

Characterizing binocularity in adult and developing mouse primary visual cortex

Jieming Fu

Charlottesville, Virginia

B.S. Chemistry, Emory University, 2017

B.A. English & Creative Writing, Emory University, 2017

M.S. Biomedical Engineering, Georgia Institute of Technology, 2019

A Dissertation presented to the Graduate Faculty of the University of Virginia in

Candidacy for the Degree of Doctor of Philosophy

Neuroscience Graduate Program

University of Virginia

April 2025

Abstract

Our visual systems are able to perceive 2-dimensional images in the eyes and combine them to perceive a 3-dimensional environment. This process, stereopsis, is a key component of depth perception and at the cellular level originates from disparity selective neurons in the primary visual cortex (V1). Unlike most other visual response properties, disparity selectivity cannot be assessed with monocular stimulation; it only emerges after the integration of binocular inputs. This makes disparity selectivity an excellent model for studying how neurons converge multiple information streams into a singular output.

Here, I performed a thorough characterization of different visual response properties that have been used to assess binocular vision: ocular dominance, interocular matching, and disparity selectivity (Chapter 2). Data was acquired using electrophysiological multichannel extracellular recordings in the V1 of awake mice as they viewed dichoptic stimuli via a polarized projector system. I demonstrated that the three binocular visual response properties were independent of each other, and that their distributions indicated that binocularity in mouse V1 was much more widespread than previously known. Furthermore, the binocular responses I observed could not be fully predicted by summation of the responses to monocular inputs, and waveform analysis showed that fast-spiking putatively inhibitory neurons also responded to binocular stimulation. Altogether, these results indicated that binocularity is prevalent throughout its namesake region in V1, but manifests in a complex manner that requires thoughtful stimulus design to uncover. Inhibitory neurons in intracortical circuits likely also contribute to binocular disparity computations performed by V1 neurons.

Experience-dependent activity during the critical period refines neural circuitry, in the visual system and beyond. Disrupted visual experience has been shown to shift ocular dominance distributions, while normal visual experience has been shown to be necessary in producing matching orientation selectivity in V1 neurons. In order to characterize the effect of visual experience on binocular development, I performed acute electrophysiological experiments on young mice starting from P14 when they opened their eyes for the first time (Chapter 3). My data showed disparity selectivity to be present at eye-opening, albeit weaker than in mature neurons, indicating that functional circuits were wired prior to eye opening but still needed experience in order to strengthen selectivity.

Together, these findings present a thorough investigation of binocularity in the adult and developing mouse visual cortex, and form a foundation for further examination of disparity selectivity computation and development, as well as future studies of binocular integration in other model systems.

Acknowledgements

I would like to first express my sincere gratitude to Dr. Jianhua Cang for his mentorship throughout my PhD. I sincerely appreciated his guidance as he both supported me and challenged me, giving me the opportunity and environment in which to learn and grow as a scientist.

I would also like to thank all my colleagues in the Cang lab, past and present. A huge thanks goes to Seiji Tanabe, for his scientific insights and extensive collaboration throughout this scientific journey. I am also grateful to Victor DePiero, Elise Savier, and Rolf Skyberg, who as senior lab members welcomed me when I began my PhD, and provided ample professional and personal advice as I began my graduate research.

I am grateful to my committee members Mark Beenhakker, Barry Condron, Alev Erisir, and Adema Ribic, for giving me their time and expert feedback. Special thanks goes to Dan Meliza, whose input late in the process of writing and defending this thesis was invaluable.

I am also thankful for the UVA Neuroscience Graduate Program coordinators Kim Knotts and Nadia Cempré for their help and support over the years.

I would also like to thank my friends in NGP and across UVA and beyond for making Charlottesville a wonderful place to live and thrive in – there are too many to name, but every one of you is important to me, and I couldn't have finished this PhD without your encouragement.

I would also like to thank my prior mentors at Emory University and the Georgia Institute of Technology, namely Machel Pardue and Andrew Feola, who seeded my interest in research and inspired me to explore a career in science. Additionally, I would like to thank Rachael Allen for being my first mentor in the Pardue lab.

My deepest gratitude goes to my family, who have supported me in my educational journey, despite the long years and distance. Thank you for instilling in me a thirst for knowledge, the discipline to work hard, and for giving me your unconditional love.

And finally, from the bottom of my heart, I want to thank my fiancé Kijoon Kim, for being the love and light of my life. We have been fortunate to come this far together, and there is so much more ahead to experience with you at my side.

Table of Contents

Title	<i>i</i>
Abstract	<i>ii</i>
Acknowledgements	<i>iii</i>
Table of Contents	<i>iv</i>
List of Figures	<i>vii</i>
Abbreviations and Acronyms	<i>viii</i>
Introduction	<i>1</i>
1.1 Organization and physiology of the visual system	<i>2</i>
1.1.1 Anatomy of the visual system	<i>2</i>
1.1.1.1 <i>The eye</i>	<i>2</i>
1.1.1.2 <i>The retina</i>	<i>4</i>
1.1.1.3 <i>Optic tract & lateral geniculate nucleus</i>	<i>4</i>
1.1.1.4 <i>Primary visual cortex</i>	<i>6</i>
1.1.1.5 <i>Higher visual areas</i>	<i>8</i>
1.1.1.6 <i>Primary versus secondary visual pathway</i>	<i>8</i>
1.1.2 Receptive fields	<i>10</i>
1.1.2.1 <i>Photoreceptors & the phototransduction cascade</i>	<i>10</i>
1.1.2.2 <i>Feedforward summation in the visual system</i>	<i>11</i>
1.1.2.3 <i>Gaps in the feedforward model</i>	<i>13</i>
1.1.2.4 <i>Receptive fields elsewhere in the visual system</i>	<i>14</i>
1.1.3 Measuring visual responses	<i>16</i>
1.1.3.1 <i>In vivo electrophysiology</i>	<i>16</i>
1.1.3.2 <i>Quantifying visually evoked electrophysiological data</i>	<i>17</i>
1.2 Binocular vision	<i>19</i>
1.2.1 Binocularity in V1	<i>20</i>
1.2.1.1 <i>Disparity-selective neurons</i>	<i>21</i>
1.2.1.2 <i>Assessing binocularity</i>	<i>22</i>
1.2.1.3 <i>Stimulus design for binocularity</i>	<i>24</i>
1.2.2 Mechanisms for disparity selectivity	<i>26</i>
1.2.2.1 <i>Introduction to the disparity energy model</i>	<i>26</i>
1.2.2.2 <i>Gaps in the disparity energy model</i>	<i>28</i>
1.3 Development of the visual system	<i>29</i>
1.3.1 General overview of embryonic visual development	<i>29</i>
1.3.1.1 <i>Formation of the optic chiasm</i>	<i>29</i>
1.3.1.2 <i>Retinotopic map wiring</i>	<i>30</i>

1.3.2	Experience-dependent visual development	31
1.3.2.1	<i>Monocular deprivation and ocular dominance studies</i>	31
1.3.2.2	<i>Studying interocular matching in naturalistic developmental conditions</i>	32
1.3.2.3	<i>Disparity selectivity and visual experience</i>	34
2	<i>Binocularity in adult mouse V1</i>	36
2.1	Abstract	37
2.2	Significance Statement	37
2.3	Introduction	38
2.4	Materials and Methods	40
2.4.1	Animals.....	40
2.4.2	Surgery	40
2.4.3	Habituation	40
2.4.4	Physiological recording	41
2.4.5	Visual stimulation.....	42
2.4.6	Data analysis	44
2.4.7	Statistics	46
2.5	Results	48
2.5.1	Systematic measurement of binocular response properties.....	48
2.5.2	Ocular dominance, interocular matching, and disparity selectivity are independent measures of binocular integration	53
2.5.3	Disparity tuning and orientation selectivity in joint parameter space	55
2.5.4	Predicting binocular tuning from responses to monocular stimuli	59
2.5.5	Specificity among cell types and cortical layers.....	62
2.6	Discussion	69
2.6.1	Ocular dominance, interocular matching, and disparity selectivity	69
2.6.2	Limitations of this study	71
2.6.3	Implications for natural behaviors and visual development.....	72
3	<i>Binocularity in developing mouse V1</i>	74
3.1	Abstract	75
3.2	Significance Statement	75
3.3	Introduction	76
3.4	Materials and Methods	78
3.4.1	Animals.....	78
3.4.2	Physiological recording	79
3.4.3	Visual stimulation.....	80
3.4.4	Data analysis and statistics.....	82
3.5	Results	83
3.5.1	Influence of visual experience on development of binocular integration.....	83

3.5.2	Developmental changes in LFP and receptive field structure.....	88
3.6	Discussion.....	91
3.6.1	Disparity selectivity in the developing visual system.....	91
3.6.2	Limitations of this study.....	92
3.6.3	Future directions.....	93
4	<i>Perspectives & Future Directions.....</i>	95
4.1	Previous studies of binocularity in mice.....	96
4.2	Is the mouse a good model for studying binocular vision?	96
4.3	Intracortical inhibition in the visual system.....	97
4.3.1	Inhibition and disparity selectivity.....	98
4.3.2	Inhibition and development	99
4.4	Disparity selectivity and stereovision	100
4.5	Concluding Remarks.....	102
	<i>References.....</i>	103

List of Figures

Chapter 1. Introduction

- Figure 1.1. Anatomy of the eye
- Figure 1.2. Schematic diagram of the mouse visual system
- Figure 1.3. Retinotopy of mouse V1
- Figure 1.4. Center-surround retinal ganglion cells
- Figure 1.5. Feedforward model for V1 simple cells
- Figure 1.6. Orientation tuning curve
- Figure 1.7. Chales Wheatstone's stereoscope design
- Figure 1.8. Schematic of retinal image disparities received by a binocular V1 neuron
- Figure 1.9. Generation of a random dot stereogram
- Figure 1.10. Disparity energy model
- Figure 1.11. Ocular dominance versus binocular matching

Chapter 2. Binocularity in adult mouse V1

- Figure 2.1. Methods and example tuning curves
- Figure 2.2. Quantification of V1 binocular response properties
- Figure 2.3. No correlation among ocular dominance, interocular matching, and binocular disparity selectivity.
- Figure 2.4. Analysis of preferred phase disparity and orientation selectivity
- Figure 2.5. Relationship between monocular and binocular responses
- Figure 2.6. Binocular response properties of fast-spiking versus regular-spiking neurons
- Figure 2.7. Binocular response properties are not specific to discrete cortical layers
- Figure 2.8. Consistency of measurements with block-structured stimulation

Chapter 3. Binocularity in developing mouse V1

- Figure 3.1. Single unit sorting and population data after eye opening
- Figure 3.2. Spontaneous and stimulus-evoked firing rates
- Figure 3.3. Example tuning curves and co-development of orientation selectivity and phase disparity selectivity after eye opening
- Figure 3.4. Local field potential changes after eye opening
- Figure 3.5. Receptive field changes after eye opening

Chapter 4. Discussion

- Figure 4.1. Changes in inhibitory innervation during the critical period
- Figure 4.2. Stereoscopic correspondence problem

Abbreviations and Acronyms

Contra	Contralateral
CSD	Current source density
dLGN	Dorsal lateral geniculate nucleus
DR	Dark rearing
ΔO	Delta orientation preference
FS	Fast-spiking
GABA	Gamma-amino butyric acid
gOSI	Global orientation selectivity index
Ipsi	Ipsilateral
ISI	Inter-spike interval
LFP	Local field potential
MD	Monocular deprivation
ODI	Ocular dominance index
PDSI	Phase disparity selectivity index
PSTH	Peri-stimulus time histogram
PV	Parvalbumin
RDS	Random dot stereogram
RF	Receptive field
RGC	Retinal ganglion cell
RS	Regular-spiking
SC	Superior colliculus
SNR	Signal-to-noise ratio
SST	Somatostatin
TTL	Transistor-transistor logic
V1	Primary visual cortex
VIP	Vasoactive intestinal peptide

Introduction

Since time immemorial, people have gazed into the night sky and told stories about the constellations splayed overhead, picking out forms and creating narratives from patterns of scattered stars. The Belt of Orion, for example, consists of three blue-white stars, spaced equally apart in a straight line. However, modern astronomy informs us that this belt-like appearance is an illusion, for the middle star Alnilam is actually the farthest away from our Earth, compared to the Alnitak and Mintaka. The belt viewed from a different angle looks rather more akin to a slingshot.

Astronomers can calculate the distance between Earth and a singular star using parallax, a phenomenon where the same object viewed from two different lines of sight will appear in slight, but perceptibly disparate positions. When observing heavenly bodies, the two different points of view are attained at different times of the year, when Earth's orbit around the sun has moved our observatories elsewhere in space. In biology, we receive information from two points of view through both eyes simultaneously. This process of stereopsis is how the visual system integrates the two-dimensional images projected onto the retinas in order to comprehend the surrounding three-dimensional environment.

This dissertation concerns binocularity in both the adult and developing visual cortex of the mouse. As an introduction, I will begin with a review of the components of the visual system and the neuron-level mechanisms that underlie visual processing, especially as they relate to binocular vision. I will also review how binocularity is defined and how it can be assessed in visual neurons. Finally, I will briefly describe neurodevelopment as it relates to the visual system, and what is known about the development of binocular neurons in the primary visual cortex.

1.1 *Organization and physiology of the visual system*

The visual system's components must together achieve several aims: capture light so that the images accurately represent the surrounding environment, translate the image information into signals that neurons can transmit, and then process the neural signals so that the environment can be perceived. Accordingly, the sensory neurons in the visual system can be defined by their receptive fields, which are the zones from which stimuli influence activity of a particular neuron. Careful characterization of receptive fields in different structures along the visual pathway reveals the iterative processes by which information is summed and fed onwards.

1.1.1 *Anatomy of the visual system*

The bilateral symmetry of the visual system is integral to some of its most important abilities, in yet another example of how structure and function are tightly entwined in biological systems. Vertebrate animal eyes come in pairs, and the most immediate benefit of having two eyes is that in the event that one eye becomes damaged, the other eye is still able to send visual inputs to the brain. During normal function, having a pair of eyes also allows for binocular vision, and subsequently stereopsis. Depending on the positioning of the eyes, the visual fields overlap to varying degrees, allowing for either a wide total visual angle and therefore better observation of all surroundings, or a narrower visual field with a large portion being binocular, leading to improved depth perception. In both cases, the pathways later in the visual system are also adapted to accommodate the segregation of information coming from the two eyes, and the eventual orderly integration of said visual information.

1.1.1.1 *The eye*

Vision begins with the process of capturing light, which begins at the eye (**Figure 1.1**). Light enters the eye through the cornea and lens, clear structures that focus the light onto the retina in a coherent image, albeit one that is upside down and reversed left-right. While this seems like a relatively straightforward process, there are many points of potential failure in this

process that could lead to a distorted image, which would in turn hinder visual perception. Opacity in the cornea or lens could prevent some light from being transmitted in full, or changes in the overall length of the eye could result in a blurry image landing on the retina. Additionally, any lack of coordination within the ocular muscles that control eye movement could result in misaligned images going to the retina, which would also in turn affect the output of binocular integration.

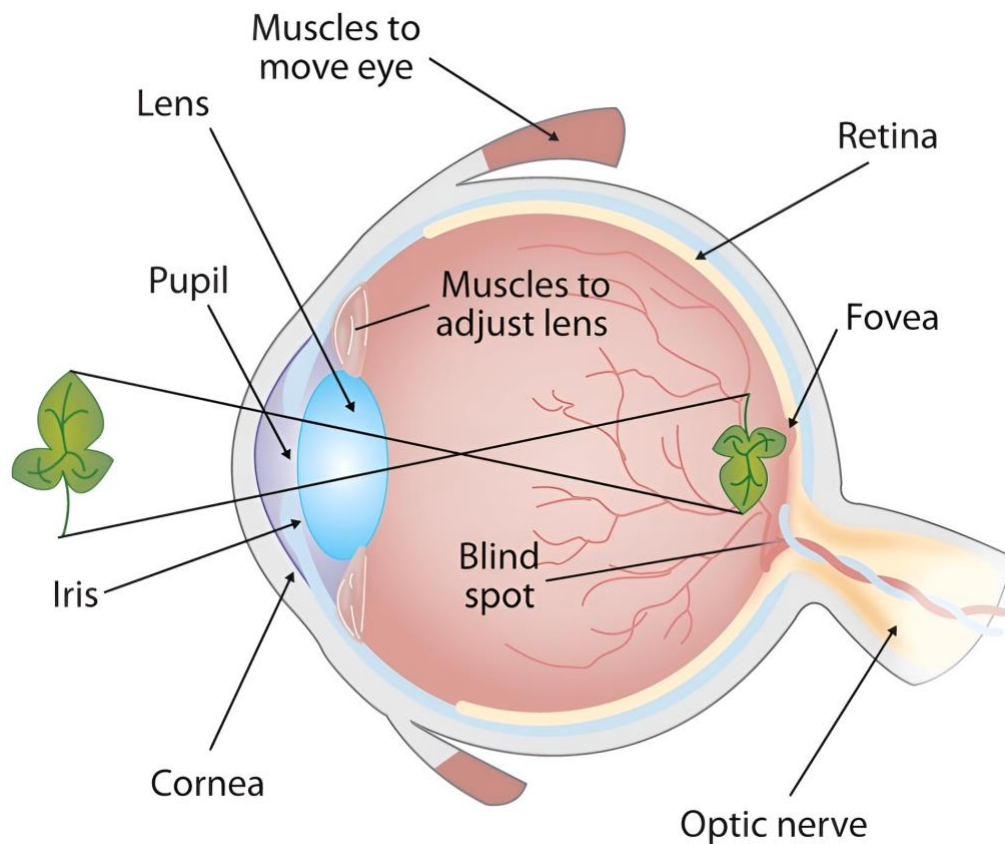


Figure 1.1. Anatomy of the eye. Light enters the anterior chamber through the cornea and pupil, and the lens focuses it to produce a coherent image on the retina. The image that lands on the retina is inversed and upside-down. Adapted from (Walters, 2020).

1.1.1.2 *The retina*

Assuming that light has been transmitted to the back of the eye as coherent images, the next step is for the retina to translate these images into neuronal signals, so that the brain can process this information.

The key cells in this process are the photoreceptors, which contain proteins that change the photoreceptor's electrical charge when struck by a photon. The signal output from the photoreceptors undergoes initial processing from interneurons in the retina, including bipolar cells, amacrine cells, horizontal cells, and more. The refined signal is then passed onto retinal ganglion cells (RGCs), which output the processed signal to the brain. RGC axons in each retina come together at the optic nerve head and then bundle together to form the optic nerves, which then project into the brain.

1.1.1.3 *Optic tract & lateral geniculate nucleus*

As the optic nerves approach the brain, the left and right eye optic nerves come together at the optic chiasm. There, the nerve fibers sort once more, bundling into tracts according to the visual field they receive information from, and then exit towards the appropriate hemisphere of the brain (**Figure 1.2**).

This crossing-over, or decussation, is only partial and affects the contralateral portions of the visual field. Axons originating from the left eye could contain information from either the left or right half of the left eye's visible range, with light coming from the right half landing within the binocular visual field. Due to the pinhole effect where light is reversed as it is projected onto the retina, light from the binocular visual field would land on the left portion of the retina, and vice versa for light from the left field of the left eye (i.e., it would land on the right portion of the retina). At the optic chiasm, axons carrying information from the peripheral visual fields would therefore cross over to the contralateral hemisphere, while axons carrying information from the central portion of the visual field would be more likely to remain on the same side.

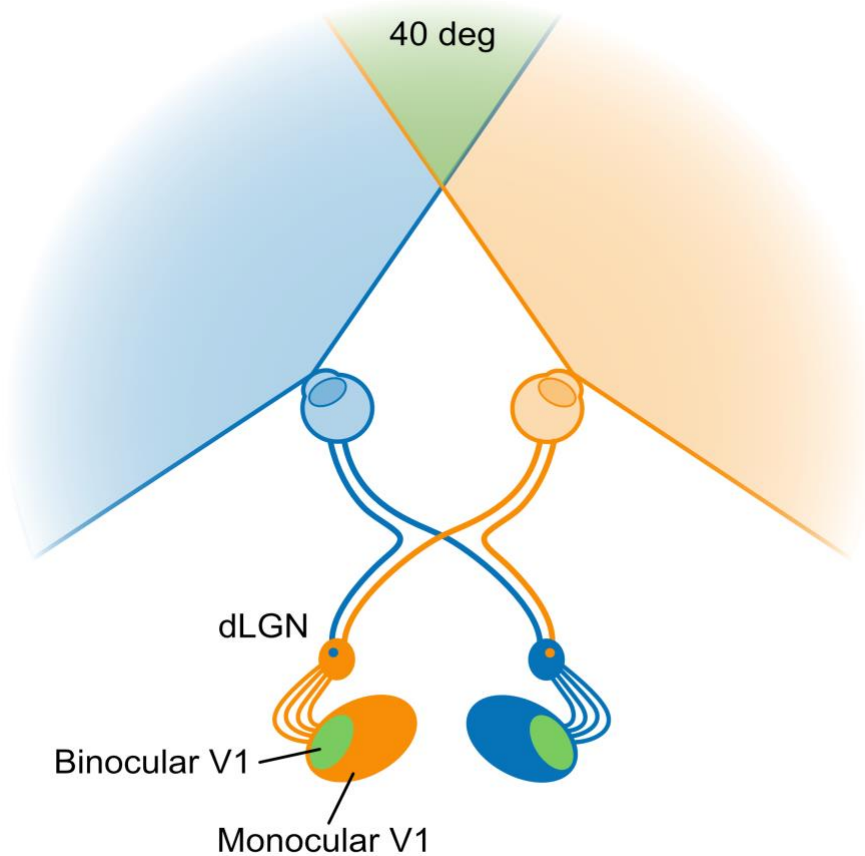


Figure 1.2. Schematic diagram of the mouse visual system. RGC axons either cross to the contralateral or stay on the ipsilateral hemisphere, leading to binocular interactions in dLGN and V1. Adapted from (Cang et al., 2023)

Around this point, it becomes more useful to refer to visual inputs as ipsilateral or contralateral, depending on where they originate relative to the structure being discussed. Upon exiting the optic chiasm, RGC axons terminate in the dorsal lateral geniculate nucleus (dLGN) of the thalamus. Projections at this point have sorted according to the appropriate visual field, but remain segregated depending on the eye they originated from. Ipsilateral projections target the ventromedial central zone of the dLGN, while contralateral inputs synapse in the surrounding zone.

This segregation between ipsilateral and contralateral projections is more pronounced in primates and cats than it is in rodents. In fact, some studies in mice have suggested that a significant proportion of their dLGN neurons in fact receive both ipsilateral and contralateral inputs (Howarth et al., 2014; Jaepel et al., 2017; Sommeijer et al., 2017; Huh et al., 2019). These include rabies tracing studies that visualize projections to the dLGN, as well as electrophysiological studies of dLGN function. However, the overall purpose of a binocular dLGN in rodents, as well as any potential preprocessing performed before inputs go to the primary visual cortex, remain unclear.

1.1.1.4 Primary visual cortex

LGN neurons then project to the primary visual cortex (V1), located in the occipital lobe. Mammalian visual cortex consists of six layers, and axons from the LGN synapse onto densely packed neurons in layer 4 of V1. In fact, primary visual cortex is also referred to as striate cortex due to the highly visible layer of axons arriving from LGN to terminate in L4.

V1 is organized in a retinotopic manner, meaning that relative spatial organization from the retina is preserved (**Figure 1.3**). Because of this intricate patterning, there is a specific zone where ipsilateral projections from the binocular visual field synapse, referred to somewhat uncreatively as the binocular region of V1.

While retinotopic maps are highly conserved across species, cortical columns are relatively rarer, present in animals such as primates and cats, but not rodents. In animals with cortical columns, information processing is organized vertically across all layers for a variety of visual properties. For example, since cats have ocular dominance columns, physiological experiments will reveal stripes of neurons that receive input from only the left or right eye in L4, before those signals converge in neurons located in more superficial cortical layers.

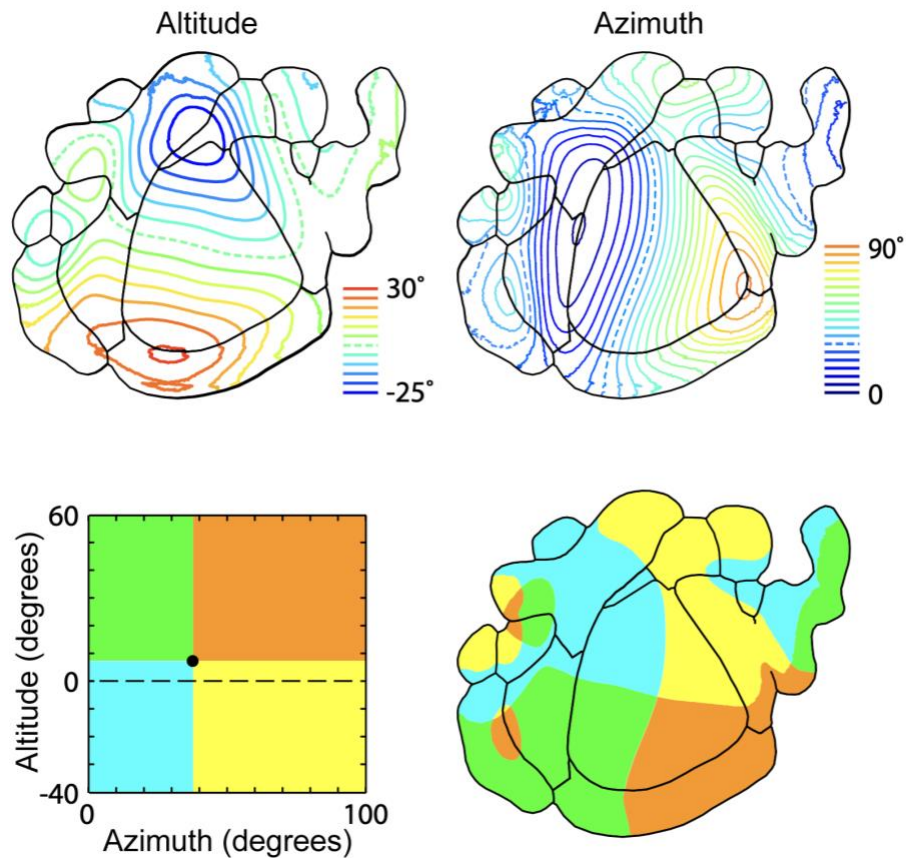


Figure 1.3. Retinotopy of mouse V1. Inputs received by V1 are organized based on where they appear in the visual field by altitude, i.e. top to bottom (top right), as well as azimuth, i.e. central to peripheral (top left). A more simplified schematic version shows that inputs from the central visual field are routed to the lateral side of V1 (bottom). Adapted from (Zhuang et al., 2017)

Rodents, on the other hand, possess a “salt-and-pepper” cortex, meaning that no such columnar organization exists. When examining another visual response property, orientation selectivity, cells with different orientation preferences will be randomly scattered throughout rodent cortex, while in primates and cats they will sort into neat windmills by orientation preference. There have been reports of structures resembling ocular dominance maps in rodents (Ringach et al., 2016; Zhou et al., 2023; Goltstein et al., 2025), but their functional relevance remains a point of contention. Computational modeling has suggested a potential link

between the retina-to-cortex sampling ratio and the presence of a columnar cortex (Jang et al., 2020).

1.1.1.5 Higher visual areas

The other areas of the visual cortex outside of V1 are collectively referred to as higher visual areas, and play roles in more advanced visual processing. The two-streams hypothesis postulates that visual information, following initial processing in V1, is passed on via two major paths. The dorsal stream goes to the parietal lobe, and is also known as the “how” stream, used to understand relative spatial location. The ventral stream meanwhile goes to the temporal lobe, and is also known as the “what” stream, used for object recognition.

Most literature examining the processing performed by the higher visual areas is produced from primate data. However, research into higher visual areas in the mouse has indicated that mouse higher visual areas are exquisitely networked and are involved in behavioral outputs such as navigation and short term memory, and respond to disparity stimuli in low frequencies (Glickfeld et al., 2014; Glickfeld and Olsen, 2017; Chioma et al., 2019).

1.1.1.6 Primary versus secondary visual pathway

The retina-dLGN-V1 pathway described thus far in the introduction has also been referred to as the primary visual pathway. The secondary visual pathway consists of projections from the retina and V1 to the superior colliculus (SC), a midbrain structure that has particular importance in rodent vision. The secondary visual pathway has been thus named because it was thought to convey information that was accessory to the visual information processed by the primary visual pathway, but studies have shown that this was an oversimplified interpretation.

The SC has traditionally been defined as a structure that plays a role in more basic functions that relate to vision, such as guiding eye movements and regulating attention. However, the vast majority of retinal axons in rodents – at least seventy percent – project to the SC and not the LGN, indicating that the SC must be playing a critical role in rodent visual

physiology, given its share of sensory input (Hofbauer and Dräger, 1985). Interest in rodent SC has also renewed interest in re-evaluating the role that the SC plays in primate brain function, uncovering such unlikely functions as assisting with abstract cognitive tasks (Peysakhovich et al., 2024). The SC is known to receive binocular inputs, and ipsilateral inputs to the SC have been shown to be important to prey capture behavior, but overall the role of binocular neurons in SC function is still being investigated (Russell et al., 2022).

1.1.2 *Receptive fields*

The receptive field of a neuron is defined as a limited zone in which a stimulus will influence a response from a sensory neuron. This definition is purposefully wide-ranging, because of the wide variety of sensory stimuli that our nervous systems accommodate and process. A receptive field for a touch neuron might encompass some area of skin where a physical stimulus would elicit a response, while the receptive field or sensory space of an olfactory neuron might be a particular chemical that binds to a neuron's specialized receptors.

In visual neuroscience, a visual receptive field may have both spatial and temporal components – that is to say, a stimulus may have to appear in a specific place in the overall visual field, or with a certain timing, or both in order to evoke a response. From the retina to visual cortex, neurons located in various structures along the visual pathway have very different receptive fields, revealing the information processing functions of these different neurons, as well as how they receive information and send it downstream.

1.1.2.1 *Photoreceptors & the phototransduction cascade*

The most basic receptive field in the visual system is that of a single photoreceptor, cells that convert photons into changes in membrane potential. In the mammalian retina, the classic photoreceptor types are rods and cones. Rods are immensely sensitive to the presence of even single photons and are therefore useful in dimly lit environments. Cones, however, are sensitive to wavelengths corresponding to different colors, and are useful in brightly lit environments where detailed perception is desirable.

Both rods and cones perform phototransduction, the process of converting photons into signals for the nervous system. In dark conditions without any photons, photoreceptors maintain a depolarized membrane potential. When a photon strikes, it causes a light-sensitive protein called an opsin to change its conformation, which in turn triggers a cascade of protein activity that results in hyperpolarization of the photoreceptor. The amount of hyperpolarization in photoreceptors varies depending on the intensity of the light, making the signal a graded

one, as opposed to elsewhere in the nervous system. In fact, signal transduction via action potentials only begins once retinal inputs are summed at RGCs.

1.1.2.2 Feedforward summation in the visual system

After the signals from multiple photoreceptors are passed along and modulated by bipolar, amacrine, horizontal cells and more, they are then integrated at a retinal ganglion cell. Despite there being upwards of 30 RGC types that have been characterized (Sanes and Masland, 2015), the stereotype of a “classic” RGC receptive field is the center-surround type.

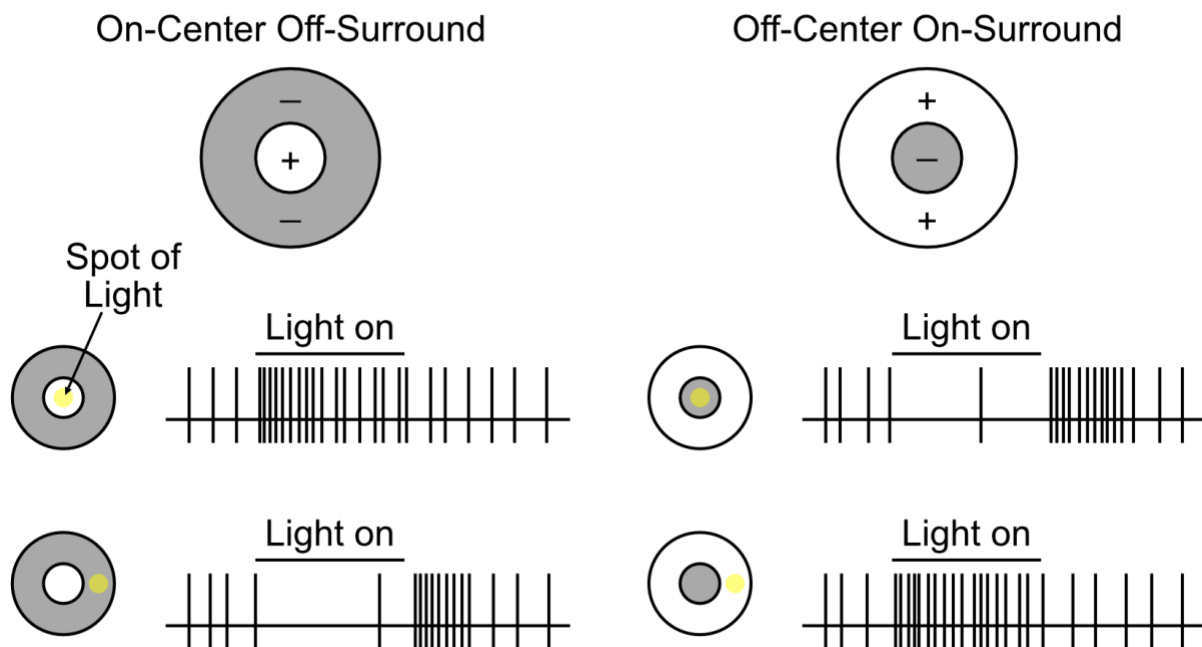


Figure 1.4. Center-surround retinal ganglion cells. An ON-center OFF-surround receptive field (top left) and an OFF-center ON-surround receptive field (top right). When light stimuli is shown to ON-zones and not OFF-zones (middle left and bottom right), the cell fires rapidly. Conversely, when light stimuli is delivered to the OFF-zones and not ON-zones, the cell’s firing is inhibited (middle right and bottom left). Adapted from (Rao, 2002).

Using the example of an ON-center OFF-surround RGC to illustrate how a center-surround receptive field functions: a bright stimulus against a dark background, displayed only to the ON zone, would induce that RGC to fire action potentials, as both the bright center of the stimulus and the dark background of the surround area would match the RGC's receptive field properties. However, if that stimulus were misaligned with the receptive field, this might result in a bright stimulus landing on the OFF-surround zone, while the dark background would land on the ON-center, and as a result the RGC would be suppressed from firing (**Figure 1.4**).

RGC receptive fields are arranged such that they tile the retina and cover the visual space. Their tiling patterns, combined with lateral inhibition supplied by horizontal cells, enable them to act as filters that enhance contrast and detect edges in images. As RGCs propagate their signals further along in the visual pathway, their projections synapse to neurons in the LGN, which also possess circular receptive fields.

When LGN projections are summed by V1 neurons, they result in V1 neurons having receptive fields that are elongated and elliptical as opposed to circular, an indication of how V1 neurons are able to respond to stimuli that have specific orientations or are moving in certain directions. In 1962, David Hubel and Torsten Wiesel described the receptive fields of neurons in cat V1 that responded well to long narrow rectangles of light, and suggested a feedforward mechanism to explain their selectivity.

In **Figure 1.5**, the circular receptive fields of the LGN neurons are arranged in a diagonal line. If a moving bar with a similar orientation was swept across the ON-centers of all these circular receptive fields at once, the combined excitatory inputs would then induce firing in the recipient V1 neuron, i.e., summation within the excitatory zone of the V1 neuron's receptive field. However, if that moving bar was rotated 90 degrees and swept across the receptive fields again, the ON zone and the flanking OFF zones would all be stimulated simultaneously. The result would be a lack of synchronized input going to the V1 neuron, which would not trigger an output action potential.

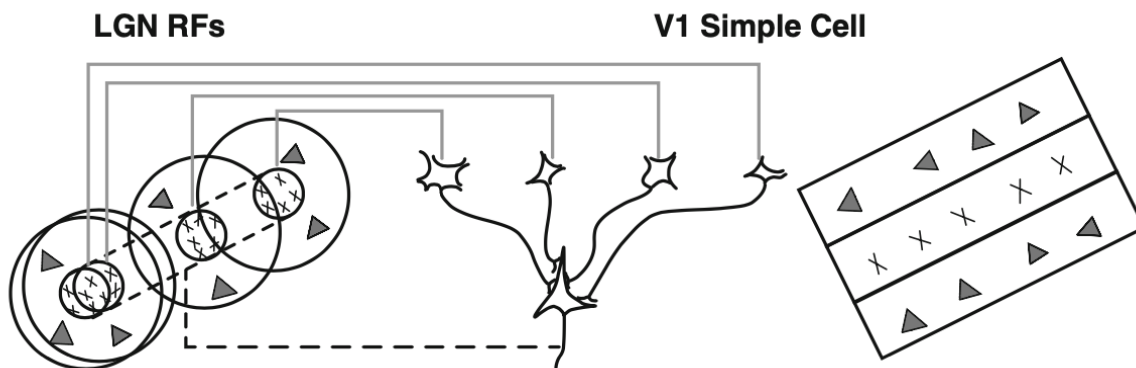


Figure 1.5. Feedforward model for V1 simple cells. Multiple LGN neurons, with their receptive fields depicted on the left, send their projections to a single V1 neuron. The resulting V1 receptive field is a summation of the LGN receptive fields, with an elongated ON region in the center flanked by OFF regions. Adapted from (Hubel and Wiesel, 1962; Scholl et al., 2013a)

This particular description applies to a category of cells that Hubel and Wiesel termed ‘simple’, because their response to a hypothetical stimulus was predictable, provided one could map out the ON and OFF zones. In contrast, complex cells were those that had preferred orientations but were spatially invariant. In other words, they were able to respond to preferred stimuli regardless of where they were in the receptive field, seemingly having no distinctive ON or OFF zones. Hubel and Wiesel suggested a hierarchical model where complex cell receptive fields might have such properties because they summed the inputs of multiple simple cells, all tuned for the same orientation. Because these simple cells’ receptive fields overlapped such that one simple cell’s OFF zone might be redundant with another cell’s ON zone, the downstream complex cell would also respond to the same preferred orientation as all of its simple cell afferents, but have no defined ON or OFF zone.

1.1.2.3 Gaps in the feedforward model

Hubel and Wiesel themselves noted that their feedforward model was based on inputs from excitatory synapses, and accordingly, there are some empirical observations that the feedforward model cannot account for alone. Nevertheless, the feedforward model is a

cornerstone achievement in our understanding of neural processing, and debates over its relative salience continue to this day, sometimes with surprising results.

Contrast invariance is an interesting example of the back-and-forth over the relevance of the feedforward model. As the contrast between a stimulus and its background increases, increased input from LGN cells should result in wider orientation tuning, according to the feedforward model. However, this is not observed in experimental settings (Skottun et al., 1987). While it was thought that this was due to the lack of inhibitory activity included in the feedforward model (Troyer et al., 1998), and that lateral inhibition was needed to accurately model contrast invariance, later studies have pointed out that changes in contrast also result in changes to the number of spikes output from LGN, which would provide an explanation for contrast invariance by feedforward excitation alone, without lateral inhibition (Finn et al., 2007).

On the other hand, the hierarchical model for complex cells was complicated by the discovery that thalamocortical inputs also go to complex cells (Hoffmann and Stone, 1971) in addition to simple cells. The hierarchical model for complex cells does not account for intracortical inputs from other complex cells and inhibitory cells (Martinez and Alonso, 2003).

Overall, the underlying principles of the feedforward model are accepted as a foundation from which other computations can be understood. We will revisit this concept as it applies to receptive fields that produce binocular disparity selectivity in [Section 1.2.2](#).

1.1.2.4 Receptive fields elsewhere in the visual system

The properties of receptive fields in higher visual areas reflect their role in processing more complex and abstract visual features. Receptive fields in these areas tend to respond to stimuli with detailed and intricate properties, including shape and texture. Through combinations of these selected features, receptive fields in higher visual areas are even capable of responding selectively to abstract object categories (Glickfeld and Olsen, 2017).

In the superior colliculus, visual receptive fields have been characterized in neurons located in the superficial layers (Wang et al., 2010b). Some SC neurons have been shown to have clear ON and OFF regions, as well as other properties similar to those found in V1 neurons, such as orientation and direction selectivity. Other SC neurons have receptive fields with features not common in other visual structures, such as narrow field vertical cells with long cylindrical receptive fields, or wide field vertical neurons with broadly expansive receptive fields.

1.1.3 *Measuring visual responses*

Neurons are discrete biological units, their function generated by a complex system of dendritic receptors, ion channels, and neurotransmitters. However, the signals regulated by these biochemical processes are sent via electrical activity propagating through axons, which means that neurons can be viewed as components of a computational circuit. When neurons are observed using electrophysiological methods, we can probe their inputs and outputs, abstracting individual neurons into mathematical functions that collect data from and govern complex biological systems.

1.1.3.1 *In vivo electrophysiology*

The electrophysiological data presented in this thesis was collected using in vivo extracellular multichannel recordings, which comes with certain benefits as well as challenges compared to other methods of recording neuron data.

In terms of benefits, in vivo recording is highly valuable for systems neuroscience because it produces neuronal recordings of a brain in its natural state. In the experimental setups described in later chapters, it is evident that these neuronal recordings are derived from a real brain processing input from visual stimuli that are designed to engage neurons in producing a binocular response.

The challenges of using in vivo recording data, aside from any technical difficulty in setting up the experiment, lie in how representative the data is of actual neuronal activity. Unlike patch-clamp electrophysiology, which allows the user to record the electrical flux of one specific neuron, extracellular multichannel data was obtained by inserting a probe into the brain and recording the total electrical activity from the nearby neurons combined. This allows for recording of either local field potentials (LFPs) or processing the data using spike sorting analysis in order to sort the data into spike trains from ostensible individual neurons. Inevitably, this means that the activity of individual neurons is being approximated to some degree, depending on the parameters used in spike sorting.

Spike sorting can be achieved through a variety of methods, ranging from manual recognition to automated algorithms (Stringer and Pachitariu, 2024). In general, all spike sorting methods aim to separate neuronal spikes from background noise fluctuations, followed by sorting neuronal spikes into clusters. In a typical workflow, spikes are first sorted according to the shapes of their waveforms, after which clusters with good-quality spikes are retained for further analysis. The goal is for the output of spike sorting to consist of spike clusters that can be trusted to originate from differentiable neurons.

1.1.3.2 Quantifying visually evoked electrophysiological data

In order to make sense of the electrophysiological data collected in these experiments, spike trains must first be analyzed together with their associated stimuli, to check if the recorded spikes were actually evoked by the stimulus. Some initial analyses that can be examined are peristimulus time histograms (PSTHs), interspike intervals (ISIs), and spontaneous spiking rates, to name a few.

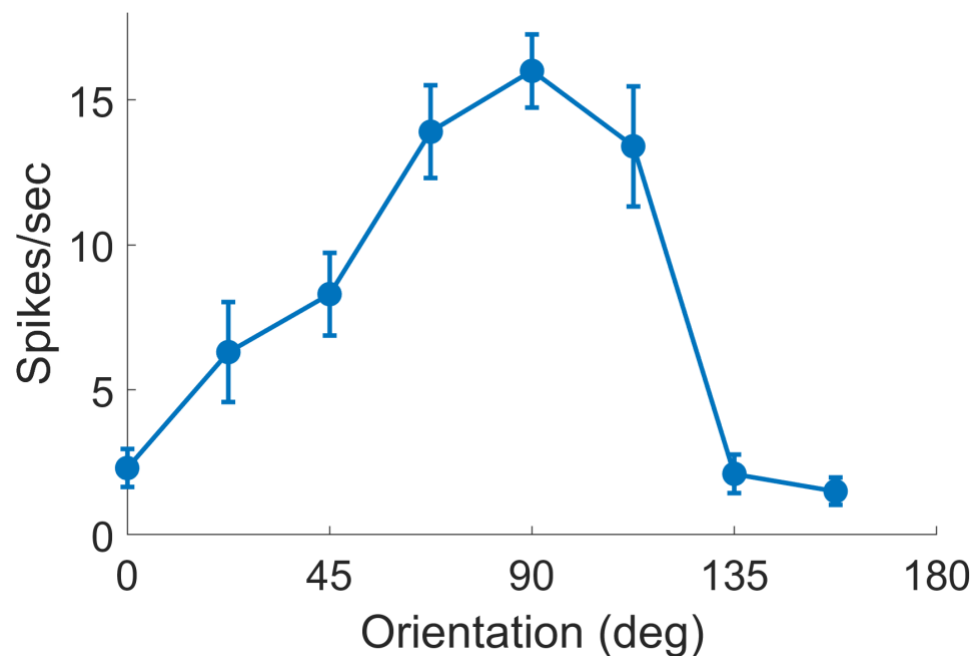


Figure 1.6. Orientation tuning curve. Original data.

One of the most useful applications of spike data is the mapping of receptive fields. In Hubel and Wiesel's landmark studies, they mapped receptive fields by hand, by recording whether neurons spiked or not when a flashing spot or bar was projected on a particular spatial location within a cat's visual field. Modern experimental rigs may allow for more complex stimuli to be shown and for more neurons to be recorded, but the general principle remains the same. Receptive field mapping is helpful for determining the optimal stimulus for a given neuron, which in turn can help uncover which inputs the neuron might be receiving in order to be responsive to that particular stimulus.

Tuning curves can also be generated in order to characterize how a neuron responds to certain properties of a stimulus. Typically, this is done with a stimulus property that exists on a continuous range, such as orientation or direction, spatial frequency, phase disparity, etc. **Figure 1.6** shows an example orientation tuning curve. The neuron fires at a low rate when the animal is seeing moving gratings oriented near the horizontal (0, 135, and 157.5), but the firing rate rises for other stimulus conditions, reaching a peak response in response to a stimulus oriented 90 degrees from the horizontal. Tuning curves can be generated for individual neurons, or normalized and examined within a population to gauge percentages of highly tuned versus untuned neurons.

1.2 Binocular vision

We have now discussed at length the eyes, receptive fields, and how all of these moving parts together capture photons and bring the signals to our brain to process, but what happens next? Somehow, our brains are able to recognize that the two-dimensional images captured by the retinas contain components of the same scene, which can be encoded and interpreted in order for us to perceive a three-dimensional world.

One of the first people to demonstrate this remarkable property of the visual system was the English inventor Charles Wheatstone. His device, the Wheatstone stereoscope, allowed for someone to view two different images simultaneously, using angled mirrors so that reflections of the images appeared aligned before both eyes at the same time (**Figure 1.7**). The two images were drawn to have a slight offset but were otherwise completely identical. Viewers using the stereoscope would know that they were looking at two paper drawings through mirrors, but feel the illusion of suddenly viewing a solid, three-dimensional object. Though later inventors continued to iterate upon this basic concept, the fundamental principle remains the same.

Wheatstone's writings were descriptive of *how* to create a stimulus that would be perceived by the eyes and brain to be stereoscopic, but what about the other way around – how do the eyes and brain perceive and encode the information needed for stereopsis? How does the brain respond to specific cues within 2-dimensional images to recognize that they are closer or further away? In this section, we will discuss disparity-selective neurons, a class of cells in the primary visual cortex that are specialized to respond to stimuli with this type of spatial offset due to the arrangement of their receptive fields. It is the output of these neurons that allows our brains to make the most of the signals collected by a binocular visual system.

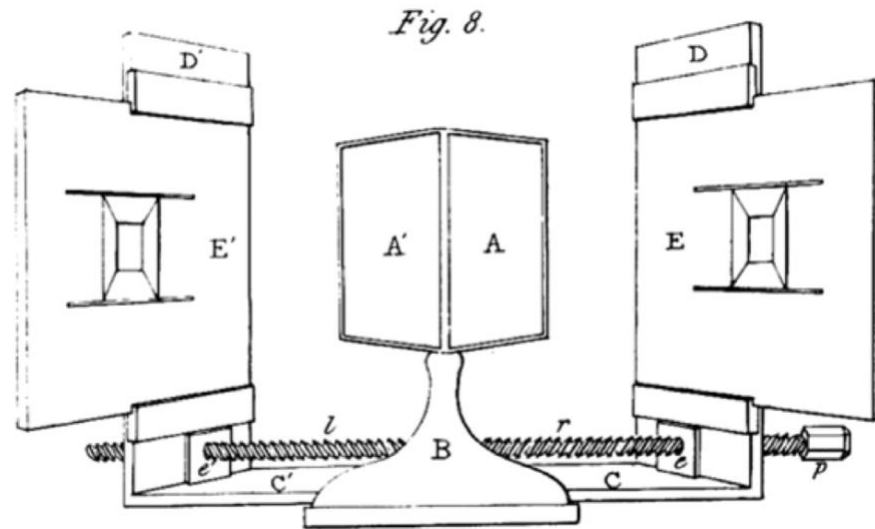


Figure 1.7. Charles Wheatstone's stereoscope design. Drawings were placed on the boards labeled by 'E', and the user would sit facing twin mirrors labeled by 'A' in order to view the drawings. Adapted from (Wade, 2002)

1.2.1 Binocularity in V1

Before delving further, it is essential to first distinguish stereopsis from the general concept of depth perception. There are a number of visual cues that contribute to the overall perception of depth, and not all require input from both eyes.

Monocular cues for depth can be grouped by their underlying cause (Banks et al., 2016). The transmission and reflection of light can shift depending on the depth – the Blue Ridge Mountains, for example, are so named because they appear blue in the distance, due to light scattering through the organic emissions from the heavily forested peaks. Other cues are based on our intuition of linear perspective, such as the relative size and overlapping of objects, as well as their texture – more visible when objects are close, and harder to view when objects are far away.

The final category of monocular cues comes from triangulation. This includes cues such as motion parallax, where objects closer to the viewer appear to move a greater distance when

the point of view shifts, as mentioned in the introduction. Disparity selectivity, and therefore stereopsis, is also a depth cue that comes from triangulation, but notably is the *only* depth cue that in a biological system requires the fusing of inputs from both eyes, rendering it extremely useful for studying neural computation.

1.2.1.1 Disparity-selective neurons

Disparity selective cells were first reported as cells in cat V1 that preferentially responded to flashing bars in the same orientation simultaneously appearing in the visual fields of both eyes (Barlow et al., 1967). Monocular stimuli, or two bars that were orthogonal to each other, elicited weaker or absent responses. Moreover, the maximum response of these neurons came when the stimuli were some distance apart, while stimuli that were too close or too far apart would fail to produce a response. In other words, these neurons were selectively responsive to stimuli with a certain disparity. Barlow and Pettigrew also noted a subset of cells that were selective for vertical disparities as well, though the range was smaller for vertical disparities compared to horizontal – and given that eyes tend to be at the same height and are separated by horizontal distance, greater sensitivity to horizontal disparity is not surprising.

Binocular disparity at the retinal level can be understood by the schematic in **Figure 1.8**, representing the images viewed by a hiker with their eyes fixed on mountains in the distance. The images of the mountains fall at about the same point on both retinas. A tree, closer to the hiker and off to one side, is located at slightly different angles from the two eyes and projects to a different location on the retina of each eye.

The significance of binocular disparity responses is therefore that in order for a disparity to exist, there must be two images that are compared against each other, in order for a disparity to exist and be detected. An image seen only through one eye contains no binocular disparity by definition, as there is no second image to compare against. Therefore, a neuron that is disparity selective is a neuron that is integrating binocular inputs, as it must be performing some type of combinatorial computation in order to produce a selective output response.

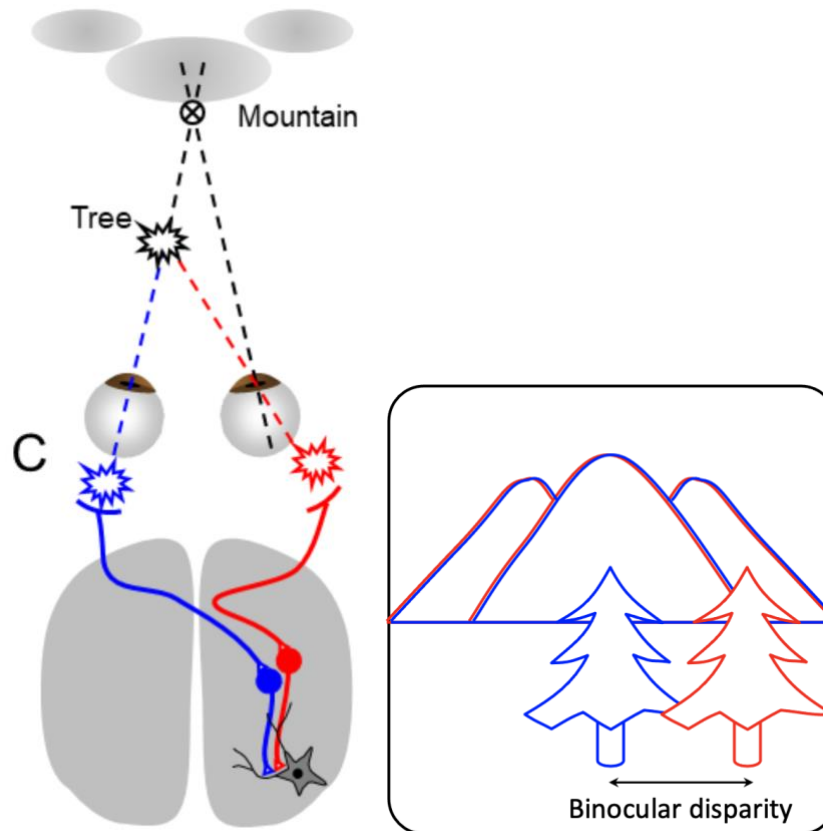


Figure 1.8. Schematic of retinal image disparities received by a binocular V1 neuron. The left schematic depicts a simplified version of how contralateral and ipsilateral inputs would converge on a binocular neuron. The left diagram represents the two retinal images superimposed upon one another so that the disparity between the tree images is noticeable.

1.2.1.2 Assessing binocularity

The ideal stimulus for probing binocularity should be one where monocular stimulation alone produces no responses of note, and only simultaneous binocular stimulation elicits a response. This statement seems self-evident, but in actuality is anything but. In the corpus of visual neuroscience literature, there exist other visual response properties of V1 neurons that can be measured by comparing the responses to inputs to the two eyes, and these have long been referred to as measures of binocularity alongside disparity selectivity.

Ocular dominance is a classic response property in V1, made famous by Hubel and Wiesel's series of papers describing experience-induced plasticity in cat V1 (Hubel and Wiesel, 1963, 1965; Wiesel and Hubel, 1963a, 1963b, 1965a, 1965b). The ocular dominance of a single neuron is obtained by recording from that neuron while stimulating through each eye individually, and then comparing the two. The stimulus can be anything that produces a neuronal response – Hubel and Wiesel used flashing spots, while other papers have used anything from drifting gratings to full-field flashes. The eye that elicits the larger response while being stimulated “dominates” the response, hence why this property is called ocular dominance. Under this paradigm, neurons are classified as monocular if they only respond when stimulated through one eye and not the other, while neurons that respond when stimulated through either eye are considered “binocular”.

Interocular matching of orientation preference is another visual response property that has been described in the literature as an assessment of binocularity. V1 neurons are known to exhibit orientation preference, i.e. a selective response for stimuli with a certain orientation, as demonstrated in the example of a tuning curve for orientation (described previously in [Section 1.1.3.2](#)). A neuron can have two orientation preferences measured, one through each eye. The majority of neurons in mature V1 have very similar orientation preferences through the two eyes, a state referred to as “matched”, but a subset of neurons have orientation preferences that are “unmatched”. Under this paradigm, neurons can be responsive when stimulated through both eyes and be either matched or unmatched, but neurons that have matched orientation preferences are considered “binocular”.

Other studies have observed that though these three response properties – ocular dominance, interocular matching, and disparity selectivity – have all been referred to as measures of binocularity at one time or another, they are not equivalent in terms of how well they describe the outputs of binocular integration. Referring back to the first statement in this subsection regarding an ideal stimulus for probing binocular integration, we can observe that ocular dominance and interocular matching do not fulfill this requirement. Both are derived from a neuron's responses to monocular stimulation, and are calculated by comparing the

responses. Once again, only disparity selectivity can be considered to capture the output of binocular integration, because it first requires binocular stimulation in order to emerge.

1.2.1.3 Stimulus design for binocularity

We have stressed the importance of binocular stimuli, but more accurately the type of stimulation used to elicit disparity selectivity should be called dichoptic presentation. The word “dichoptic” comes from the Ancient Greek διχῶ, meaning “two”, and ὀπτικός, meaning “optical”. In practice, dichoptic presentation refers to a stimulus where images are presented to the two eyes simultaneously but independently, such as in a stereoscope.

In experimental settings, a variety of dichoptic stimuli have been used to probe binocularity. V1 responds well to moving bars, which extended to Barlow and Pettigrew’s initial studies of disparity selective neurons responding to light flashing through moving slits. Drifting gratings were adapted for dichoptic presentation by turning them into binocular gratings with phase disparity, where the spatiotemporal frequency of the stimulus remained the same between the two eyes, but the cycles could be either in phase or varying degrees out of phase.

A potential side effect of using drifting gratings to assess binocularity may be that it may evoke particularly high responses from orientation preference matched cells, which would in turn skew the population of neurons perceived to be binocular towards those that are already orientation matched. For a method to observe binocularity regardless of the orientation preferences of a neuron, we turn to yet another type of dichoptic stimulus: the random dot stereogram.

The random dot stereogram (RDS) is a dichoptic pattern that generates the perception of stereoscopic vision using only patterns of randomized dots, which inherently contain no orientation. Developed at Bell Labs in the 1960s by Dr. Bela Julesz, the basic principle of generating an RDS stimulus is to start with a pattern of random dots, shift a small portion of the dots, and fill in the gap with more randomly distributed dots. When the original image and the

altered image are shown together to the two eyes, the shifted patch appears at a different depth than the rest of the image (**Figure 1.9**).

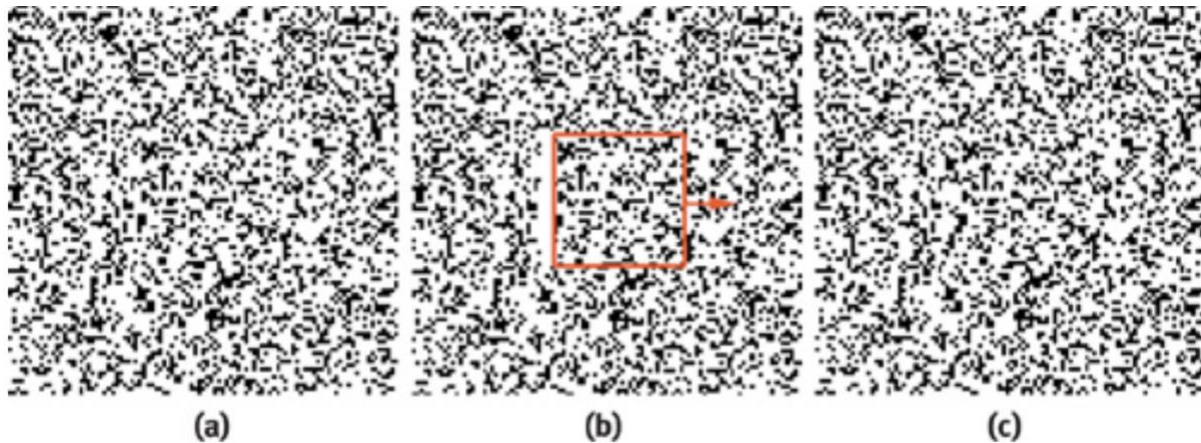


Figure 1.9. Generation of a random dot stereogram. After an image of random dots is generated (a), a patch is selected and shifted (b). The remaining gap is then filled by more random dots (c). When (a) and (c) are viewed in the two eyes, they evoke an illusion of a floating square. Adapted from (Policarpo, 2004)

The very fact that RDS images create a visual illusion of a floating patch of dots is extraordinary, given that there is no other information in the images that can be used to support that perception. The dots are randomly spaced out, with no obvious cues such as areas of high or low contrast, edges, or shapes, and yet the brain still manages to define an area to be at a different depth than the surround. What this reveals is that the visual system fuses images from the two eyes to create a single percept very early in its processing pipeline, before object recognition happens (Poggio and Poggio, 1984). This aspect of the visual system was described as “cyclopean” by Bela Julesz, invoking the monster from Greek mythology with only one eye in its forehead (Julesz, 1971; Read, 2005). Contrary to the parable, perhaps our visual systems must recognize the whole elephant before it starts identifying the parts.

Random dot stereograms have been used to characterize disparity selectivity in primates, and only recently have been used in murine experiments with differing results (Chioma et al., 2019, 2020; Samonds et al., 2019). Some groups report that mouse V1 has cells

that can respond to RDS, while others report very low or altogether absent responses. Our systematic investigation of mouse disparity selectivity has concluded that mice exhibit strong responses to phase disparity stimuli but weak responses to RDS stimuli, especially when compared to neurons in the V1 of the tree shrew (Tanabe et al., 2022). We posit via modeling that this may be due to differences in cortical connectivity between the mouse and the tree shrew; the tree shrew's visual system and brain organization greatly resembles other primate brains, and this very well may also be true of its V1 at the microcircuit level.

1.2.2 Mechanisms for disparity selectivity

One major question that arose following the discovery of disparity selective neurons was exactly how these neurons were selective for disparities in the first place. For many a given neuron, the distance of the disparity between the stimuli that triggered the neuron's highest response rate was within the confines of the receptive field in either eye. How were neurons encoding disparity in the inputs from these receptive fields?

A widely acknowledged solution to this problem comes in the form of the disparity energy model, which describes an elegant computational process by which offsets in spatial structure in turn produces a phase difference between the receptive fields of the two eyes. The phase difference between the receptive fields is what allows for the disparity selective properties of a binocular neuron.

1.2.2.1 Introduction to the disparity energy model

According to the disparity energy model, disparity selectivity arises from the feedforward interaction of monocular inputs to a V1 binocular cell (**Figure 1.10A-C**). Recall that in the Hubel and Wiesel feedforward model, the LGN receptive fields were largely identical, and it was their sequential spatial arrangement that determines what orientation of stimulus triggers the biggest response. In the disparity energy model, the monocularly receptive fields may differ in terms of spatial arrangement or receptive field shapes, resulting in a phase shift where the ON and OFF zones of the receptive fields are in and out of phase with each other

(Ohzawa and Freeman, 1986, 1986; DeAngelis et al., 1991; Anzai et al., 1997; Ohzawa et al., 1997).

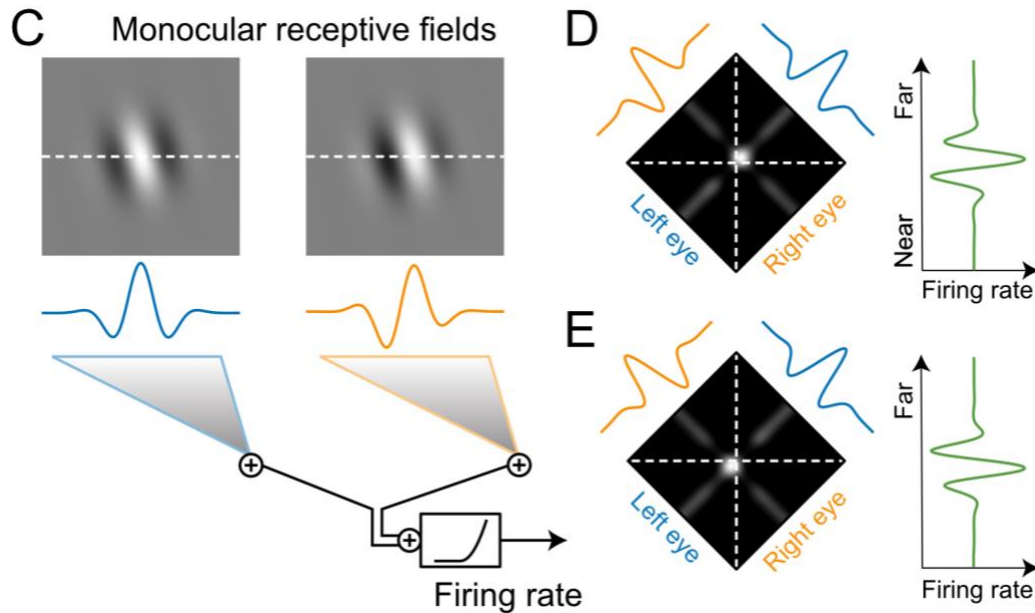


Figure 1.10. Disparity energy model. Signals received through monocular receptive fields are linearly combined, then passed through an output nonlinearity to produce a disparity selective output. The disparity energy model predicts different responses based on the overlap between different receptive field arrangements. A small shift in the structure of one monocular receptive field can result in the preferred disparity changing by several degrees, as shown in the bright “hotspots”. Adapted from (Cang et al., 2023)

When stimuli are shown to both eyes and the inputs are combined at a binocular V1 neuron, the output nonlinearity combines with the offsets between the receptive fields together give rise to binocular disparity selectivity (**Figure 1.10D-E**). Only a narrow selection of binocular stimuli can match the idiosyncrasies of monocular receptive fields and trigger binocular cell firing. In this way, though the receptive fields through neither the left nor right eyes seem selective enough to distinguish between minute differences in spatial positioning of otherwise identical stimuli that indicate depth, the combination of the two monocular receptive fields achieves that specificity.

The disparity energy model posits that the disparity selectivity of a neuron can be predicted if its receptive field structure. Logically, it follows that if the presence of offset binocular receptive fields is sufficient to compute the products of binocular integration, the weights of the inputs, i.e. ocular dominance, would not contribute to disparity selectivity. Accordingly, multiple studies have shown that the ocular dominance of a neuron does not correlate to its disparity selectivity.

1.2.2.2 Gaps in the disparity energy model

The disparity energy model has been hugely influential in visual neuroscience and has inspired computational models for other visual functions such as face recognition, depth perception in motion, and more. However, the disparity energy model is similar to other feedforward models in that it has oversimplified some aspects of binocular circuit dynamics.

One of the most significant gaps is that the disparity energy model is a purely feedforward model, and does not incorporate any potential inputs from inhibitory neurons that would be present in intracortical feedback within V1 itself. However, our results and other studies indicate that inhibitory inputs are crucial to generating disparity selectivity, and differences in connectivity can result in vast differences between visual responses between different animal models (See Section 4.4.1 for further discussion).

The disparity energy model also does not include inputs coming from other visual input cues that would influence depth perception. Updated versions of the disparity energy model by other research groups incorporate aspects such as luminance in order to more closely model how disparity selective neurons would respond to real-world conditions (Chen et al., 2021). That being said, the principles of the disparity energy model have been successfully applied in applications of computer vision using simulated neurons, showing its viability as a general explanation for mechanisms underlying binocularity (Martins et al., 2011, 2018).

1.3 *Development of the visual system*

The development of the visual system is an intricate process of growth followed by refinement. In the earliest stages, axon guidance cues lead retinal projections to terminate at the correct targets in order to form an organized retinotopic map. Spontaneous retinal waves propagate through the immature visual system, guiding the establishment of proper connections. Later, visual experience during the critical period then serves to stabilize or alter these connections, and determine which synapses should be kept and strengthened, and which should be pruned.

1.3.1 *General overview of embryonic visual development*

The visual system, along with all nervous tissues, arise from the ectoderm layer of the developing vertebrate embryo. After the neural tube forms, the rostral end differentiates into tissues that eventually form the brain, starting with primary brain vesicles. The prosencephalon, or forebrain, is the most rostral of these vesicles, and in turn will split into the diencephalon and the telencephalon, later cerebrum. From the diencephalon, two buds grow laterally and develop into the optic cups, which give rise to the retina.

1.3.1.1 *Formation of the optic chiasm*

After retinal ganglion cells differentiate in the inner retina, their cell bodies migrate outwards, while their axons grow back towards the thalamus via the optic stalks, which will eventually develop into the optic nerves. At the growing diencephalon, RGC axons form the optic chiasm, an important step in the development of binocular wiring.

Axons from the dorsal region of the central retina are the first to enter what will become the optic chiasm, at embryonic day 12. A complex of radial glial cells, along with other membrane-bound proteins with immunological and structural functions, induce the axons to cross over the midline and form the optic chiasm (Soares and Mason, 2015). Axons that bypass this glial cell complex do not cross over, and instead form the ipsilaterally projecting neurons

that synapse into their own region of dLGN. Tracing studies have indicated that this initial batch of ipsilateral-projecting axons is eventually pruned, but not before providing a path for follower axons to also project ipsilaterally.

1.3.1.2 Retinotopic map wiring

When RGC projections first begin to make connections to neurons in the SC and LGN, they must gradually refine the synapses formed until an accurate retinotopic map is formed. At the cellular level, signaling from axon guidance molecules binding to their respective receptors provides a local framework for developing neurons to migrate to the correct targets. In the visual system, if axon guidance cues such as ephrins are knocked out, retinotopic maps in crucial structures such as V1 are then formed incorrectly (Feldheim et al., 2000, 2004; Cang et al., 2005). Similar to other brain structures in development, a gradient of ephrin expression along the dorsal-ventral axis indicates the spatial organization of individual axons seeking out their designated termination zones. Aside from ephrins, Wnt/ryk gradients are also present in the retinal D-V axis, and disruption of these gradients leads again to incorrect retinotopic map development (Hindges et al., 2002).

Besides molecular cues, spontaneous neuronal activity during development are also major players in early circuit wiring. The spontaneous waves propagating retinal ganglion cells are divided into three stages, ordered based on the time they emerge. In mice, stage I and II waves begin firing prior to birth and around the time of birth, respectively, and are driven by acetylcholine signaling (Bansal et al., 2000). Stage II waves fire infrequently and propagate across the retina, and so assist in wiring retinotopic maps between RGCs and corresponding neurons at structures further up the visual pathway (Butts, 2002). When spontaneous activity from the retina is blocked, neurons still form connections, but their axonal arbors become large and diffuse, indicating a lack of spatial specificity in synapse stabilization; this has been observed in both retinogeniculate (retina to LGN) and retinocollicular (retina to superior colliculus) synapses (Grubb et al., 2003; McLaughlin et al., 2003). Finally, spontaneous activity is not limited to originating from the retina; early spindle bursts in the cortex are correlated with

stage II retinal waves from the contralateral eye (Ackman et al., 2012), while later spindle bursts can be triggered by stimulating the contralateral eye with light (Hanganu et al., 2006).

Stage III waves begin firing around postnatal days 10-12, a few days prior to eye opening. These waves are driven by glutamate signaling, and partly due to differences in firing rate, RGCs of similar signs tend to fire as clusters, as in ON-ON RGCs fire together, and OFF-OFF RGCs fire together (Stacy et al., 2005). This information is conveyed up the visual pathway and helps differentiate inputs from different populations of RGCs.

1.3.2 Experience-dependent visual development

Mice open their eyes around 14 days after birth, overlapping with the aforementioned stage III retinal waves. From this point onwards, activity in the visual system becomes gradually reflective of the surrounding environment, and outcomes can vary greatly depending on the quality of that environment.

1.3.2.1 Monocular deprivation and ocular dominance studies

In order to understand how something works, one can start by taking it apart. That is essentially the approach used by Hubel and Wiesel in their landmark experiments using monocular deprivation to induce alterations of ocular dominance in kittens (Wiesel and Hubel, 1963a). Experimental young animals had one eyelid sutured shut for several weeks, starting around the time of eye opening. After the sutures were removed, V1 neurons were less responsive when stimulated through the formerly sutured eye, indicating that a lack of visual experience through that particular eye led to a shift in ocular dominance toward the consistently stimulated eye. This was not seen when the animals were older when the eyelid was sutured. These experiments demonstrated the existence of experience-dependent plasticity during a critical period of development, as Hubel and Wiesel demonstrated that ocular dominance in the visual cortex was malleable, but only during a brief window of time. Subsequent studies into the neuronal circuitry behind experience-dependent plasticity have

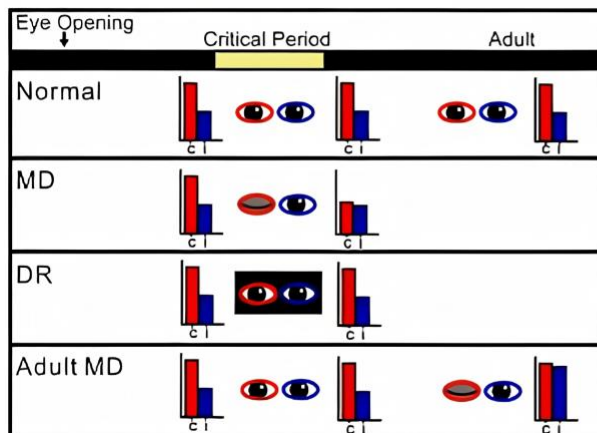
illuminated the cellular mechanisms and increased detail of the parameters of the critical period.

1.3.2.2 Studying interocular matching in naturalistic developmental conditions

Interocular matching is another, but more physiologically relevant, experience-dependent process where, over the course of the critical period, V1 neurons change from having different orientation preferences through the two eyes to having matched orientation preferences.

Like ocular dominance, interocular matching is malleable by differences in visual experience during the critical period. However, if a wild-type animal undergoes normal development, the ratio of contralateral-to-ipsilateral input representation in the cortex does not change significantly. It can be shifted to different ratios if visual experience is altered during the critical period, but these are the result of experimental intervention and fall outside the course of normal development.

A Ocular dominance plasticity



B Binocular matching

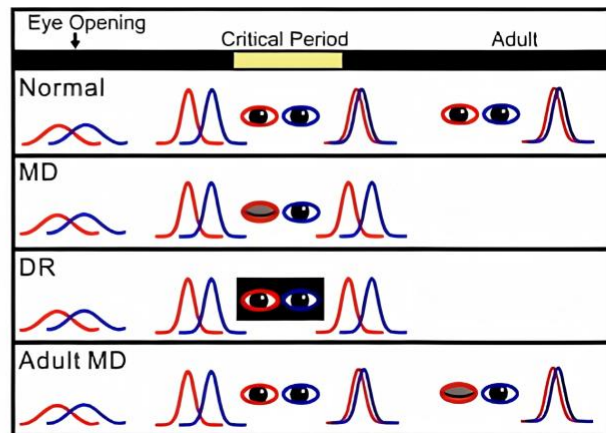


Figure 1.11. Ocular dominance versus binocular matching. Ocular dominance (left) does not change under normal developmental conditions, but can be manipulated with monocular deprivation or dark rearing. Interocular matching (right) matures during normal development, but is halted if visual experience is disrupted through MD or DR.

In interocular matching, however, neurons start mismatched before the onset of the critical period, and become matched by the end of the critical period (Wang et al., 2010a, 2013). For interocular matching, the change from mismatched to matched is essential to the process of normal visual development (**Figure 1.11**). The mismatch of orientation preferences prior to eye opening was significant, a mean difference of about 35 degrees – e.g., if the contralateral eye stimulus that evokes the most spikes for a certain cell was a horizontal bar (0 degrees), the ipsilateral eye stimulus for that same cell would be a bar tilted at an angle of 35 degrees. This difference shrank to about 18 degrees by P22, showing that mere days of visual experience was enough to induce a significant change in the interocular matching of binocular cells (Wang et al., 2013).

These observed values for mismatched orientation preference were obtained by obtaining the preferred orientation for each eye by stimulating them separately, and then calculating an orientation selectivity index from the two values. It has since been reported that in ferrets, showing binocular stimuli to animals in the critical period reveals another, third preferred orientation, that differs from the preferred orientations through the contralateral and ipsilateral eyes. Moreover, the binocular preferred orientation at eye opening, i.e., the start of the critical period, seemed to be the most “influential” on the preferred orientation measured monocularly (Chang et al., 2020).

In mice, it has been reported that neurons in the binocular zone shift between responding solely to monocular input to responding to binocular input, and vice versa, during the critical period, and also that convergence of interocular matching observed in layer 2/3 neurons does not correlate with the orientation preferences in binocular layer 4 neurons (Tan et al., 2020). Unlike the study done by Chang et al., however, a cell that responded to “binocular input” in this paper was defined as a cell that fired in response to both right and left eye monocular stimuli, whereas a true binocular stimulus would be delivered to both eyes simultaneously. This study also measured orientation preference at P22, P29, and P36, and our previous studies have shown that orientation preference is already significantly developed by P22.

1.3.2.3 *Disparity selectivity and visual experience*

While ocular dominance is useful for probing mechanisms involved in critical period plasticity, and interocular matching is reflective of biological changes that should happen in a normal critical period, neither truly characterize the development of binocular vision, especially the process of stereopsis. Both ocular dominance and interocular matching are assessments of how inputs from each individual eye are represented in the visual cortex, and in order to capture this, the eyes are probed independently using monocular stimuli.

There is a noticeable dearth of literature on binocular disparity selectivity during development. Whether owing to the animal models used in earlier disparity selectivity studies – primarily cats and primates, which are not as prevalent in developmental neuroscience literature as rodent animal models – or greater interest in the computations mechanisms that contribute to disparity selectivity as opposed to the developmental processes, the fact is that the majority of disparity selectivity studies were performed using adult animals.

In monkeys, partial monocular deprivation – as in, animals were allowed intermittent binocular vision every day, no significant shifts in ocular dominance or contrast sensitivity were reported, but disparity selectivity still declined (Sakai et al., 2006). Similar results were reported in cats, using monocular deprivation (Vorobyov et al., 2007) and surgically-induced strabismus (Scholl et al., 2013b).

In a study using monocular deprivation to study disparity selectivity in mice, the authors reported that four days of monocular deprivation, initiated around P28-30, decreased their disparity selectivity (Scholl et al., 2017). It is interesting to note that the time window in which monocular deprivation was induced is later in this paper than those used in previously discussed interocular matching papers. In fact, the authors compared disparity selectivity measured at P25, which they termed “pre-critical period” to nondeprived animals at P30, and found no significant differences. They used this evidence to validate that the decline in disparity selectivity they observed was due solely to decreased visual experience during the critical period.

In summary, the visual system's structures and circuit-level mechanisms have adapted in a multitude of ways to extract information from binocular inputs and make use of them in order to eventually perceive depth. During development, neural activity is necessary for shaping and refining these exquisite circuits. In the following chapters, I will describe my findings from characterization studies of binocular neurons in both the adult and developing mouse primary visual cortex.

2 Binocularity in adult mouse V1

The contents of this chapter were published as “Widespread and multifaceted binocular integration in the mouse primary visual cortex.” Jieming Fu, Seiji Tanabe, Jianhua Cang. *Journal of Neuroscience* [Published Aug 21 2023].

Jieming Fu^{1,2,*}, Seiji Tanabe^{3,*}, and Jianhua Cang^{2,3}

1. Neuroscience Graduate Program 2. Department of Biology; 3. Department of Psychology

University of Virginia, Charlottesville, VA 22904, USA

*. These authors contributed equally to this work.

Correspondence and requests for materials should be addressed to Jianhua Cang, cang@virginia.edu

Abbreviated title: Binocular integration in mouse V1.

Number of figures and tables: 8 figures.

Number of pages: 41.

Number of words: Abstract: 187; Introduction: 649; Discussion: 1647.

Conflict of Interest: The authors declare no competing financial interests.

Acknowledgements:

We thank Sotiris Masmanidis at UCLA for supplying the multielectrode silicon probes. This work was supported by US National Institutes of Health (NIH) grants (EY026286 and EY020950) and Jefferson Scholars Foundation to J.C.

2.1 *Abstract*

The brain combines 2-dimensional images received from the two eyes to form a percept of 3-dimensional surroundings. This process of binocular integration in the primary visual cortex (V1) serves as a useful model for studying how neural circuits generate emergent properties from multiple input signals. Here, we perform a thorough characterization of binocular integration using electrophysiological recordings in the V1 of awake adult male and female mice, by systematically varying the orientation and phase disparity of monocular and binocular stimuli. We reveal widespread binocular integration in mouse V1 and demonstrate that the three commonly studied binocular properties – ocular dominance, interocular matching, and disparity selectivity – are independent from each other. For individual neurons, the responses to monocular stimulation can predict the average amplitude of binocular response, but not its selectivity. Finally, the extensive and independent binocular integration of monocular inputs is seen across cortical layers, in both regular-spiking and fast-spiking neurons, regardless of stimulus design. Our data indicate that the current model of simple feedforward convergence is inadequate to account for binocular integration in mouse V1, thus suggesting an indispensable role played by intracortical circuits in binocular computation.

2.2 *Significance Statement*

Binocular integration is an important step of visual processing that takes place in the visual cortex. Studying the process by which V1 neurons become selective for certain binocular disparities is informative about how neural circuits integrate multiple information streams at a more general level. Here, we systematically characterize binocular integration in mice. Our data demonstrate more widespread and complex binocular integration in mouse V1 than previously reported. Binocular responses cannot be explained by a simple convergence of monocular responses, contrary to the prevailing model of binocular integration. These findings thus indicate that intracortical circuits must be involved in the exquisite computation of binocular disparity, which would endow brain circuits with the plasticity needed for binocular development and processing.

2.3 Introduction

Neural circuits in the visual system combine inputs from the two eyes and transform them into signals that are then utilized to guide animal behavior. In humans, the process of binocular integration is key to stereoscopic vision, as it uses the small difference between the two retinal images (i.e., binocular disparity) to encode depth (Cumming and DeAngelis, 2001). More generally, early stages of binocular integration are an excellent model for studying how neural circuits combine multiple streams of signals into one and generate useful emergent properties for subsequent processing.

The prevailing view of binocular integration came from a series of studies done in the cat primary visual cortex (V1), which led to the “disparity energy model” (Ohzawa et al., 1990, 1996, 1997). In cats, binocular convergence occurs downstream of V1 layer 4. Convergence of the feedforward geniculocortical projections creates oriented receptive fields (RFs) in layer 4 neurons (Hubel and Wiesel, 1962; Priebe and Ferster, 2012), which, according to the disparity energy model, are then combined to generate selectivity for binocular disparity. Specifically, the model posits that the two monocular RFs have different degrees of spatial offset, and only specific disparities that match this offset would cause the neuron to discharge due to spiking threshold. Although this model has been successful in explaining many experimental observations in cat and monkey V1 (Cumming and Parker, 1997; Prince et al., 2002; Tsao et al., 2003; Anzai et al., 1999), it is important to note that it is purely feedforward and only considers excitatory connections.

The mouse has been a useful model in binocular vision studies, especially for ocular dominance (Espinosa and Stryker, 2012), a measure of relative response magnitude of individual V1 neurons through the two eyes. Studies have also investigated how V1 neurons match their orientation preference through the two eyes, which is driven by visual experience during a critical period in early life (Wang et al., 2010a, 2013; Gu and Cang, 2016). A few recent studies reported large proportions of “monocular” neurons in the binocular zone of mouse V1 (Salinas et al., 2017; Huh et al., 2019; Jenks and Shepherd, 2020; Tan et al., 2020, 2021),

inconsistent with the results of many previous studies (Gordon and Stryker, 1996; McGee et al., 2005; Mrsic-Flogel et al., 2007; Kameyama et al., 2010). This discrepancy could be due to technical differences, but also highlights the potential confusion caused by the classification of “monocular” and “binocular” neurons in studies where the two eyes were never stimulated simultaneously (Cang et al., 2023). The nomenclature “monocular” implies a specific wiring pattern, whereas in fact it refers to a neuronal property measured at the level of spikes. Indeed, studies in a number of species, including mice, indicate that ocular dominance is not directly related to having selectivity to binocular disparity (LeVay and Voigt, 1988; Read and Cumming, 2004; Kara and Boyd, 2009; Scholl et al., 2013a; Chioma et al., 2020). However, how V1 neurons transform monocular inputs into binocular responses in mice has not been systematically studied.

Here, we set out to study binocular integration in mouse V1 by interleaving monocular and binocular stimulations using dichoptic presentation. We found that mouse V1 neurons heavily dominated by one eye or having mismatched orientation preference were just as likely to be tuned to phase disparity as neurons with more balanced activation or matched preference through both eyes. Consequently, almost all neurons in the V1 binocular zone showed evidence of binocular integration. In addition, for individual neurons, monocular responses were poorly associated with responses to binocular stimulation. Since a simple feedforward model would dictate that any binocular response was the result of converging monocular inputs, this decoupling of monocular and binocular responses indicates that binocular integration is unlikely to be explained by feedforward mechanisms alone. Rather, intracortical circuits must play a major role in binocular integration. This mechanism may provide visual circuits with the plasticity they need for binocular processing.

2.4 *Materials and Methods*

2.4.1 *Animals*

Male and female C57BL6 mice (n=28; 16M & 12F) beyond 8 weeks of age (63-117 days) were used for all experiments. All animals were approved by the Institution for Animal Care and Use Committee at the University of Virginia.

2.4.2 *Surgery*

Mice were placed under isoflurane anesthesia (5% for induction, 2% for maintenance, in O₂, ~0.5 L/min, VetFlo, Kent Scientific) for implantation of a custom-designed titanium headplate to immobilize the head during recordings. Atropine (0.3 mg/kg in 10% saline) and dexamethasone (2.0 mg/kg in 10% saline) were administered subcutaneously, and the core body temperature was monitored and maintained at 37°C (Frederick Haer Company) for the duration of surgery. Artificial tears (Henry Shein Medical) were administered to prevent drying and injury to the corneas. The mouse's head was held in place using a stereotaxic frame equipped with ear bars (Kopf Instruments), after which the scalp was resected to expose a portion of the occipital skull centered over binocular V1, and subsequently the headplate was adhered using Metabond (Parkell). Mice were placed on a heating pad to recover from isoflurane until bright, alert, and responsive, after which they were returned to their home cages. Post-operative monitoring continued for 4 days.

2.4.3 *Habituation*

Following headplate surgery, mice were habituated to the electrophysiological recording rig for at least 4 days prior to recording. Mice were head-fixed to a post that allowed them to run on a cylindrical Styrofoam wheel (6 in diameter) that could freely rotate around its axis. Each habituation session lasted for 30 minutes, and mice were limited to 1 session per day. Recording proceeded once mice displayed no signs of distress or agitation while on the running wheel.

2.4.4 *Physiological recording*

At least 12 hours prior to recording, a craniotomy was performed while the mouse was placed under isoflurane anesthesia. The craniotomy was positioned above the left visual cortex (~2.0 mm diameter, ~3.15 mm lateral & ~0.5 mm anterior from lambda; **Figure 2.1B**). The craniotomy was covered with agarose (2.5%) and Quik-Cast silicone epoxy (World Precision Instruments), which was removed immediately prior to recording.

Mice were head-fixed and allowed to run freely on the running wheel for the duration of recording. A silicone multielectrode probe (64M, 64D, or 128AxN models, Masmanidis Lab, UCLA) (Yang et al., 2020) was attached to an data acquisition system (RHD 128-Channel Headstage, Intan Technologies) to record electrophysiological signals during visual stimulation. The probe was centered over the craniotomy, and following penetration into the cortex, the area was covered with agarose (2.5%), into which a reference wire was immersed. The probe was advanced until the tip channels were embedded in white matter. Analog voltage signals were digitized at a 20 kHz sampling rate (RHD Evaluation System, Intan Technologies), and the timing of visual stimulation condition changes were recorded with transistor-to-transistor (TTL) pulses simultaneously with voltage signals, to enable later offline synchronization for analysis.

After the recording session ended, the probe was retracted, the craniotomy was covered with agarose and Quik-Cast, and animals were returned to their home cages. Recording continued on consecutive days until the recording area showed visible signs of damage, after which animals were euthanized according to IACUC protocols.

Spikes in the voltage time series were sorted into separate units using MountainSort (Chung et al., 2017). The spike waveform of each detected spike-like event was projected onto a 1D feature space. The spike-sorting algorithm comprises a series of nonparametric statistical tests for unimodality. Noise overlap is the fraction of “noise events” in a cluster, i.e., spike-like events not associated with this or any of the other clusters. Spike clusters were considered

single units if they passed criteria for noise overlap (<0.08), indicating that spike waveforms were distinguishable from randomly sampled noise waveforms, and isolation (>0.96), indicating that spike waveforms were distinguishable from clusters of other spike clusters in feature space (**Figure 2.1C, D**). Single units were then retained for further analysis.

2.4.5 Visual stimulation

Visual stimuli were generated in MATLAB using the Psychophysics Toolbox package (RRID: CDR_002881) (Kleiner et al., 2007). Stimuli were shown to mice using a combined projector and polarization modulator system, as described previously (Tanabe et al., 2022). Briefly, the graphics processor (AMD Radeon Pro WX 7100) generated left-eye and right-eye images on the top and bottom half of every video frame, respectively. The projector (Optoma HD27HDR) then displayed the two halves in interleaved video frames at 120 Hz, so that frames intended to be viewed by the left and right eyes were shown in alternating sequence. The left eye and right eye received the images asynchronously, with the left eye preceding by 8.3 ms. These frames were then filtered through a polarization modulator (DepthQ Passive Bundle) and projected onto a polarization-preserving screen (Stewart Film RP 150). Animals viewed the stimulus frames through passive polarization filters that were mounted in 3D-printed frames and secured to the head-fixing post to maintain a constant position in front of the animal's eyes. The passive filters allowed the animal to view left-eye-intended frames only with the left eye, and vice versa for the right eye (**Figure 2.1A**), and each eye received stimulation at 60 Hz. Gamma correction was applied for a linear transformation from grayscale values to luminance (range 6 to 87 cd/m^2), and crosstalk with this system was measured with a photometer to be 1.9%. A custom 3D printed shield was used to prevent light from the projector from generating photoelectric artifacts in the physiological recording data. The viewing distance from the mouse to the projector screen was 25cm, consistent with previous mouse studies (Samonds et al., 2019).

The visual stimulus was centered over the estimated receptive field (RF) locations of the neuronal population being recorded. In order to map the RF, we used either a contrast-

reversing bar on a gray background, or a flashing bright bar on a dark background. RFs needed to be within 20 degrees of the contralateral visual field from the vertical meridian on the horizontal axis, and within the stimulus screen along the vertical axis. If the RF was not located within these boundaries, the probe was retracted and reinserted in a location closer to the retinotopic center of the visual field. After 3 to 4 neurons had their RFs mapped with sufficient confidence, the average position of the RF centers was used as the visual stimulus center position.

We used a contrast-reversing checkerboard pattern (reversal rate 0.5 Hz, $10^\circ \times 10^\circ$) presented to both eyes to estimate the depth of the electrode contacts relative to the cortical layers. The checkerboard patch was centered at the average position of the previously mapped RFs and covered an area of $50^\circ \times 50^\circ$.

Drifting sinusoidal gratings were used to assess the orientation and disparity tuning of V1 neurons. Gratings were presented in a circular patch (radius 30°) that was centered over the average of the previously mapped RFs. Disparity in binocular gratings was generated by shifting the phase of the sinusoid seen by the right eye, and referred to as phase disparity. The orientation of binocular gratings ranged from 0° (vertical orientation, drifting rightward) to 157.5° , in 22.5° counterclockwise steps. The full range of phase disparity from 0° to 360° , in 45° steps, was tested for each orientation of the grating. The stimulus set also included monocular gratings for the left and right eyes, at the orientations specified above, and a control condition in which both eyes were shown a gray screen, for a total of 81 conditions. Stimulus conditions were presented in a pseudorandom order, where every condition was presented at least once before any condition was repeated, and recording continued until each stimulus had been repeated at least 10 times. Each trial consisted of a stimulus-on duration of 1 s, followed by an inter-stimulus interval of 0.5 s. The spatial frequency and temporal frequency of gratings were fixed at 0.04 cycles/degree and 2 Hz, respectively, and gratings were presented with full contrast.

2.4.6 Data analysis

Spike timing was aligned with the onset timing of the stimulus. Tuning functions were then constructed by calculating the firing rate during the response window for each stimulus condition. The response time window was set to be 60 ms delayed to the stimulation.

Tuning functions generated from the responses to monocular grating stimuli were used to calculate the ocular dominance index (ODI) and quantify the degree of interocular mismatch of orientation preference (ΔO) of a cell. We calculated the trial-averaged firing rate for each condition, and generated two orientation tuning functions, one for monocular stimulation of the contralateral eye r_i^C , and one for the ipsilateral eye r_i^I , where the subscript i denotes the i -th orientation. The response to the blank condition, r_0 , was subtracted from the r_i^C and r_i^I , and values after subtraction were truncated at zero to avoid negative firing rates.

In order to calculate ODI, the peak of the tuning function associated with the contralateral eye was estimated using the zeroth- and first-order harmonics of orientation tuning:

$$a^C = \frac{1}{m} \sum_{i=1}^m r_i^C + \frac{1}{m} \left| \sum_{i=1}^m r_i^C e^{j2\theta_i} \right|$$

where j is the imaginary number, m is the number of orientation conditions, and θ_i is the orientation in units of radians. The same formula was used to calculate the a^I associated with the ipsilateral eye. The ODI was then calculated by comparing the peak between the contralateral and ipsilateral eyes, and normalizing the output to a value between -1 and 1:

$$ODI = \frac{a^C - a^I}{a^C + a^I}$$

For comparisons involving the strength of orientation tuning, a global orientation selectivity index (gOSI) was calculated by taking the ratio between the amplitudes of the zeroth- and first-order harmonics of the orientation tuning (Mazurek et al., 2014):

$$\text{gOSI} = \frac{|\sum_{i=1}^m r_i^C e^{j2\theta_i}|}{\sum_{i=1}^m r_i^C}$$

The angle of the vector sum $\text{Arg}(\sum_{i=1}^m r_i^C e^{j2\theta_i})/2$ was the estimated preferred orientation for the contralateral eye stimulation. Taking the absolute difference of the preferred orientations through the contralateral and ipsilateral eyes yielded ΔO .

The strength of disparity tuning in response to binocular gratings was quantified using the phase disparity selectivity index (PDSI). To calculate PDSI, we used the same method as described above to calculate the zeroth- and the first-order harmonics. The array of binocular conditions in our experimental design resulted in multiple phase disparity tunings r_i^B , one for each orientation. The PDSI was then calculated as the ratio between zeroth- and first-order harmonics of the phase disparity tuning r_i^B (Scholl et al., 2013a):

$$\text{PDSI} = \frac{|\sum_{i=1}^k r_i^B e^{j\varphi_i}|}{\sum_{i=1}^k r_i^B}$$

where k was the number of phase disparity tested, and φ_i was the i -th phase disparity. To assign a single PDSI value to a cell, we selected the PDSI from all the orientations that had the largest modulation amplitude of the first harmonic.

The recorded neuronal population was also classified into putative fast-spiking (FS) inhibitory neurons versus regular-spiking neurons. A well-characterized feature of FS neurons is that their spike waveforms are narrow, specifically that their voltage polarity can switch in less than 0.2 ms (Bruno and Simons, 2002; Atencio and Schreiner, 2008). In order to differentiate between these two types of cells, we calculated the slope of the waveform at a time window where fast-spiking cells would have completed a polarity switch already, while regular-spiking cells would have not (Niell and Stryker, 2008). For this analysis, we took the spike template from the channel with the largest amplitude and extracted 3 time samples, centered at 0.5 ms after the negative peak. A linear regression of these 3 voltage values was used to approximate the slope of the waveform around those timepoints.

The local-field potential (LFP) was the extracellular voltage time series bandpass filtered between 1 – 120 Hz (2nd-order Butterworth filter). The LFP was trial-averaged across all contrast reversals of the checkerboard pattern. Strong negative sinks typically occurred in a limited range of depth. We estimated the deepest point of the sink using spline interpolation and used that as the center of layer 4 of V1. If necessary, the probe depth was then adjusted so that the tip penetrated about 250-300 μm deeper into the cortex, in order to span all cortical layers. The current-source density was used to verify the existence of a sink (Mitzdorf, 1985). We then subtracted this depth from the position of the electrode contact on the microprobe where each neuron's spikes were detected. This was the relative depth of each neuron with respect to layer 4.

2.4.7 Statistics

Neurons in this study were determined to be visually responsive if they passed a bootstrapped permutation test (Siegle et al., 2021), where based on their firing patterns, we were able to reject the null hypothesis that firing rate during visual stimulation was indistinguishable from the firing rate in response to a blank stimulus condition. Deviation from the null hypothesis of the original observed data was quantified using the chi-square value:

$$\chi^2 = \frac{\sum_i (r_i - r_0)^2}{r_0}$$

In this equation, r_i and r_0 represent the trial-average firing rates of the i -th stimulus condition and the blank condition, respectively. Random permutation was used to estimate the null distribution of the chi-square value. The trial-to-trial firing rate, including the firing rate of the blank condition, was randomly permuted so that any association between the firing rate and any given stimulus condition was lost. This permuted data was then used to recalculate a null chi-square value, and this process was repeated 1000 times in order to generate a null chi-square value distribution. The 95th percentile of this null distribution was used as the cutoff for visual responsiveness – that is to say, only neurons that had an original chi-square value greater

than the 95th percentile of the randomly permuted distribution were considered significantly responsive to visual stimulation.

The MATLAB Statistics and Machine Learning Toolbox was used for all statistical tests. Spearman's partial rank correlation coefficient was used to quantify correlation between response indices. Hartigan's dip test was used to verify unimodality for distributions (Hartigan and Hartigan, 1985). The Mann-Whitney U test was used to compare data from different groups of cells. Further details on the number of cells and animals, as well as statistical tests used for specific comparisons, are provided in Results. We did not utilize statistical methods to predetermine sample sizes, and animals were not assigned to control or experimental groups because such considerations were inapplicable to the design of this characterization study.

2.5 Results

2.5.1 Systematic measurement of binocular response properties

To systematically measure the relationship between monocular and binocular responses of individual V1 neurons, we used a dichoptic display system to present drifting sinusoidal gratings of different orientations, either binocularly with specific phase disparity, or monocularly to either the ipsilateral or contralateral eye (**Figure 2.1A**). Neurons were recorded from all cortical layers of the binocular zone of V1, using a 64-channel silicon microprobe spanning the entire cortical depth (**Figure 2.1B, C, D**). Many neurons displayed response properties that were not expected from a simple convergence model. For example, the neuron in **Figure 2.1E** showed a complete dominance of the contralateral eye over the ipsilateral eye (**Figure 2.1E**; orange vs blue). A neuron with such a strong ocular dominance would be traditionally classified as monocular, and one would expect it to be insensitive to any stimulus to the ipsilateral eye. In striking contrast to this expectation, this neuron was in fact tuned to the phase disparity of the binocular gratings. At the preferred orientation (90°), this neuron was most responsive when the gratings in the two eyes were opposite in phase (i.e., a phase disparity of 180°) and the response was reduced at other disparities (black curve). The tuning to phase disparity is unequivocal evidence that this neuron, despite its strong ocular dominance, integrates signals originating in the two eyes. In other words, binocular integration in mouse V1 does not necessarily produce a simple combination of monocular signals, thus highlighting the need for a careful characterization using well-designed stimulus sets.

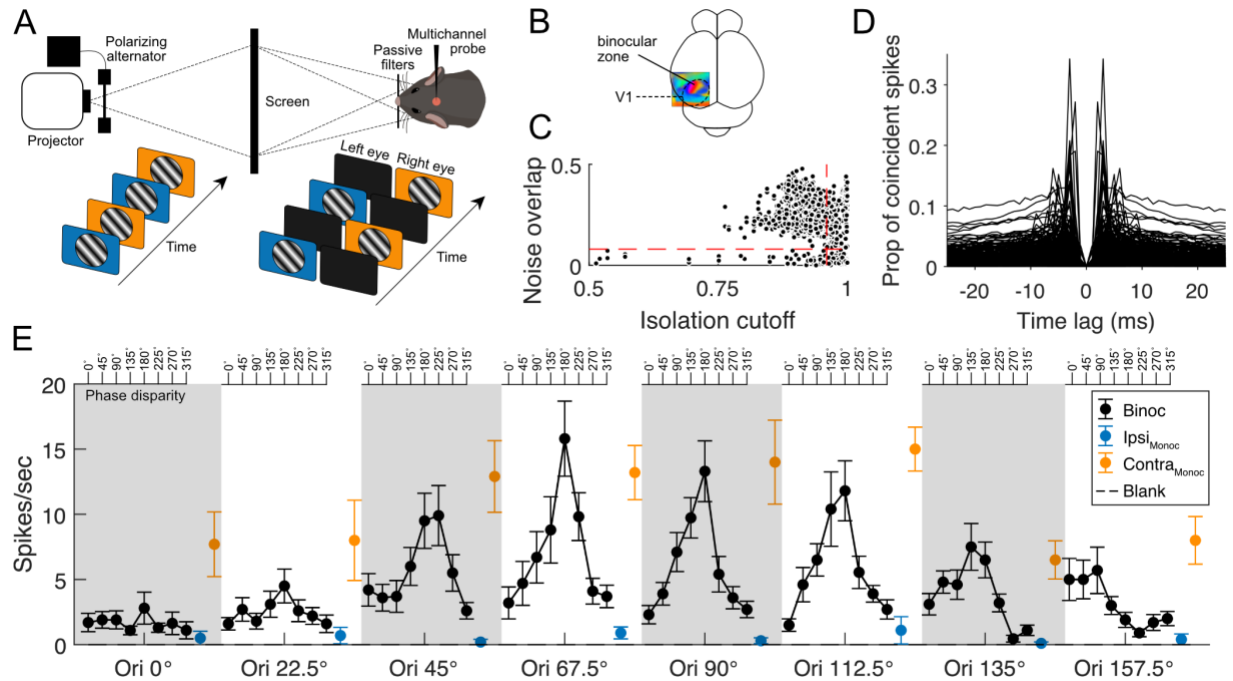


Figure 2.1. Methods and example tuning curves.

- A. Schematic diagram of dichoptic stimulus system. *Bottom left*: Stimulus frames for the left and right eyes were interleaved (120 frames/sec) and the alternating frames had different polarities after passing a polarizing modulator. *Bottom right*: The animal viewed the projected images through a pair of passive polarization filters such that each eye only viewed alternating frames that had a matching polarization.
- B. Intrinsic signal imaging was used to identify the V1 binocular zone. The azimuthal visual field through the ipsilateral eye is represented in color (central-peripheral: blue-red).
- C. Spike sorting into single units. Spike-waveforms that were considered for further analysis as single units had to pass two criteria, noise overlap < 0.08 and isolation cutoff > 0.96 .
- D. Autocorrelograms of all single-unit spikes. Each line is an isolated single unit, and spike counts within each bin was divided by the total number of spikes of that unit. A clear dip around short delay times ($\tau < 2$ ms) is present.
- E. Example tuning curves from a phase disparity selective neuron. Binocular stimuli were shown at 8 orientations and 8 phase disparities, allowing for the generation of 8

disparity tuning curves (black), one per orientation. The responses to monocular stimulation are shown in orange (contralateral) and blue (ipsilateral).

Across the population of recorded neurons in V1 ($n = 594$, 13 mice), 47.5% ($n = 282$) showed significant responses to the stimulus set (see Methods for details of classifying responsiveness). There was a wide variety of ocular dominance, which we were able to quantify in neurons that responded significantly to monocular stimulation through the contralateral and/or ipsilateral eye ($n = 244$). Some neurons were comparably driven by stimulation through either eye (e.g., **Figure 2.2A**), whereas others were dominated by one eye, the contralateral eye in most cases (e.g., **Figure 2.2B**). The distribution of ocular dominance index (ODI) spanned the entire range of -1 and 1, with a small bias towards the contralateral eye (median = 0.12) (**Figure 2.2C**). For the subset of neurons that were significantly responsive to monocular stimulation through both eyes ($n = 136$), we estimated the preferred orientation associated with each eye and compared interocularly. Many neurons had similar orientation preferences between the two eyes (e.g., **Figure 2.2D**), whereas a minority had orientation preferences that were quite different (e.g., **Figure 2.2E**). We calculated the difference in the preferred orientation (ΔO) between the two eyes for each neuron. The population distribution of ΔO values had a peak near 0° with a skewed tail that tapered off at higher ΔO values (median = 27.4° ; **Figure 2.2F**), largely consistent with previous results in anesthetized mice (Wang et al., 2010a, 2013; Sarnaik et al., 2014; Gu and Cang, 2016; Levine et al., 2017). Also consistent with previous findings (Wang et al., 2010a; Levine et al., 2017), the degree of interocular matching depended on the strength of orientation tuning ($\rho = -0.435$, $p < 0.001$, between ΔO and the OSI of the non-dominant eye; **Figure 2.2J**), but not on the response amplitude ($\rho = -0.148$, $p = 0.092$, between ΔO and the peak amplitude of the non-dominant eye; **Figure 2.2K**); and the strength of orientation tuning was significantly matched interocularly ($\rho = 0.242$, $p < 0.01$; **Figure 2.2L**).

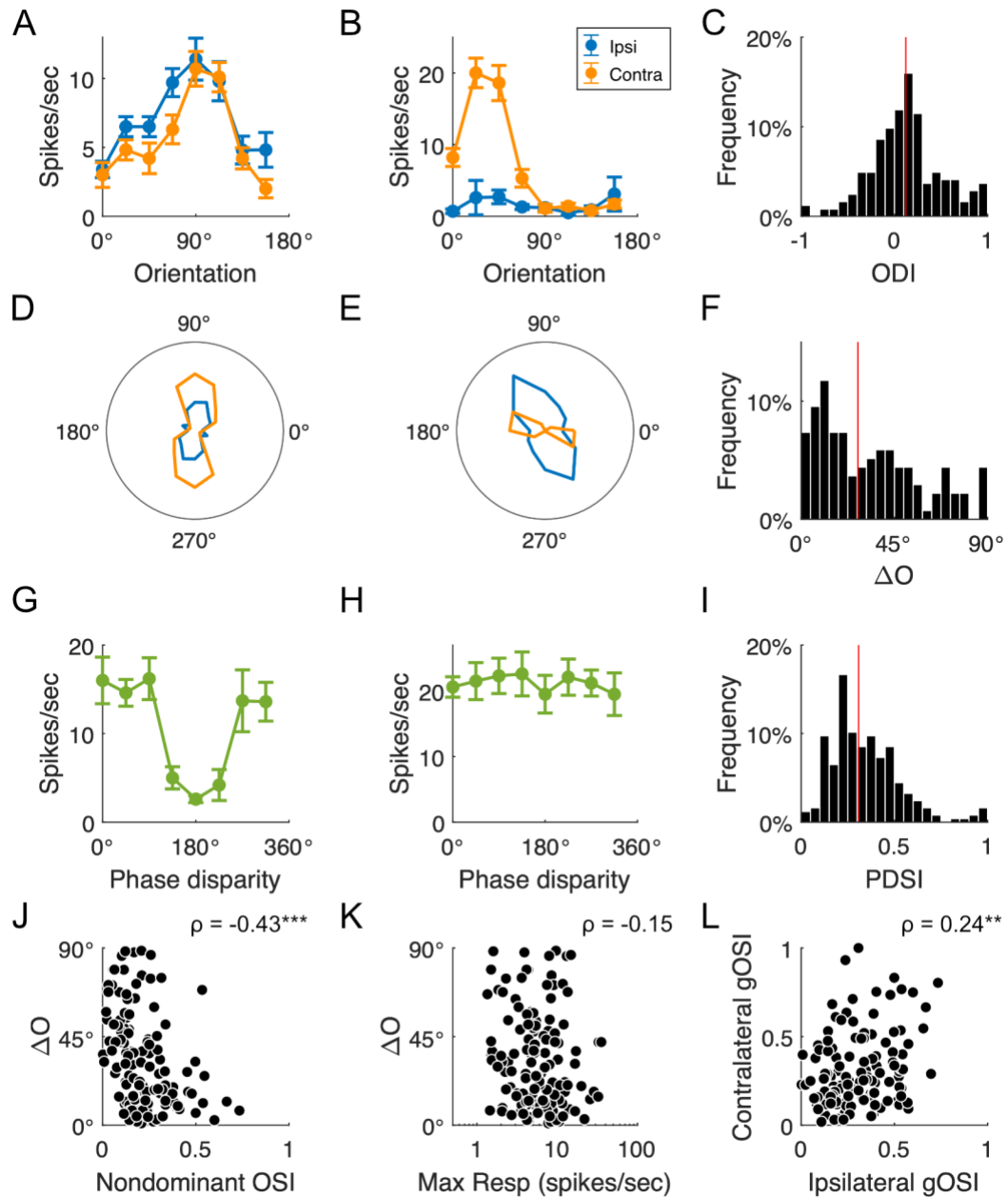


Figure 2.2. Quantification of V1 binocular response properties.

- A.** Example monocular orientation tuning curves. This neuron was balanced in its response to contralateral and ipsilateral stimulation (orange and blue, respectively; ODI -0.13).
- B.** Orientation tuning curves from a neuron that is dominated by contralateral stimulation (ODI 0.82).

- C. Histogram of ODI across the population (n=244). The population had a small bias toward the contralateral eye's dominance, with a median ODI of 0.12 (red vertical line).
- D. Example orientation tuning curves represented in polar coordinates. The angle and radial distance represent the stimulus orientation and response magnitude, respectively. The tuning curve was duplicated to complete the full range of angles. This neuron had matched orientation preference through the two eyes ($\Delta O = 4.5^\circ$).
- E. Example orientation tuning curves from a neuron mismatched in orientation preference through the two eyes ($\Delta O = 52.7^\circ$).
- F. Histogram of ΔO values across the population (n = 136), with a median of 27.4° (red vertical line).
- G. Example phase disparity tuning curve. This neuron was tuned to the phase disparity of the binocular grating (PDSI = 0.32).
- H. Example phase disparity tuning curve from a nonselective neuron (PDSI = 0.03).
- I. Histogram of PDSI values across the population (n = 246), with a median of 0.31 (red vertical line).
- J. ΔO was correlated with gOSI through the nondominant eye (Spearman correlation, $\rho(129) = -0.435$, $p < 0.001$).
- K. The magnitude of ΔO was not correlated with the peak spike rate in response to the non-dominant eye (Spearman correlation, $\rho(129) = -0.148$, $p = 0.09$).
- L. Correlation of gOSI through the two eyes (Spearman correlation, $\rho(129) = 0.242$, $p = 0.005$).

The characterization of ocular dominance and interocular matching of orientation preference is limited to responses to monocular stimulation. As illustrated in **Figure 2.1**, we also examined these neurons' responses to binocular stimulation of various disparities in the same recordings. Many neurons were tuned to the phase disparity of a binocular grating (e.g., **Figure 2.2G**). Others responded strongly to binocular gratings, without obvious tuning to the phase disparity (e.g., **Figure 2.2H**). We measured the strength of disparity tuning by calculating a phase disparity selectivity index (PDSI) for each orientation of the stimulus. We then chose the PDSI associated with the strongest modulation by phase disparity to represent the strength of disparity tuning. Most visually responsive neurons displayed significant phase disparity selectivity (median = 0.31; **Figure 2.2I**, $n = 246$; with $n = 148$, i.e., 60.2%, greater than 0.25, a level of high selectivity).

2.5.2 *Ocular dominance, interocular matching, and disparity selectivity are independent measures of binocular integration*

Binocular integration is often assumed to depend primarily on the convergence of feedforward monocular inputs representing the two eyes, which are the same projections that create orientation tuning. This assumption would lead to certain expectations of the relationship among ocular dominance, interocular matching, and disparity selectivity of individual V1 neurons. For example, neurons that receive balanced innervation from the two eyes may be more likely to have interocularly matched orientation preference and show strong disparity tuning. We found no evidence for such relationships. Neurons with balanced monocular responses (i.e., ODI near 0) could have very different values of ΔO and PDSI, ranging from mismatched to matched and from non-selective to highly selective (**Figure 2.3A and 2.3B**). On the other hand, neurons with strong ocular dominance (i.e., ODI near 1 or -1) could still be highly selective for phase disparity (**Figure 2.3C and 2.3D**). Across the population, there is no correlation between ODI and ΔO ($\rho = -0.010$; $p = 0.91$; **Figure 2.3E**), or between ODI and PDSI ($\rho = -0.110$; $p = 0.22$; **Figure 2.3F**). Furthermore, there is also no correlation between ΔO and PDSI ($\rho = -0.138$; $p = 0.12$; **Figure 2.3G**). These three measures of binocular responses are therefore independent from each other, and they likely encode orthogonal features of binocular stimuli.

These data suggest that a simple convergence of monocular inputs is unlikely to be the deciding mechanism of binocular integration.

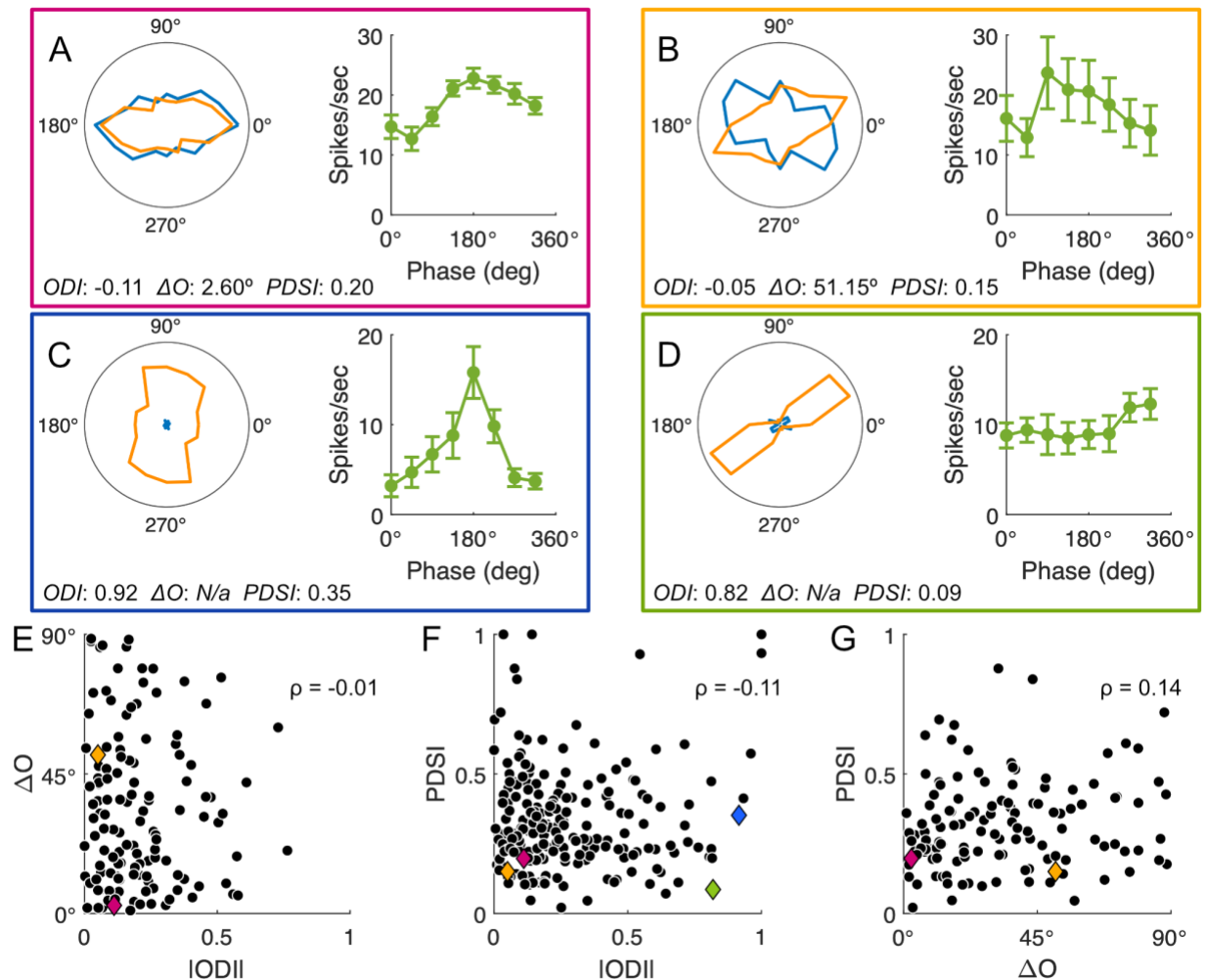


Figure 2.3. No correlation among ocular dominance, interocular matching, and binocular disparity selectivity.

A - D. Four example neurons showing different level of ocular dominance, interocular matching, and phase disparity selectivity. Monocular orientation tuning curves of each neuron are shown to the left in polar plots (contralateral in orange and ipsilateral in blue) and disparity tuning curve to the right (green curve). The associated ODI, ΔO (if responsive to both monocular simulations), and PDSI are shown in the bottom. No systematic relationship is seen among the three measures.

- E. No significant correlation was found between ΔO and ODI (Spearman partial ranked correlation, $\rho(129) = -0.010$, $p = 0.090$). Example cells from panels A and B are labeled in magenta and yellow, respectively.
- F. No significant correlation was found between PDSI and ODI (Spearman partial ranked correlation, $\rho(200) = -0.110$, $p = 0.218$). Example cells from panels A, B, and C are labeled in magenta, yellow, and blue, respectively.
- G. No significant correlation was found between PDSI and ΔO (Spearman partial ranked correlation, $\rho(125) = -0.138$, $p = 0.123$). Example cells from panels A and B are labeled in magenta and yellow, respectively.

Additionally, few cells in our dataset had monocularly dominated ODI values (e.g., $|\text{ODI}| > 0.80$, $n = 16/244$, i.e., 6.6%) and a large portion of those that did show high disparity selectivity (e.g. $\text{PDSI} > 0.25$ & $|\text{ODI}| > 0.8$, $n = 6/16$, i.e. 37.5%; **Figure 2.3F**). In other words, neurons in the mouse V1 binocular zone do not form distinct contralateral, ipsilateral, or binocular groups, as suggested by some recent studies. Instead, binocular integration is widespread and almost all neurons are binocular.

2.5.3 Disparity tuning and orientation selectivity in joint parameter space

Orientation tuning and phase disparity tuning are often measured separately. This would be fine if separate populations of dLGN afferents truly converged to produce the two tuning properties. Orientation tuning would reflect the property of the dLGN afferents converging from the contralateral eye's compartment, whereas phase disparity tuning would reflect the property of the dLGN afferents converging across the contra- and ipsilateral compartments. Given that our data suggest that the convergence is unlikely the only mechanism for the production of phase disparity tuning, we explored the tuning in the joint parameter space of orientation and phase disparity. Specifically, each combination of orientation and phase disparity of a binocular grating comprises a vector, or a position on a surface. A schematic illustrating these two variables is shown in **Figure 2.4A**. Binocular gratings with a phase disparity of 90° and

orientation of 0° (blue outline, left), once rotated 180° , become identical to gratings with a phase disparity of 270° and orientation of 180° (blue outline, right). Similarly, gratings with a phase disparity of 270° and orientation of 0° (pink outline, left) are identical to those with a phase disparity of 90° and orientation of 180° (pink outline, right). Due to the inverted nature by which the two axes wrap around, the phase disparity and orientation conditions that define the points on this map can also be understood as tiling the surface of a Klein bottle (Tanaka, 1997; Tanabe et al., 2022).

We illustrated each neuron's firing rate for each parameter combination in a heatmap. Many neurons had heatmaps with a clearly defined hotspot (**Figure 2.4B**). Due to the way in which the orientation and phase disparity axes wrap around, hotspots located near the edges appear split across two areas of the heatmap (**Figure 2.4B**, left; lower left quadrant and the upper right quadrant). Given this complex topological structure, a single vertical slice of the heatmap may not serve as a representative of phase disparity tuning. We thus calculated the preferred phase disparity for each vertical slice of the heatmap and plotted it and the associated PDSI (gray scale) for the corresponding orientation (**Figure 2.4C**; $n=246$). Interestingly and unexpectedly, the PDSI was similarly high in many orientations, including both 0° (vertical) and 90° (horizontal) (Wilcoxon's signed rank, $p=0.5$). In other words, in mouse V1, phase disparity tuning is not limited to horizontal disparity of vertical gratings, as one would expect from stereoscopic depth perception.

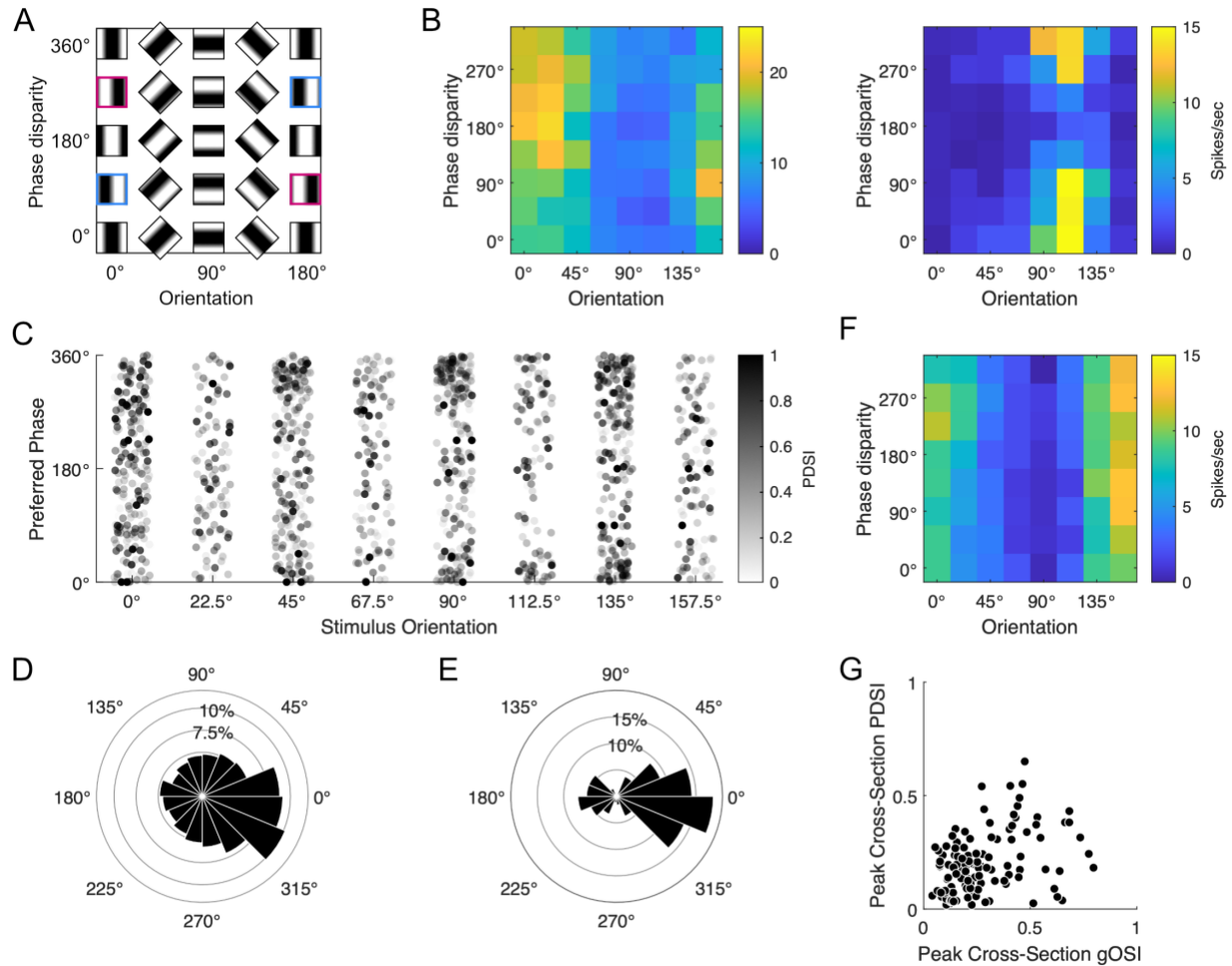


Figure 2.4. Analysis of preferred phase disparity and orientation selectivity.

- A.** Schematic illustrating the systematic variation of stimulus orientation (x-axis) and phase disparity (y-axis). The two red and two blue squares mark the identical stimulus condition (see text for details).
- B.** Each neuron's response to a particular stimulus orientation and phase disparity is represented in a position on a 2-d heatmap. Two example neurons are shown with localized hotspots on the heatmap.
- C.** Distribution of the preferred phase disparity separately for each orientation. Each dot represents a column of the heatmap of a given neuron, with its degree of disparity selectivity (PDSI) shown in grayscale. The preferred phase disparity tended to cluster around 0°, particularly for tuning curves that had higher PDSI values (darker data points,

where the estimation of preferred disparity is more accurate with stronger phase disparity tuning).

- D. Distribution of preferred phases represented in a polar histogram, including all data points in panel C.
- E. Distribution of preferred phases, where for each neuron, only the orientation which induced the highest PDSI was included. A strong bias toward phase disparity 0° is seen (and also 180°), with gaps near orthogonal phase disparities 90° and 270° .
- F. Example heatmap from a neuron with a vertically elongated hotspot.
- G. Relationship between orientation selectivity and disparity selectivity. For each neuron, we identified the peak in the heatmap and calculated the gOSI and PDSI from the two cross-sections that run through the peak.

Furthermore, in several of the orientations (e.g., 90°), there were biases toward phase disparity of 0° and 180° . The bias was partially visible in the pooled distribution of the preferred phase disparity across all stimulus orientations (**Figure 2.4D**; circular mean 338.6°). We examined this bias further by selecting the preferred disparity associated with the highest PDSI for each neuron. The bias in the preferred phase disparity became much clearer (**Figure 2.4E**), showing a bimodal distribution, with peaks at 0° and 180° , and dips at 90° and 270° (Hartigan's dip test, $p < 0.001$). Mouse V1 neurons were therefore most strongly driven by a binocular grating that had the same phase in both eyes or the opposite phase across the eyes.

In a small subset of the neurons, the hotspot was elongated vertically, indicating weak phase disparity tuning but strong orientation tuning (**Figure 2.4F**). In contrast, few neurons had a hotspot stretching across the orientation axis. We therefore analyzed the relationship of the strength of tuning along the phase disparity axis and the orientation axis. To do this, we generated two cross-sections that ran through the heatmap peak: one cross-section along the orientation axis and the other along phase disparity axis. We calculated the gOSI and the PDSI of the respective cross-sections. In the scatter plot comparing these values (**Figure 2.4G**), there was a noticeable dearth of points in the upper left corner, i.e., few neurons were highly phase

disparity selective but not orientation selective. This result could reflect a hierarchical processing mechanism in which orientation tuning is generated prior to the phase disparity tuning.

2.5.4 *Predicting binocular tuning from responses to monocular stimuli*

We next examined how binocular tuning might derive from upstream monocular processes. We noticed that in many neurons, the strongest phase disparity tuning was observed when the binocular grating was given the orientation that elicited the strongest monocular response (**Figure 2.5A**). The shape of the phase disparity tuning had the characteristics of a sinusoid, wherein the baseline and amplitude both reach their peaks at the preferred orientation. To quantify this relationship, we decomposed the phase disparity tuning curve into its 0-th order (F_0 , the mean) and 1-st order Fourier components (F_1 , the vector sum). Both F_0 and F_1 peaked at the same orientation for this example neuron (**Figure 2.5B**; black solid and black dashed, respectively), and both curves closely resembled the orientation tuning obtained with contralateral eye stimulation. For this neuron, the orientation tuning of the contralateral eye stimulation accurately predicted the orientation tuning of both F_0 and F_1 .

In other neurons, the monocular responses were good predictors of F_0 , but poor predictors of F_1 (**Figure 2.5C**). Orientation tuning of F_0 had a clear peak at 67.5° for this neuron (**Figure 2.5D**), resembling the peak of the contralateral eye stimulation. In contrast, the orientation tuning of F_1 had two peaks, including one that hardly elicited responses when the grating was monocular (orientation 157.5° ; **Figures 2.5D**). This shape was dissimilar to the orientation tuning of either contralateral or ipsilateral stimulations.

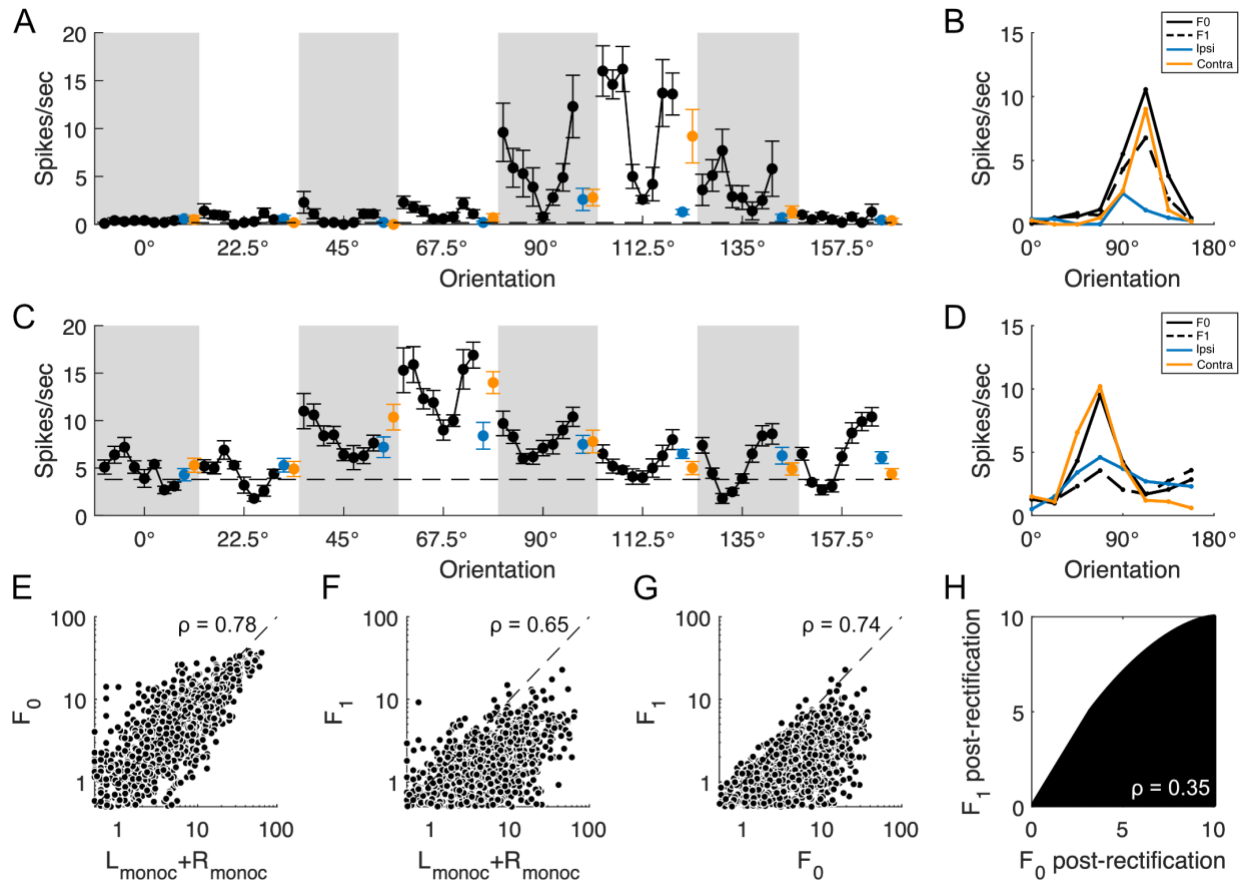


Figure 2.5. Relationship between monocular and binocular responses.

- A.** Tuning curves of an example neuron. This neuron showed the strongest disparity tuning at the orientation it preferred monocularly (112.5°).
- B.** Orientation tuning of the F_0 (black solid) and the F_1 (black dashed) components of the phase disparity tuning curves from panel **A**. Superimposed are the monocular orientation tuning curves (blue for ipsilateral and orange for contralateral). F_0 and F_1 as a function of orientation have indistinguishable shapes, and the monocular responses are good predictors of their magnitude.
- C.** Tuning curves from an example binocular neuron whose disparity tuning was dissociated from the monocular orientation tuning. Strong disparity tuning was obtained with an orientation (157.5°) that was perpendicular to its preferred orientation.
- D.** Same plot as panel **B**, but for the neuron in **C**. F_0 and F_1 as a function of orientation are dissociated from each other, and the monocular responses are good predictors for the

magnitude of F_0 but not for F_1 .

- E. Scatter plot of F_0 and the sum of the responses to monocular stimulation. Each dot corresponds to one point of the orientation tuning curve in **D**. The dots fell along the diagonal, showing a high correlation.
- F. Scatter plot of F_1 and the sum of the monocular responses. Most dots fell below the diagonal and filled the gap between the diagonal and the horizontal axis. F_1 was dissociated from the monocular responses.
- G. Scatterplot of F_1 and F_0 , with most dots filling the entire space between the diagonal and the horizontal axis.
- H. Simulation of spike threshold effect on relationship between F_0 and F_1 . Sinusoids with all possible combinations of F_0 and F_1 was generated (i.e., no correlation between F_0 and F_1) and then passed through a threshold nonlinearity. The output was then decomposed into F_0 and F_1 , whose amplitudes are shown in this plot. The upper left corner of the plot was missing, which created a moderate level of spurious correlation when in fact they have zero correlation in the subthreshold voltage.

To quantify the similarities of the four orientation tuning curves, we first summed the two monocular orientation tuning curves (contralateral L_{monoc} and ipsilateral R_{monoc}) and then compared with the binocular response (F_0 and F_1). If binocular combination is as simple as a linear summation, as postulated in the disparity energy model, we would expect the summed orientation tuning curve to be a good predictor of the orientation tuning curves of both F_0 and F_1 . This was indeed true for the F_0 component, where F_0 plotted against $L_{\text{monoc}} + R_{\text{monoc}}$ fell along the identity line ($\rho=0.776$; $p<0.001$; **Figure 2.5E**). However, the F_1 component did not follow this pattern. F_1 plotted against $L_{\text{monoc}} + R_{\text{monoc}}$ not only fell below the identity line, it also scattered across a wide range between the horizontal axis and the identity line ($\rho=0.650$; $p<0.001$; **Figure 2.5F**). The large scatter was partially due to the discrepancy in orientation tuning between F_0 and F_1 (**Figure 2.5G**). Despite the high value of the rank correlation between F_1 and F_0 ($\rho=0.742$; $p<0.001$), the actual relationship was in fact poor. This is because F_1 cannot exceed F_0 due to the rectification by the firing threshold (**Figure 2.5H**), which limits points from falling above the

identity line. Therefore, our data suggest that the orientation tuning of F1 is dissociated from the monocular orientation tunings. This finding indicates that the F0 of phase disparity tuning is largely relayed from monocular processes, whereas the F1 of phase disparity tuning is likely generated by a separate mechanism in downstream circuits where binocular combination has already occurred.

2.5.5 *Specificity among cell types and cortical layers*

We next classified the recorded neurons into fast-spiking and regular-spiking neurons and analyzed their binocular response. The fast-spiking neurons are known to overlap with a specific subtype of inhibitory interneuron that express the molecular marker parvalbumin (PV) (Kawaguchi and Kondo, 2002). When the waveforms of all visually responsive neurons in the dataset were superimposed, we observed two distinct patterns of waveforms (**Figure 2.6A**). To separate these two categories quantitatively, we calculated the slope of the spike at 0.5 ms after spike detection. A histogram of the slope values showed a bimodal distribution with a clear split at slope of 0 (**Figure 2.6B**). We classified neurons with a negative slope as fast-spiking ($n = 67$), and neurons with a positive slope as regular-spiking ($n = 179$). The fast-spiking population had weaker orientation tuning than the regular-spiking counterpart ($z = -3.610$; $p < 0.001$; **Figure 2.6C**). The fast-spiking population also had weaker phase disparity tuning than the regular-spiking counterpart ($z = -3.829$; $p < 0.001$; **Figure 2.6D**). These results are independent confirmations of previously published results on their orientation selectivity and disparity selectivity (Niell and Stryker, 2008; Liu et al., 2009; Scholl et al., 2015). We next applied the classification to our measurement of binocular response properties. The low selectivity metrics of fast-spiking neurons could be obscuring any pattern that was otherwise present in the remaining regular-spiking population. This was not the case. Even after splitting the population into the two classes, we found no correlation between ODI and ΔO (**Figures 2.6E, F**), between PDSI and ODI (**Figures 2.6G, H**), or between PDSI and ΔO (**Figures 2.6I, J**).

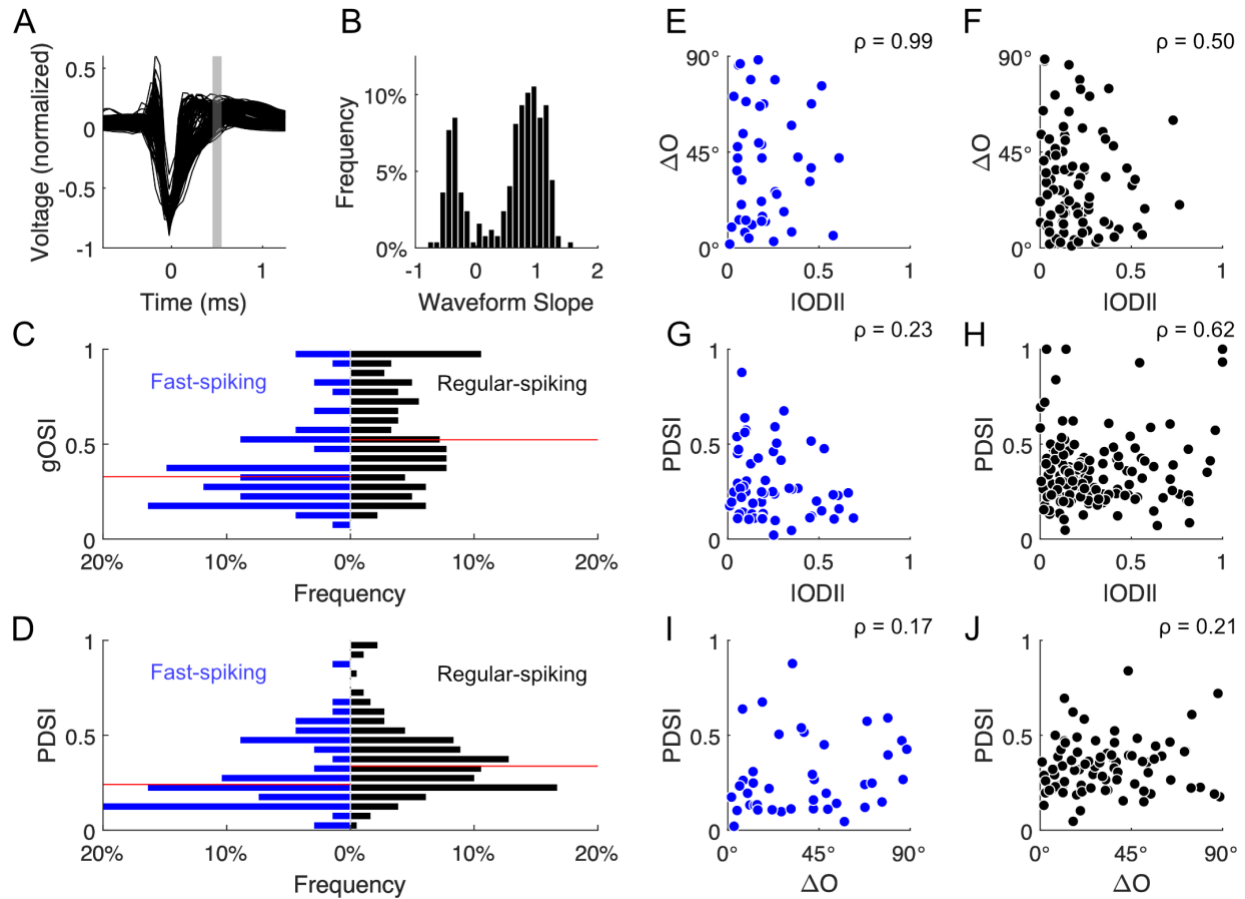


Figure 2.6. Binocular response properties of fast-spiking versus regular-spiking neurons.

- A.** Aggregated spike waveforms display distinct populations of fast-spiking and regular-spiking neurons. Area shaded in gray indicates the time window where the slope of the waveform was estimated for quantification.
- B.** Bimodal distribution of estimated waveform slopes. Positive values belong to regular-spiking, where negative values belong to fast-spiking, or putative PV inhibitory interneurons.
- C.** Population of fast-spiking neurons displayed broader orientation tuning than regular-spiking neurons (Wilcoxon rank-sum, $z = -3.61$, $p = 1.29e^{-4}$).
- D.** Population of fast-spiking neurons displayed broader phase disparity tuning than regular-spiking neurons (Wilcoxon rank-sum, $z = -3.81$, $p = 1.36e^{-4}$).
- E.** No significant correlation was found between ΔO and ODI within fast-spiking neurons (Spearman correlation, $\rho(42) = 0.001$, $p = 0.994$).

- F. No significant correlation was found between PDSI and ODI within regular-spiking neurons (Spearman correlation, $\rho(85) = -0.072$, $p = 0.504$).
- G. No significant correlation was found between PDSI and ΔO within fast-spiking neurons (Spearman correlation, $\rho(58) = -0.159$, $p = 0.225$).
- H. No significant correlation was found between ΔO and ODI within regular-spiking neurons (Spearman correlation, $\rho(140) = -0.042$, $p = 0.624$).
- I. No significant correlation was found between PDSI and ODI within fast-spiking neurons (Spearman correlation, $\rho(41) = 0.213$, $p = 0.170$).
- J. No significant correlation was found between PDSI and ΔO within regular-spiking neurons (Spearman correlation, $\rho(82) = 0.138$, $p = 0.210$).

Next, we examined binocular responses across cortical depth. We measured the local-field potential (LFP) in response to a contrast-alternating checkerboard pattern and used it to determine the center of layer 4 (**Figure 2.7A-B**; see methods for details). A sink occurred in a specific window in depth after a short delay from both LFP and current-source density analysis (71.4 ms; 500 μm from the tip of the probe). We found no evidence of layer specificity in any of the binocular response metrics: ODI, ΔO , or PDSI (**Figures 2.7C, D, E**).

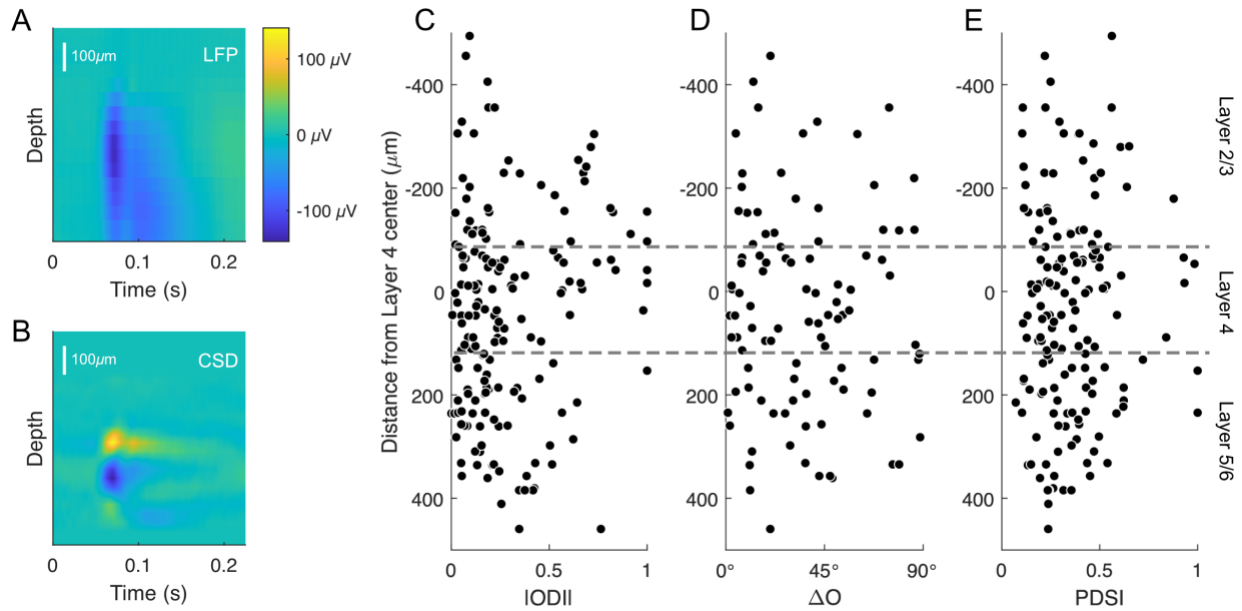


Figure 2.7. Binocular response properties are not specific to discrete cortical layers.

- A.** Example LFP as a function of time and depth in the cortex. Time $t=0$ s was when the stimulus switched polarity, and depth $z=0$ was the position of the channel closest to the tip of the microelectrode probe. Dark blue represents negativity.
- B.** Current source density (CSD) calculated from **A**. The region with strongest negativity in the LFP was also where the strongest negativity appeared in the CSD.
- C.** No layer specificity was found with ocular dominance.
- D.** No depth specificity was found with ΔO .
- E.** No depth specificity was found with the width of phase disparity tuning.

Finally, we asked whether stimulus design could impact our observations of binocular integration. Thus far, we had interleaved monocular and binocular stimulations to rule out any potential complications arising from neuronal adaptation to the statistics of sensory stimulation. If the stimuli were to be presented in a series of blocks, the statistics of the stimulus would have varied from one block to the next. It is conceivable that neurons change their response property as an adaptation to the statistics of the sensory stimuli, which could make direct comparisons between monocular and binocular responses difficult to interpret. To test whether such adaptation might influence our measurements, we acquired an additional dataset where we presented all the monocular stimulation in the first block to measure ocular dominance and interocular matching, followed by all the binocular stimulation in the second block to measure phase disparity selectivity (“two block design”; $n = 22$ mice, including 7 used in the “one block” design). We observed no major differences between the population distributions of ODI, ΔO , or PDSI when using one stimulus recording block versus two blocks, nor any correlation between the response indices (**Figure 2.8**).

Together, our results indicate that regardless of stimulus design, cortical depth, and cell type, binocular integration in mouse V1 is widespread, and importantly this integration process does not simply depend on a convergence of feedforward monocular inputs.

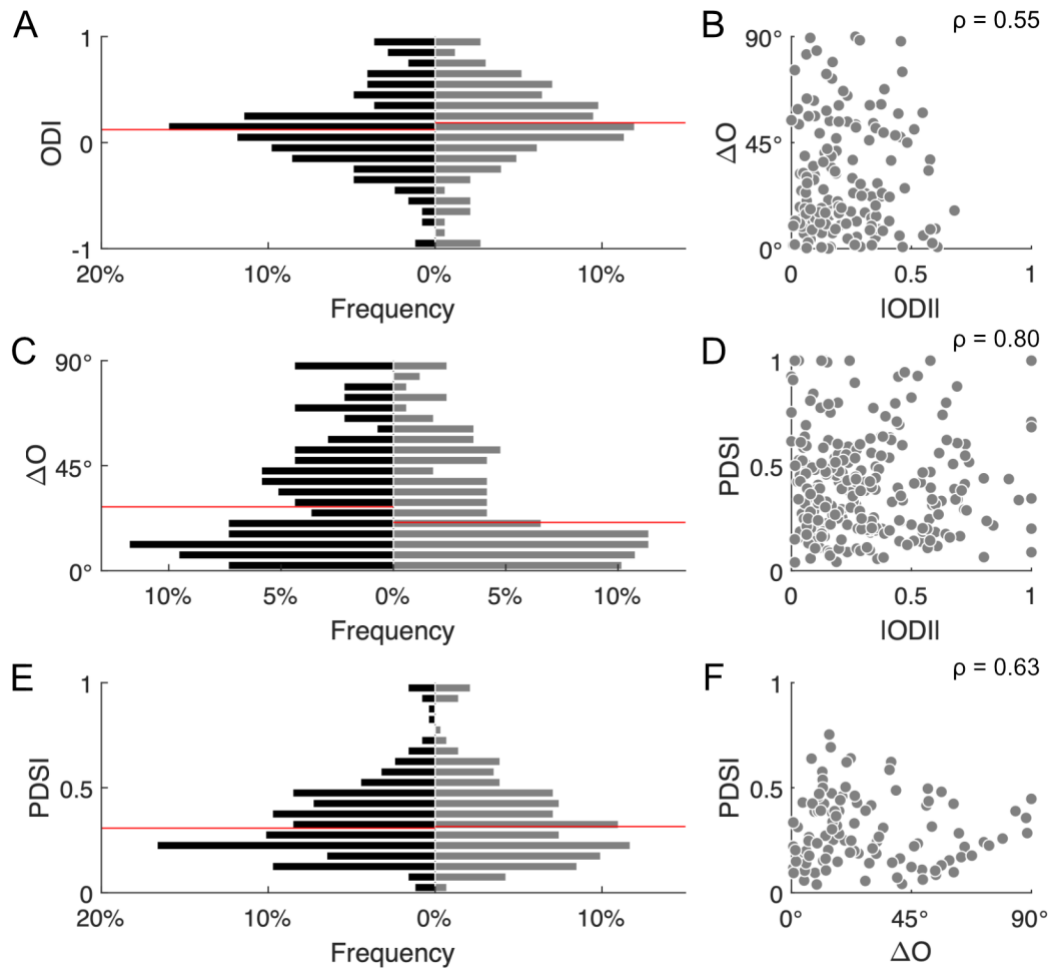


Figure 2.8. Consistency of measurements with block-structured stimulation.

- A.** Comparison of ODI distribution obtained with the interleaved stimulation versus the block-structured stimulation. *Left:* ODI obtained with interleaved stimulation, as in **figure 2.1D**. Median ODI (0.12) is indicated in red. *Right:* ODI obtained with block-structured stimulation. The monocular stimulation block preceded the binocular stimulation block. Median ODI (0.19) is indicated in red.
- B.** No significant correlation was found between ΔO and ODI with the block-structured stimulation (Spearman correlation, $\rho(155)=0.048$, $p=0.552$).
- C.** *Left:* ΔO obtained with interleaved stimulation, as in **figure 2.1D**. Median ΔO (27.4°) is indicated in red. *Right:* ΔO obtained with block-structured stimulation. Median ΔO (20.7°) is indicated in red.

- D. No significant correlation was found between PDSI and ODI with the block-structured stimulation (Spearman correlation, $\rho(245)=-0.016$, $p=0.801$).
- E. *Left*: PDSI obtained with interleaved stimulation, as in **figure 2.1D**. Median PDSI (0.31) is indicated in red. *Right*: PDSI obtained with block-structured stimulation. Median PDSI (0.32) is indicated in red.
- F. No significant correlation was found between PDSI and ΔO with the block-structured stimulation (Spearman correlation, $\rho(106)=-0.048$, $p=0.625$).

2.6 Discussion

In this study, we tested the extent of binocular integration in mouse V1 and found that almost all responsive neurons showed evidence of binocular integration. Even neurons that were heavily dominated by one eye showed clear tuning to the phase disparity of a binocular grating, unequivocally demonstrating binocular interaction. Our data do not support the notion that neurons dominated by one eye are relaying signals from an upstream monocular structure, as implied by their classification nomenclature of “monocular cells.” Furthermore, we showed that ocular dominance, interocular matching, and disparity selectivity are independent measures of binocular integration. Finally, we found no direct association between phase disparity tuning and orientation tuning, suggesting that the two properties are generated via separate mechanisms. The major mechanism for creating phase disparity tuning is likely intracortical circuitry, unlike the convergence of geniculocortical projections for orientation tuning.

2.6.1 Ocular dominance, interocular matching, and disparity selectivity

Ocular dominance is a measure of binocularity that has been long studied in the visual cortex (Hubel and Wiesel, 1962). Decades of ocular dominance studies have significantly advanced our understanding of visual development and plasticity, as well as their critical period regulation (Hofer et al., 2006; Espinosa and Stryker, 2012; Priebe and McGee, 2014; Kaneko and Stryker, 2017; Ribic, 2020). However, these studies may have led to the notion that separate groups of monocular and binocular neurons exist even within the binocular zone of V1. For example, several recent studies using 2-photon calcium imaging reported large proportions of monocular neurons (> 50%) in layer 2/3 of mouse binocular V1 (Salinas et al., 2017; Huh et al., 2019; Tan et al., 2020). The notion of purely monocular neurons in binocular V1 might be an acceptable approximation of layer 4 in cats and monkeys, where geniculocortical projections form alternating stripes of ocular dominance (Levay et al., 1978). However, it would raise important questions about the nature of binocular integration if monocular cells indeed exist at such a large population *after* the convergence of eye-specific inputs, which takes place in V1

layer 4 in mice (Gordon and Stryker, 1996) and even to some extent in the dLGN (Guido et al., 1989; Howarth et al., 2014).

A careful study of binocular integration requires an apparatus that presents visual stimuli dichoptically to the subject. The tuning to binocular disparity shows the neuron's sensitivity to binocular interactions. A truly monocular neuron could never have this property, and therefore, disparity tuning is direct evidence of binocular integration. Here we found widespread disparity selective neurons in the mouse binocular V1, across all cortical layers. Together with the observed ODI distribution, our data demonstrate that almost all neurons in the binocular V1 show evidence being influenced from both eyes. The reported "monocular cells" in recent mouse studies were likely due to the lower sensitivity in calcium imaging and the lack of true binocular stimulation (Cang et al., 2023). More generally, we found a lack of correlation between ocular dominance and disparity selectivity. This result is consistent with findings across multiple studies performed in cats, monkeys, and mice (LeVay and Voigt, 1988; Read and Cumming, 2004; Kara and Boyd, 2009; Scholl et al., 2013a; Chioma et al., 2020). In other words, disparity tuning and ocular dominance are independent measures of the binocular integration process in V1. Notably, this is inconsistent with the disparity energy model (Ohzawa and Freeman, 1986; Ohzawa et al., 1990, 1997), which predicts that more strongly tuned neurons should have a more balanced ocular dominance.

The original feedforward model of binocular integration also assumed that a neuron's monocular RFs in the two eyes should be similar (including orientation), except for offsets in position or phase, for the neuron to be useful in representing stereoscopic depth (Anzai et al., 1999). Again, we did not find such a relationship between disparity selectivity and interocular matching of orientation preference. More generally, the disparity energy model postulates that neuronal responses to binocular stimulation can be predicted from the measured responses to monocular stimulation, up to a first-order approximation. Our data showed that this was reasonably the case for the average binocular response magnitude, but not for the degree of disparity selectivity.

Together, our study has revealed considerable discrepancies between actual binocular responses and the ones predicted by the disparity energy model. One way to reconcile these discrepancies is to consider a neuronal population in which binocular convergence has the same mechanism as the disparity energy model, but the population is synaptically coupled via intracortical connections. To a first-order approximation, each neuron's response property closely follows the disparity energy model. When the stimulus drive is sufficiently strong as for a sinusoidal grating, neurons in the population influence each other through nonlinear interactions. The response of a particular neuron in such a coupled network will depend on the strength and feature of the stimulus, due to the propagation and recurrent feedback of signals across the population. We have implemented such a recurrent network model in a recent study (Tanabe et al., 2022), which was able to explain the observed stimulus-dependent differences in disparity tuning between mice and tree shrews. It also predicts a reduced disparity tuning of inhibitory neurons in mice, a prediction validated by the observed tuning of fast-spiking neurons. Whether recurrent intracortical connectivity indeed underlies binocular integration will have to be studied in the future.

2.6.2 Limitations of this study

One limitation of our study is the lack of eye tracking data. Disconjugate eye movements could potentially wash out disparity tuning if they are unchecked. Mice are known to make disconjugate eye movement under freely moving conditions (Meyer et al., 2020). Under head-fixed conditions, it is less clear. Vergence eye movements are likely smaller than what is detectable with current eye tracking methods (Samonds et al., 2019). The sheer fact that we saw strong disparity tuning is evidence that vergence eye movements are small enough that it does not wash out the tuning. In order to study how vergence eye movements might affect the encoding of disparity, future studies would need to develop new methods of eye tracking with an accuracy several magnitudes higher.

Another limitation was that running speed was not recorded. In the mouse visual cortex, locomotion is known to amplify the sensory signal (Niell and Stryker, 2008). When we

include running states into the same condition as stationary states, we expect an increase in the mean and variance of firing rates across all stimuli. One possibility we could explore in future studies is whether locomotion amplifies sensory signals of certain stimulus features (e.g., orientation) more than others (e.g., disparity).

2.6.3 *Implications for natural behaviors and visual development*

Much of the studies using cats and primates involve the mechanisms for stereoscopic depth perception. Stereopsis is particularly advantageous for animals with frontally facing eyes, but it is not clear whether the same advantage holds for mice with laterally facing eyes. Recent studies have shown that mice are capable of solving some stereoscopic tasks (Samonds et al., 2019; Boone et al., 2021). On the other hand, it is also possible that evolutionary pressure has led mice to use binocular vision in very different ways.

Binocular vision is best understood in terms of the geometry of visual projections from the environment onto the retina. For the study of binocular vision in humans, eye movement tracking is vital, because visual projection geometry will critically depend on the point of fixation. The same does not necessarily hold for the study of binocular vision in mice. One of the patterns of eye movement that mice make is in response to head movement. A compelling explanation is that those eye movements serve to stabilize their gaze despite head movement (Meyer et al., 2020). During head movement, there is a transient period during which the retinal images become misaligned, and binocular vision may be useful to the animal in that time period.

The magnitude of misalignment depends critically on the interocular distance. For instance, suppose there is an object in the upper, binocular visual field, and the head is rotated clockwise along the roll axis. The left eye sees the object from a higher viewpoint than the right eye. Geometrically, the projection of the object to the left eye is in a shallower angle than the projection to the right eye. The disparity produced by this head rotation is directly proportional to the interocular distance. To compute the magnitude of the eye movement for realigning the images, the interocular distance will be a necessary parameter. For a developing mouse, whose

interocular distance continues to change with the growth of the head, this might be a challenge. A mechanism that allows continuous recalibration, such as synaptic plasticity, might resolve this challenge during development. Having the primary circuitry for this computation in the cortex, as opposed to the geniculocortical projections, might help in the continuous recalibration.

Another product of the activity-dependent development is the matching of orientation preference (Wang et al., 2010a; Chang et al., 2020), which raises the question of how the development of phase disparity tuning might mirror it, and whether the two properties develop on a slightly offset time course. The paucity of the current literature on this subject makes it difficult to speculate on how exactly the two processes might codevelop, but we hope that future studies will help us understand how the wiring for orientation tuning and phase disparity tuning are determined during the course of development.

In conclusion, we have found widespread and multifaceted binocular integration in mouse V1, which includes neurons that are heavily dominated by one eye. The practice of classifying and separating out these neurons as being part of a monocular mechanism will consequently underestimate the role of recurrent circuits in binocular integration. Our results indicate a critical role of intracortical circuits in binocular computation. Future studies will be needed to reveal the exact cortical circuits, determine how developmental plasticity shapes them, and understand how binocular integration and development help mouse behavior.

3 Binocularity in developing mouse V1

The contents of this chapter are in preparation for publication under the working title “Experience-dependent co-development of orientation and phase disparity selectivity in the mouse binocular primary visual cortex.” Jieming Fu, Seiji Tanabe, Jianhua Cang.

Jieming Fu^{1,2}, Seiji Tanabe³, and Jianhua Cang^{2,3}

1. Neuroscience Graduate Program; 2. Department of Biology; 3. Department of Psychology

University of Virginia, Charlottesville, VA 22904, USA

Correspondence and requests for materials should be addressed to Jianhua Cang, cang@virginia.edu

Abbreviated title: Experience-dependent development in mouse binocular V1.

Number of figures and tables: 5 figures.

Number of pages: .

Number of words: Abstract: 207; Introduction: 636; Discussion: 1183.

Conflict of Interest: The authors declare no competing financial interests.

Acknowledgements:

We thank Sotiris Masmanidis at UCLA for supplying the multielectrode silicon probes. This work was supported by the US National Institutes of Health (NIH) grant EY034779 to J.F., and NIH grants (EY026286 and EY020950) and Jefferson Scholars Foundation to J.C.

3.1 *Abstract*

Two-dimensional images from the eyes are combined in the brain to create an understanding of three-dimensional surroundings, in a process called stereopsis. The neurons in the primary visual cortex (V1) are the first in the primary visual pathway to integrate these two streams of information. The complex circuitry underlying binocular integration is one of many sensory processing pathways that is experience-dependent during development. While it has been demonstrated that disparity selectivity, like other visual response properties, can be altered by manipulating visual experience during the critical period, little is known about how disparity selective circuits function in animals at the start of their visual experience acquisition period, and whether disparity selectivity matures over the course of the critical period with more visual experience.

To better understand how binocular circuits develop with visual experience, we performed acute electrophysiological recordings in young mice ranging between the day of eye opening to two weeks after eye opening. We observed a steady co-development of both orientation and phase disparity selectivity, as well as changes in other measures of synaptic activity and circuit wiring, particularly in the early days immediately after eye opening. Altogether, our data suggest that circuits performing binocular integration may be strengthened by visual experience during the critical period.

3.2 *Significance Statement*

The visual critical period is a crucial part of neural development when experience profoundly shapes how the brain's circuits wire together to process sensory and other inputs. Our data here demonstrate that during the initial days right after eye opening, neurons in mouse primary visual cortex rapidly strengthen their selectivity to certain stimuli. While other studies have shown that depriving the visual system of experience during the critical period can reduce binocularity responses, our study examines how initial exposure to visual inputs in an unaltered system contributes to circuit development.

3.3 Introduction

Exposing the early visual system to experience-guided input is a crucial step in shaping functional circuits, since any absence of or alteration to visual experience during this critical period can create a permanent reduction in the responses of primary visual cortex (V1) neurons.

Ever since the discovery that short periods of monocular deprivation (MD) during a critical window of development is sufficient to create permanent deficits in adult vision, MD has become accepted as a model paradigm for probing mechanisms of plasticity in sensory cortex. While these studies have illuminated many molecular interactions underpinning experience-dependent plasticity, most protocols for monocular deprivation – particularly in mice – begin several days into the visual critical period (Hofer et al., 2006; Espinosa and Stryker, 2012; Hooks and Chen, 2020). Therefore, while this manipulation is enough to induce permanent changes to circuit wiring, it does not accurately capture the changes happening during the induction of sensory experience to the visual system.

During the days right after eye-opening, the visual system shifts from being shaped by spontaneous activity from retinal waves, to activity driven by light entering the eyes. Dark rearing studies have shown that in the absence of visual experience, neurons throughout the visual system undergo systemic structural changes, such as decreases in dendritic spine counts and lack of myelination (Valverde, 1971; Tian and Copenhagen, 2001; Osanai et al., 2022). Clearly, the timely induction of experience to the naïve visual system is crucial in reaching typical developmental milestones.

Disparity selectivity inherently requires a V1 neuron to integrate information received from two separate eyes in order to produce an output, which makes it a promising and yet understudied avenue through which to study circuit development. Neurons that are phase disparity selectivity are responsive only to particular combinations of binocular stimuli, and such responses cannot be elicited with monocular stimuli alone. Previous studies have examined how the interocular matching of orientation selectivity matures with visual experience and decreases

in dark-reared mice (Tan et al., 2020), and shown that monocular deprivation in mice during the midst of the critical period decreases some phase disparity selectivity (Scholl et al., 2017).

However, findings regarding the circuit properties of these binocular integrative processes prior to visual experience remain sparse. Ferret research regarding interocular matching suggests that for orientation selectivity, there is a binocular orientation preference at eye opening that exists alongside the unmatched monocular orientation preferences, and that visual experience serves to align all three orientation preferences (Chang et al., 2020). However, other research suggests that the cortex is slower to respond to ipsilateral input, in comparison to contralateral input (Honnuraiah et al., 2024), which would suggest that phase disparity selectivity should be weak or altogether absent at eye opening, and that the onset of visual experience allows the cortex to rapidly wire binocular integration circuits, albeit incomplete ones that are still susceptible to manipulations such as monocular deprivation.

In this study, we looked at the interaction between onset of visual experience and the dynamics of binocular integration, by performing acute electrophysiological recording in the binocular V1 of young mice from the day of eye opening until 15 days later. We found that over the course of the precritical and early critical period, orientation and phase disparity selectivity strengthen together in binocular V1, over the course of about 9-10 days, but overall matures to near-adult levels by the timepoint when monocular deprivation protocols in other studies begin. Receptive field structure becomes clearer over the course of the early critical period as well. Overall, these results suggest that there is an initial maturation of binocular integration circuit wiring that stabilizes fairly early into the critical period, pointing to experience-dependent plasticity perhaps existing in two stages, akin to a “first draft” phase early in the precritical and critical periods, and an “editing” phase in the middle to late critical period.

3.4 *Materials and Methods*

3.4.1 *Animals*

Male and female C57BL6 mice (n=36; 19M & 17F) between 13 and 30 postnatal days of age were used for all experiments. Use protocols for animals were approved by the Institution for Animal Care and Use Committee at the University of Virginia.

Mice were placed under isoflurane anesthesia (5% for induction, 2% for maintenance, in O₂, ~0.5 L/min, VetFlo, Kent Scientific) for implantation of a custom-designed titanium headplate to immobilize the head during recordings, and to create a craniotomy to allow access to the brain for electrophysiological recording, as previously described (Fu et al., 2023). Atropine (0.3 mg/kg in 10% saline) and dexamethasone (2.0 mg/kg in 10% saline) were administered subcutaneously, and the core body temperature was monitored and maintained at 37 deg C (Frederick Haer Company) for the duration of surgery. Artificial tears (Henry Shein Medical) were administered to prevent drying and injury to the corneas. The mouse's head was held in place using a stereotaxic frame equipped with ear bars (Kopf Instruments). The scalp was resected to expose a region of the occipital skull, centered over binocular V1, after which a titanium headplate was adhered using Metabond (Parkell).

After waiting ~5 minutes for Metabond to fully cure, a craniotomy was performed to allow access to binocular V1 for electrophysiological recording. The craniotomy was positioned above the left visual cortex (~2.0 mm diameter, ~3 mm lateral & ~0.5mm anterior from lambda), with the exact distance lateral of lambda adjusted based on the animal's age. This lateral distance was approximated from intrinsic imaging of binocular V1 performed in a subset of animals. The craniotomy was then covered with agarose (2.5% in 10% saline) and Quik-Cast silicone epoxy (World Precision Instruments) to protect the area prior to recording.

Mice were given a subcutaneous injection of carprofen (5mg/kg) and placed on a heating pad to recover from isoflurane anesthesia until bright, alert, and responsive.

Electrophysiological recording proceeded after mice were allowed to recover from anesthesia for a minimum of 4 hours.

3.4.2 *Physiological recording*

Mice were head-fixed and allowed to run on a free-moving wheel for the duration of recording. A silicone multielectrode probe (128 AxN Sharp model, Masmanidis Lab, UCLA)(Yang et al., 2020) was attached to a data acquisition system (RHD 128-Channel Headstage, Intan Technologies) to record electrophysiological changes during visual stimulation. The probe was centered over the craniotomy, and following insertion into the cortex, the area was covered with agarose (2.5%) into which a reference wire was immersed. The probe was advanced until tip channels were embedded in white matter. Analog voltage signals were digitized at a 20 kHz sampling rate (RHD Evaluation System, Intan Technologies), and the timing of visual stimulation condition changes were recorded with transistor-to-transistor (TTL) pulses simultaneously with voltage signals, to enable later offline synchronization for analysis.

After the recording session had ended, the probe was retracted, and animals were euthanized according to IACUC protocols.

Spikes in the voltage time series were sorted into single units using the MountainSort spike sorting algorithm (Chung et al., 2017), which consists of a series of nonparametric statistical tests for unimodality. The algorithm projected the waveform of each spike-like event that it detected onto a 1-dimensional feature space. Spike clusters were considered single units if they passed the threshold criteria for both noise overlap and isolation. Noise overlap is defined as the fraction of “noise events” in a spike cluster, i.e. spike-like events that were not associated with any particular cluster. A lower noise overlap value indicated that a spike waveform was better distinguished from randomly sampled noise waveforms. Isolation indicated whether a spike waveform was distinguishable from other spike clusters in the 1-dimensional feature space. For the purposes of this study, spike events that had a noise overlap <0.08 and isolation >0.96 were retained for further analysis.

3.4.3 Visual stimulation

Visual stimuli were generated in MATLAB using the Psychophysics Toolbox package (RRID: CDR_002881)(Kleiner et al., 2007). Stimuli were shown to mice using a combined projector and polarization modulator system, as described previously (Tanabe et al., 2022; Fu et al., 2023). Briefly, the graphics processor (AMD Radeon Pro WX 7100) generated left-eye and right-eye images on the top and bottom half of every video frame, respectively. The projector (Optoma HD27HDR) then displayed the two halves in interleaved video frames at 120 Hz, so that frames intended to be viewed by the left and right eyes were shown in alternating sequence. The left eye and right eye received the images asynchronously, with the left eye preceding by 8.3 ms. These frames were then filtered through a polarization modulator (DepthQ Passive Bundle) and projected onto a polarization-preserving screen (Stewart Film RP 150). Animals viewed the stimulus frames through passive polarization filters that were mounted in 3D-printed frames and secured to the head-fixing post to maintain a constant position in front of the animal's eyes. For this study, the design of the passive polarization filters was customized for the age of the animal and the size of their head, in order to minimize light leaking from around oversized filters. The passive filters allowed the animal to view left-eye-intended frames only with the left eye, and vice versa for the right eye, and each eye received stimulation at 60 Hz. Gamma correction was applied for a linear transformation from grayscale values to luminance (range 6 to 87 cd/m²), and crosstalk with this system was measured with a photometer to be 1.9%. A custom 3D printed shield was used to prevent light from the projector from generating photoelectric artifacts in the physiological recording data. The viewing distance from the mouse to the projector screen was 25cm, consistent with previous mouse studies (Samonds et al., 2019).

The visual stimulus was centered over the estimated receptive field (RF) locations of the neuronal population being recorded. We used a flashing bright square on a dark background to roughly determine the center of the RF. RFs needed to be within 20 degrees of the contralateral visual field from the vertical meridian on the horizontal axis, and within the stimulus screen along the vertical axis. If the RF was not located within these boundaries, the probe was

retracted and reinserted in a location closer to the retinotopic center of the visual field. After 3 to 4 neurons at different depths along the probe had their RFs mapped with sufficient confidence, the average position of the RF centers was used as the visual stimulus center position.

We used a contrast-reversing checkerboard pattern (reversal rate 0.5 Hz, $10^\circ \times 10^\circ$) presented to both eyes to estimate the depth of the electrode contacts relative to the cortical layers. The checkerboard patch was centered at the average position of the previously mapped RFs and covered an area of $50^\circ \times 50^\circ$.

Drifting sinusoidal gratings were used to assess the orientation and disparity tuning of V1 neurons. Gratings were presented in a circular patch (radius 30°) that was centered over the average of the previously mapped RFs. Disparity in binocular gratings was generated by shifting the phase of the sinusoid seen by the right eye, and referred to as phase disparity. The orientation of binocular gratings ranged from 0° (vertical orientation, drifting rightward) to 157.5° , in 22.5° counterclockwise steps. The full range of phase disparity from 0° to 360° , in 45° steps, was tested for each orientation of the grating. The stimulus set also included monocular gratings for the left and right eyes, at the orientations specified above, and a control condition in which both eyes were shown a gray screen, for a total of 81 conditions. Stimulus conditions were presented in a pseudorandom order, where every condition was presented at least once before any condition was repeated, and recording continued until each stimulus had been repeated at least 10 times. Each trial consisted of a stimulus-on duration of 1 s, followed by an inter-stimulus interval of 0.5 s. The spatial frequency and temporal frequency of gratings were fixed at 0.04 cycles/degree and 2 Hz, respectively, and gratings were presented with full contrast.

A white noise stimulus was used to confirm the estimated RF center, as well as provide a more precise mapping of RF structure in recorded neurons (Ringach, 2002). The white noise stimulus design consisted of a square patch (30° by 30°) centered over the estimated RF center. The patch was then further split into squares that were 2° in height and width, and randomly

assigned a contrast value of bright, dark, or gray. Each frame was randomly generated, with independent versions for each eye, and the contrast values of each stimulus location was saved for RF analysis. The white noise patterns were refreshed at a rate of 20 frames/second until sufficient data had been gathered for RF analysis, for a total of 20-25 minutes.

3.4.4 Data analysis and statistics

This study used largely the same data processing pipeline as described in our previous study of binocular visual response properties in adult mouse cortex, including methods of determining visually response neurons, generating tuning functions, and LFP analysis.

RFs mapped using sparse white noise were analyzed by generating peristimulus time histograms of spike activity for possible combination of stimuli conditions – location of a stimulus square in the grid, whether the square was bright or dark, and whether the square appeared in the left or right eyes. Heatmaps were then generated for every neuron to map the receptive fields depending on the stimulus condition. In order to quantify the salience of receptive fields, we computed a signal-to-noise ratio (SNR) by comparing the variability of the RF heatmaps against the variability of a null hypothesis heatmap. The null version was generated by building heatmaps from the PSTH of the response 300 frame refreshes after the stimulus onset, in order to sample noise unrelated to any stimulus.

The MATLAB Statistics and Machine Learning Toolbox was used for all statistical tests. The Kruskal-Wallis test with Bonferroni correction was used to compare outcomes at different developmental timepoints, and further details on the number of cells and animals, as well as test statistics, are provided in Results. We did not utilize statistical methods to predetermine sample sizes, and animals were not assigned to control or experimental groups because such considerations were inapplicable to the design of this characterization study.

3.5 Results

3.5.1 Influence of visual experience on development of binocular integration

To study the development of binocular integration after the onset of visual experience, we used a 64-channel silicon microprobe that spanned the entire cortical depth (**Figure 3.1A**) to record from neurons at all layers. These recordings were performed in acute experiments from young mice spanning from the day of eye opening (aged between P12 and P14), until 15 days after eye opening (**Figure 3.1B**). Across the population of recorded neurons in V1 ($n=1078$), the proportion of neurons that were responsive to visual stimulation varied with age and visual experience. Notably, on the day of eye opening, a far lower proportion of neurons were visually responsive when compared with populations even one day later.

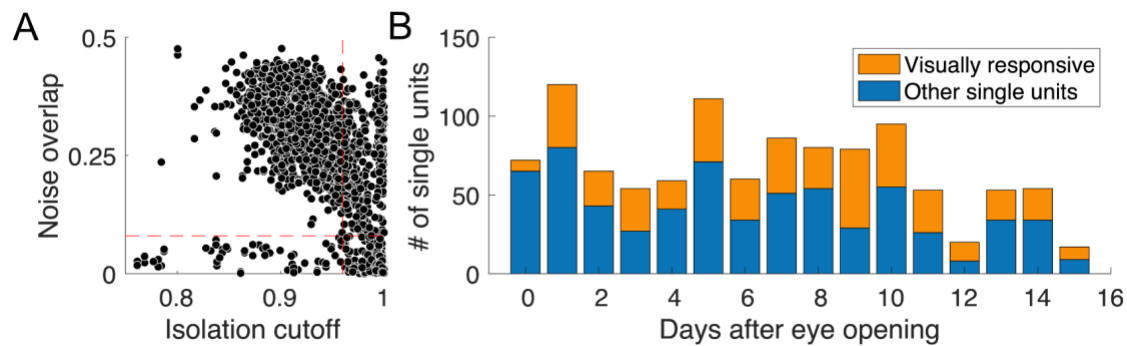


Figure 3.1. Single unit sorting and population data after eye opening.

- A.** Spikes were sorted into single units. Waveforms marked for further analysis as single units needed to fulfill two criteria: noise overlap < 0.08 and isolation cutoff > 0.96 , indicated by red dashed lines.
- B.** Number of visually responsive and non-visually responsive single units per day after eye opening.

In order to determine whether neurons at eye opening were less visually responsive independent of an overall decrease in firing rate, we examined the average spontaneous firing rate (**Figure 3.2A**) and average stimulus-evoked firing rate (**Figure 3.2B**). While spontaneous

firing rates on average did not change commensurate with visual experience ($\chi^2(5)=9.93$, $p=0.07$), stimulus-evoked firing rates were significantly lower around eye opening compared to all later timepoints ($\chi^2(5)=15.5$, $p=0.008$). However, other developmental changes to binocular integration properties, as described below, were observed to take place over the course of several days following eye opening, and cannot be explained entirely by the decrease in stimulus-evoked firing rate on the day of eye opening.

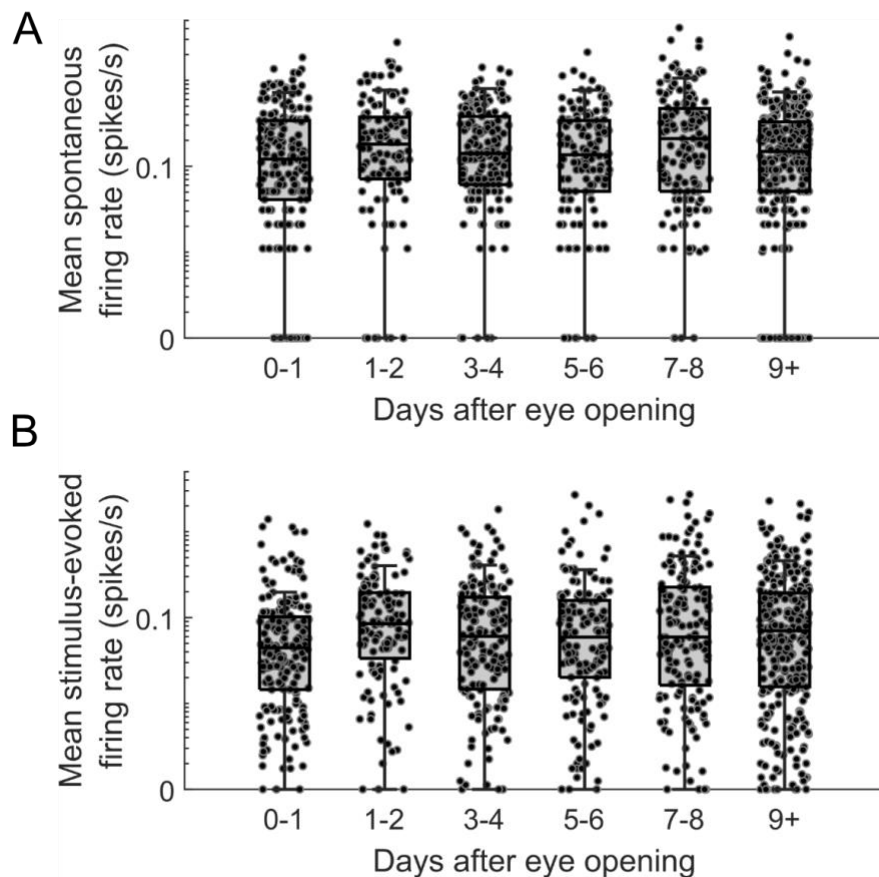


Figure 3.2. Spontaneous and stimulus-evoked firing rates.

- A. Spontaneous firing rate of single units did not significantly change across days after eye opening ($\chi^2(5)=9.93$, $p=0.07$).
- B. Stimulus evoked firing rate of single units was significantly depressed at day of eye opening ($\chi^2(5)=15.5$, $p=0.08$).

One such effect of visual experience is particularly apparent when observing how responses to binocular gratings become increasingly selective with additional days post eye-opening. From the day of eye opening to about two days later, responses to binocular gratings were barely discernable (**Figure 3.3A**, 2-D heatmap visualization of binocular responses in **Figure 3.3B**), while after about 3-4 days of visual experience, some selectivity to orientation was noticeable (**Figure 3.3C and D**). After around 7 days of visual experience, the recorded population contained many neurons that were both orientation and phase disparity selectivity, akin to the visual responses we characterized in adult mouse V1.

As the developmental changes we observed consisted of both orientation selectivity and phase disparity selectivity strengthening together, as visualized in the gradual appearance of a “hotspot” in the example 2-D heatmaps over time, we quantified the overall selectivity of a neuron to both orientation and phase disparity selectivity with a new index. In order to calculate this index, the 2-D heatmap for a neuron’s binocular grating responses first required “untwisting”, due to the manner in which the orientation axis in 180-degree space and the phase disparity axis in 360-degree space wrap around in an inverted manner. As shown in **Figure 3.3G**, a binocular grating with orientation 0° and phase disparity 90° is identical to a binocular grating with orientation 180° and phase disparity 270° (both outlined in blue). Following untwisting of the 2-D heatmap (**Figure 3H**), we calculated a combined orientation-and-phase-disparity selectivity index by taking the ratio between the amplitudes of the zeroth- and first-order harmonics of the 2-D tuning heatmap. This is mathematically equivalent to the method used to compute a global orientation selectivity index in other visual neuroscience literature (Mazurek et al., 2014), which prompted us to extend its application from a 1-dimensional visual response property such as orientation selectivity to our 2-dimensional visual response characterization.

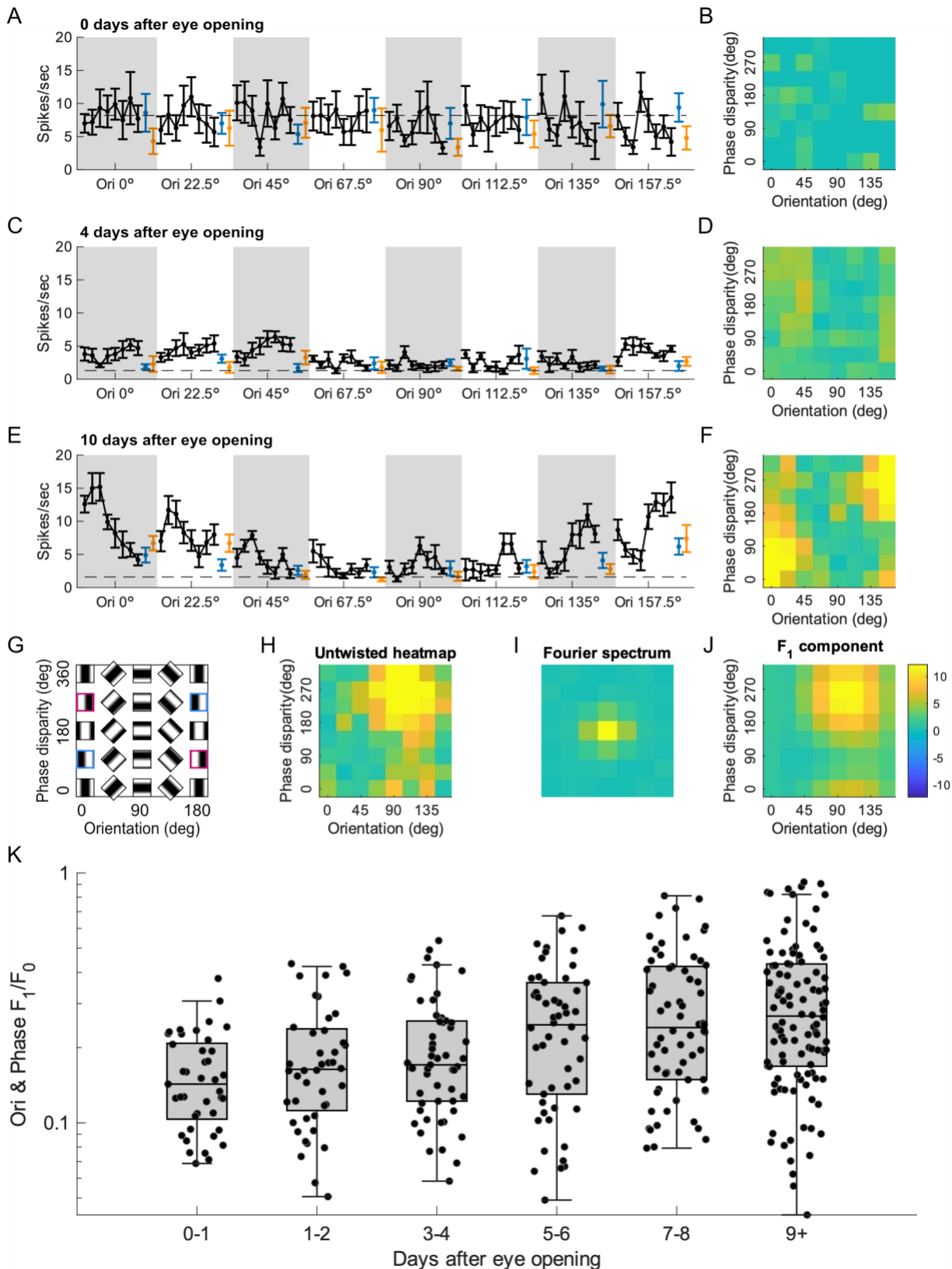


Figure 3.3. Example tuning curves and co-development of orientation selectivity and phase disparity selectivity after eye opening.

- A. Example tuning curves from a neuron at day of eye opening.
- B. Binocular responses from the example in A, to orientation and phase disparity combinations, represented as a 2-D heatmap.
- C. Example tuning curves from a neuron 3 days after eye opening.
- D. Binocular responses from the example in C, to orientation and phase disparity combinations, represented as a 2-D heatmap.
- E. Example tuning curves from a neuron 7 days after eye opening.
- F. Binocular responses from the example in E, to orientation and phase disparity combinations, represented as a 2-D heatmap.
- G. Schematic indicating how orientation and phase disparity axes wrap around in an inverted fashion. The conditions outlined in magenta and blue are in fact identical to one another, as detailed previously (Fu et al., 2023).
- H. The same 2-D heatmap from F, after untwisting.
- I. The 0th (center) and 1st order Fourier components of the untwisted heatmap in H.
- J. Inverse Fourier transform using the 0th and 1st order Fourier components derived in I. The resulting 2-D heatmap possesses most characteristics of the original heatmap in H.
- K. Selectivity to both orientation and phase disparity was represented with the ratio of F_1 to F_0 . This ratio steadily increases in the initial days after eye opening ($\chi^2(5)=41.83$, $p<0.001$), showing the maturation of both orientation and phase disparity selectivity with the accumulation of visual experience.

The F_1/F_0 ratio for orientation and phase disparity selectivity noticeably increased across days after eye opening, taking approximately 8-9 days to reach a level after which the average F_1/F_0 ratio plateaued ($\chi^2(5)=41.83$, $p<0.001$). This increase in the average F_1/F_0 ratio resulted not only from an increase in the highest ceiling of selectivity, but also from an increase in the floor, i.e. the neurons that were least selective for particular combinations of orientation and phase disparity still saw an increase in their selectivity. This indicates that the maturation of

binocular integration is happening across all visually responsive neurons in binocular V1 as a population, rather than a select few neurons achieving high levels of binocular responsiveness.

3.5.2 Developmental changes in LFP and receptive field structure

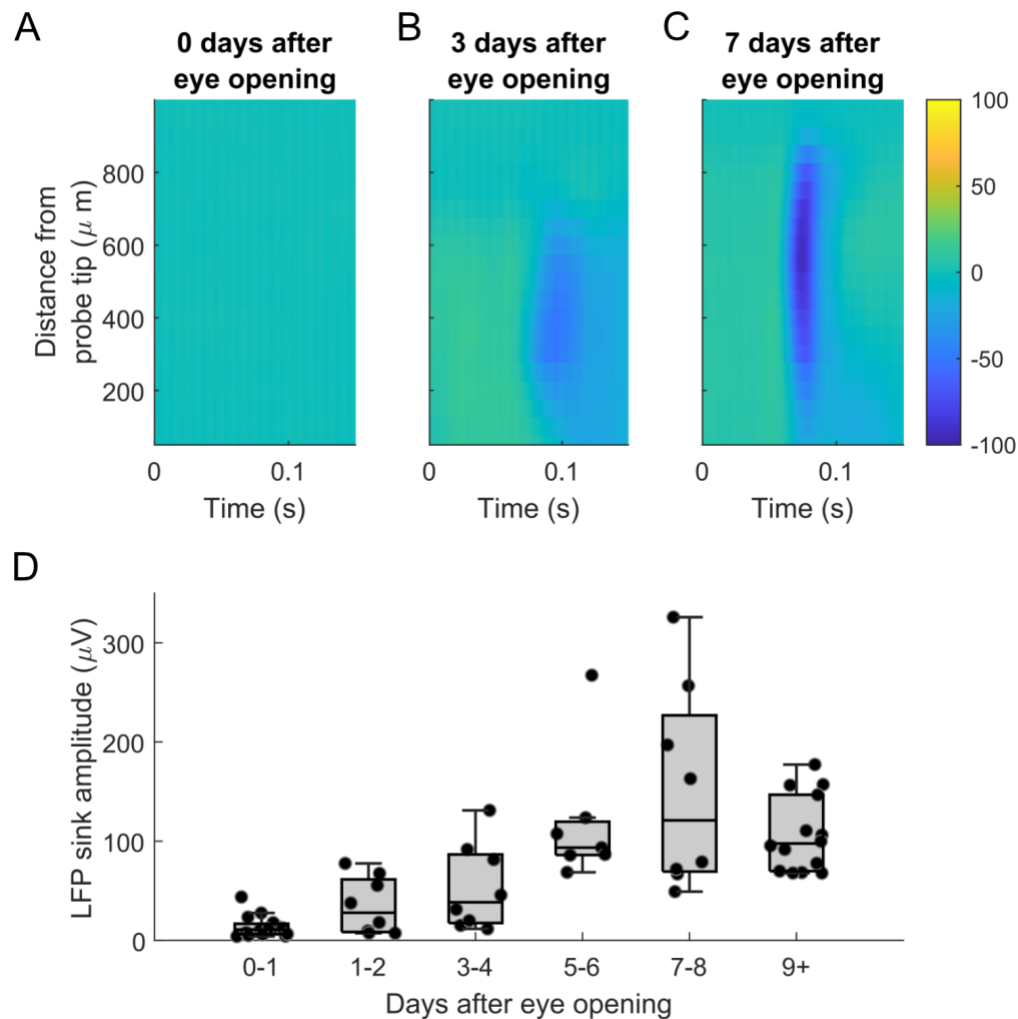


Figure 3.4. Local field potential changes after eye opening.

- A.** Example LFP on the day of eye opening as a function of time and depth in the cortex. Time $t=0$ s corresponds to when the stimulus switched polarity.
- B.** Example LFP at 3 days after eye opening as a function of time and depth in the cortex.
- C.** Example LFP at 7 days after eye opening as a function of time and depth in the cortex.

- D. The absolute value of the LFP sink amplitude at the most negative part of the voltage sink, plotted against days after eye opening. Significant growth in the sink amplitude is apparent between 0 and 6 days after eye opening ($\chi^2(5)=40.45$, $p<0.001$).

In addition to changes in binocular integration, we observed changes in other indications of V1 function. Previously, we had used the local field potential (LFP) response to a contrast-alternating checkerboard to approximate the cortical layer that neurons were located in, as the center of the negative sink evoked by the stimulus can be understood to occur at the depth of layer 4. However, in recordings occurring between 0 and 2 days after eye opening, this negative sink was almost absent (**Figure 3.4A**), and only began to be discernible at around 3-4 days after eye opening (**Figure 3.4B**). At around 6-7 days after eye opening, the negative sink is clearly distinguishable (**Figure 3.4C**), and the peak amplitude of the sink plateaus through the rest of the recording period (**Figure 3.4D**). The increase in LFP sink depth was statistically significant ($\chi^2(5)=40.45$, $p<0.001$).

The receptive field structure of binocular V1 neurons also became more defined throughout early development and after visual experience. Receptive fields in both the ipsilateral and contralateral eyes, mapped with either bright or dark spots, were so faint as to be almost non-visible on the day of eye opening (**Figure 3.5A**), but became better defined after several days of visual experience (**Figure 3.5B**). We quantified RF salience by combining all 4 receptive field mapping combinations (eye and stimulus luminance) into a singular image, and then calculating a signal-to-noise ratio (SNR) to assess all receptive field combinations together. The SNR increased as days after eye opening increased ($\chi^2(5)=45.33$, $p<0.001$).

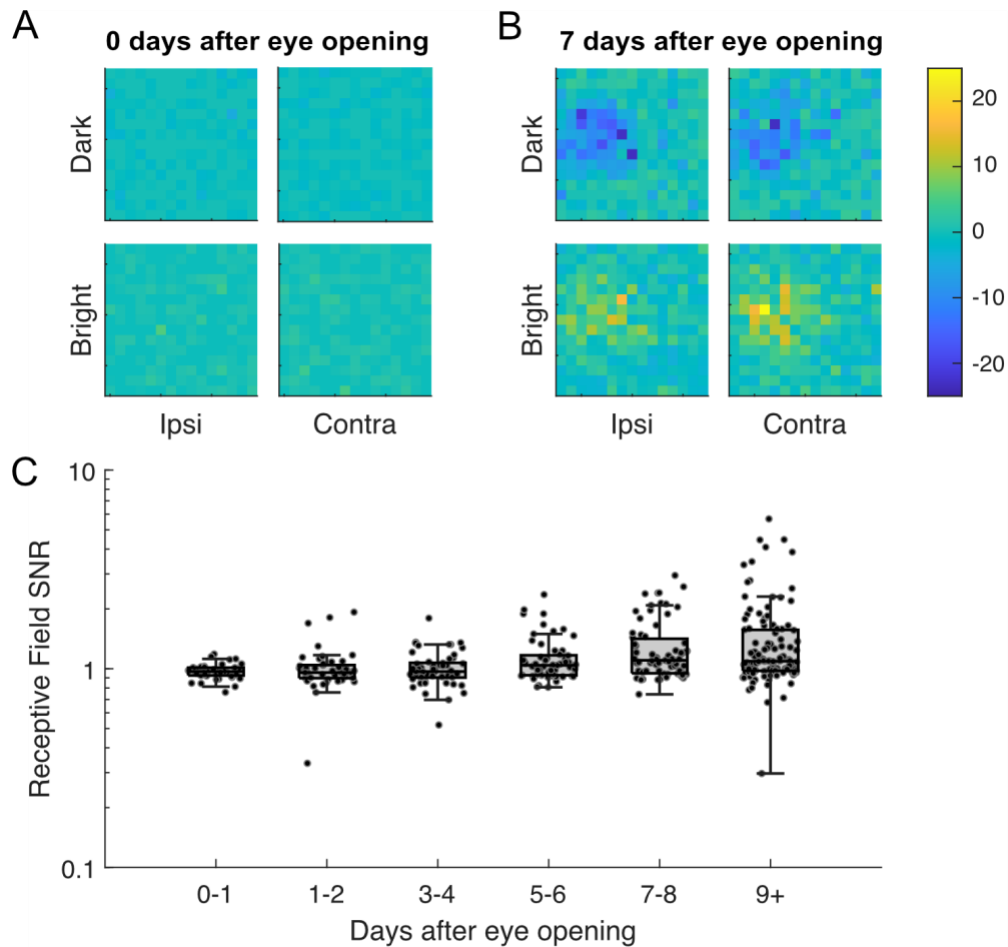


Figure 3.5. Receptive field changes after eye opening.

- A.** Example receptive field structures mapped with sparse noise, on the day of eye opening. Responses to dark and bright spots are on the top and bottom rows, and responses to spots shown to the ipsilateral or contralateral eyes are in the right and left columns, respectively.
- B.** Example receptive field structures 7 days after eye opening.
- C.** The signal-to-noise ratio (SNR) of all four receptive field mappings, plotted against days after eye opening. The SNR steadily increased with the accumulation of visual experience ($\chi^2(5)=45.33$, $p<0.001$).

3.6 Discussion

In this study, we measured binocular response properties in mouse V1 from the day of eye opening until 15 days post-eye opening, and found that both orientation and disparity selectivity were present at eye opening but weak. As we recorded from mice with progressively more visual experience, both visual properties strengthened, and from 8-9 days after eye opening onwards they had plateaued. Additionally, we observed evidence of maturation in other measures of neural activity such as the LFP and the population salience of receptive fields. Our data support that binocular disparity selectivity is a visual response property that matures dramatically as the visual system accumulates additional experience, but questions remain about neurons that are inherently capable of disparity selectivity at eye opening, i.e. prior to any visual experience.

3.6.1 Disparity selectivity in the developing visual system

Our recordings on the day of eye opening suggest that a subset of binocular neurons possess disparity selectivity at the time of eye opening, independent of experience-dependent input. This raises the possibility of these neurons serving as “anchors” or “pioneers” for the further refinement of disparity selectivity in V1. Spontaneous activity from the retina and LGN is sufficient to drive the initial formation of functional circuits (Hagihara et al., 2015), with further refinement occurring after visual experience is introduced into the system. It therefore follows that some proportion of neurons in binocular V1 receives a sufficient quantity of feedforward projections from the dLGN to be disparity selective at eye opening. Our observations on the maturation of LFP sink amplitude and receptive field structure are consistent with other reported values (Hoy and Niell, 2015; Thompson et al., 2017), which lends credence to the reliability of our observations of maturing disparity selectivity as well.

The fact that we observed no strongly selective neurons at this earliest timepoint could be due to a number of factors. The most salient reason could be that we recorded a significantly lower stimulus-evoked mean firing rate on the day of eye opening, as opposed to any other timepoint in the dataset. However, even with data from the first timepoint excluded, we still

observed orientation and disparity selectivity increasing in strength over time. Another possibility is that inhibitory neurons and other intracortical inputs are important for shaping strong selectivity, as has been described for orientation selectivity (Li et al., 2012; van Versendaal and Levelt, 2016). Inhibitory neurons are also known to change their firing patterns and inputs over the course of the critical period, meaning that the signals they send to binocular neurons could vary greatly over the timepoints during which our visual response property data was collected.

If these initially selective neurons do guide the development of disparity-selective neurons, why might untreated amblyopia result in a permanent loss of stereovision? Particularly in the case of strabismus-related amblyopia, where both retinas are receiving coherent images, albeit misaligned ones. One possibility is that V1 neurons require consistently aligned binocular input in order to strengthen disparity selectivity, and in cases of strabismus, the images received in the retina shift in the magnitude of their misalignment, depending on the direction the eyes are focused toward.

3.6.2 *Limitations of this study*

One obvious limit of this study is therefore a lack of eye-tracking data, to follow the eye movements made by young mice during this period of early visual exposure. This data may be especially difficult to obtain from young animals on the day of eye opening, because while the eyes have opened, the eyelids may remain narrowed for extended periods of time. This increases the difficulty of obtaining a clear image of the pupil for image recognition-based eye tracking.

The changes we observed in the LFP could have been due to developmental changes other than circuits rewiring in response to visual experience. Synapse density in the cortex increases rapidly during the third postnatal week (Lohmann and Kessels, 2014; Südhof, 2018), which overlaps with the period after eye-opening during which we were recording, and so our observation that the LFP sink amplitude was rapidly increasing could have been due to an increase in synaptic activity throughout the cortex. Some studies have also suggested that very

young mice in their second week of postnatal development undergo a transitory period of brain activity, where cortical networks slip in and out of a quiescent state without obvious behavioral affects (Shen and Colonnese, 2016; Domínguez et al., 2021). This could explain the low stimulus-evoked mean firing rate we observed, but could also have troubling implications for the deepening LFP amplitude sinks that we recorded from 0 to 3 days after eye opening. The initial lack of LFP we observed could have been due to network quiescence.

Finally, many of the binocular response properties we recorded were based on responses to drifting grating stimuli, where we used a spatial frequency of 0.04, consistent with previous studies from our group (Skyberg et al., 2022), and mouse V1 neurons overall have been reported to respond to higher spatial frequencies in the event of mismatched frequency preference between the two eyes (Salinas et al., 2017). However, visual experience has been reported to shift spatial frequency preference towards higher frequencies as development progresses, which might mean that the precise spatial frequency of a stimulus plays a smaller role in evoking peak responses in a younger animal (Nishio et al., 2021).

3.6.3 *Future directions*

Future studies on binocular development in V1 should aim to track individual binocular neurons longitudinally, likely using two-photon imaging or chronic electrophysiological methods. 2P imaging may be less desirable for these studies, given that it is less adept at capturing the full extent of activity in neurons with low firing rates, which in turn creates issues for the analysis of visual response properties (Cang et al., 2023).

Existing behavioral assessments for binocularity in mice include the visual cliff test and its relative, the pole descent task; gap crossing tasks, and prey capture behavior (Russell, 1932; Fox, 1965; Hoy et al., 2016; Samonds et al., 2019). A limitation shared by all of these tasks is that they can be performed with monocular vision, which would greatly increase the chance of obtaining a false positive, i.e. a determination that an animal is using stereovision when in actuality it is not. On the other hand, young mice might be less motivated to perform complex behaviors such as prey capture, or perform poorly at tasks such as pole descent due to a lack of

coordination or grip strength. In these scenarios, young mice would perform more poorly on stereovision behavioral tasks than anticipated.

In conclusion, we have found evidence of maturing binocular vision in young mice following the advent of visual experience, accompanied by dramatic changes in the overall stimulus-evoked field potential of the binocular visual cortex, as well as the structure of binocular receptive fields. These results indicate that disparity selectivity, and by extension binocular integration, is a visual response property that is refined and strengthened through experience-dependent input. However, the impact of this maturation in disparity selectivity upon the development of stereovision itself is unclear, and merits future study by way of longitudinal tracking or animal behavior.

4 Perspectives & Future Directions

Disparity selectivity provides a unique opportunity for studying information processing in the visual system. In this dissertation, I present a thorough characterization of visual responses to binocular stimuli. In adult V1, the majority of neurons in the binocular region are responsive to dichoptic stimuli in some way, but the complexity of their presentation can lead to an underestimation of the prevalence of binocular neurons in the early visual system. In developing V1, neurons responsive to disparity stimuli are present from eye opening, and their strengthening selectivity over time points to the importance of visual experience in refining these integrative circuits.

In this chapter, I will discuss my findings in the broader context of visual neuroscience literature and explore the applicability of these results to actual stereovision, as well as studies performed using different animal models. We will revisit the role of inhibitory inputs in computing binocular integration, as well as the role they play in the developing brain.

4.1 *Previous studies of binocularity in mice*

We show in Chapter 2 that the visual response properties of ocular dominance, interocular matching, and disparity selectivity are not correlated, though all have been used to assess binocularity of V1 neurons in the past. Other studies have observed the lack of correlation between ocular dominance and disparity selectivity, though it has been suggested that ocular dominance may play a role in normalizing the response if the inputs to the two eyes differ in contrast (Mitchell et al., 2023).

What should we make of the differing reports on whether mice visually respond to random dot stereograms? As briefly mentioned in the introduction, we observed minimal responses from mouse V1 to RDS, and so the disparity selectivity assessments in this dissertation's data chapters was all quantified from responses to phase disparity. However, other groups have reported disparity tuning in mice after RDS stimulation (Samonds et al., 2019; Chioma et al., 2020; Boone et al., 2021). However, these studies reported a relatively minor percentage of neurons in V1 being responsive to RDS stimuli, which is consistent with both our observations in mice using RDS.

4.2 *Is the mouse a good model for studying binocular vision?*

Much has been written on whether the mouse is even a good model system for studying vision at all (Huberman and Niell, 2011; Priebe and McGee, 2014; Seabrook et al., 2017). The earliest studies on the neural mechanisms were performed in the cat, and primate research continues to be a source of high-quality data because of the close resemblance between their visual system and that of humans. Primates also rely on vision in a significant way to engage with their environment, which can be assessed with trained behaviors.

In contrast, mice were not an intuitive choice of a model system for visual neuroscience. Mice have poor visual acuity, lack many ocular structures and brain organization that are important to visual processing in humans, and appear to rely more on olfactory and auditory inputs to navigate their environment. However, once mouse V1 neurons were characterized and

it was demonstrated that visual manipulations in the mouse could be used to study plasticity (Gordon and Stryker, 1996), the mouse was widely adopted as a model system due to its cost-effectiveness and the wealth of compatible genetic tools (Leinonen and Tanila, 2018). In recent years, the tree shrew has attracted significant interest (Fitzpatrick, 1996). Despite appearing physically similar to rodents or squirrels, the tree shrew is evolutionarily closer to primates, which is mirrored in its brain and eyes. Further investigations of binocular processing might be more complete if data from mouse studies is complemented with data from animal models that more closely resemble the human visual system.

That being said, the mouse occupies a unique role as an animal model due to its utility and ubiquity. The wide variety of genetic tools that can be applied to the mouse allow researchers to alter genes and circuits with relative ease, especially once optogenetics come into play. These can be then assessed with functional behavioral assays that depend on vision, such as social recognition of other mice and prey capture (Hoy et al., 2016; Young et al., 2018). If ipsilateral inputs to V1 are ablated, the success rate of prey capture decreases, suggesting that stereovision plays some role in this behavior (Johnson et al., 2021). Finally, the mouse brain and specifically the visual system has been the subject of the MICrONS project, an ambitious connectomics projects that thus far has mapped portions of mouse V1 and higher visual areas through a combination of *in vivo* calcium imaging and electron microscopy reconstruction (Bae et al., 2025; Ding et al., 2025). Ultimately, the mouse is a powerful model for studying vision, so long as researchers make use of the plethora of tools available, but with some awareness of how the mouse visual system can and cannot recapitulate aspect of human vision.

4.3 *Intracortical inhibition in the visual system*

The most basic feedforward models that we have discussed thus far only account for excitatory synapses, but as has been noted throughout this dissertation, the importance of inhibitory input cannot be discounted, particularly given their clear contribution to binocular integration. We know that cortical activity in awake animals is actually dominated by inhibitory neurons, indicating their importance in conscious perceptual processes (Haider et al., 2013).

4.3.1 *Inhibition and disparity selectivity*

Inhibitory inputs contribute in a multitude of ways to cortical computations other than disparity selectivity. As mentioned earlier in Section 1.1.2.3 regarding updated versions of the feedforward model, it is known that PV interneurons mediate gain control to maintain selectivity despite shifts in contrast (Troyer et al., 1998; Callaway, 2004). SST neurons contribute to surround suppression by responding selectively to large stimuli and inhibiting all other neuron types in the cortex – excitatory, PV, and VIP (Adesnik et al., 2012; Niell and Scanziani, 2021).

With regards to disparity selectivity, both the data presented in this dissertation and other studies indicate that PV interneurons are themselves disparity selective, but weakly selective in comparison to excitatory neurons. Because PV neurons draw their inputs from surrounding excitatory neurons, their weak selectivity may be a result of pooling inputs from neurons with vastly disparate tuning, given the salt-and-pepper organization of mouse V1 (Scholl et al., 2015). This could be one reason why mouse neurons respond weakly to random dot stereograms (Tanabe et al., 2022); the pooled gain control effect is so strong that it results in a dampening of any disparity selectivity, as the excitatory neurons that send the strongest inputs to a nearby PV neuron receive the strongest inhibition feedback in return (Znamenskiy et al., 2024). In a tree shrew's columnar cortex, this instead results in sharpened disparity selectivity. Further exploration of this topic could examine whether temporary inhibition of PV activity in mouse V1 can increase RDS disparity selectivity.

Finally, it should be noted that the proportion of fast-spiking versus regular-spiking neurons reported in Chapter 2 is on the high end of the proportion of PV neurons in the cortex as described in the literature, which ranges anywhere between 10-30% (DeFelipe et al., 2013). The explanation for this apparent discrepancy may range from technical to idiosyncratic. First, it has been documented that automated spike-sorting technology, while improving at a rapid pace, struggles with sorting neurons with low SNR or bursting firing rates (Buccino et al., 2022), which could account for an overrepresentation of cells with higher firing rates in the single unit dataset. Other studies have shown that inhibitory neurons are not evenly distributed

throughout the cortex, but rather may form “hot zones” in certain columnar areas and layers (Meyer et al., 2011).

4.3.2 *Inhibition and development*

Inhibitory innervation serves as a key switch regulating cortical plasticity. In mice lacking a GABA-synthesizing protein, merely reducing GABA levels was sufficient to prevent OD plasticity, while administering additional GABA via benzodiazepines could rescue the phenotype (Hensch et al., 1998). PV cells especially play a major role in regulating the developmental timeline of the cortex.

Prior to the onset of the experience-dependent critical period, inhibitory input to pyramidal cells is dominated by SST cells, particularly in L2/3. As the critical period opens, PV cells mature and begin to fire more, increasing the strength of their inputs to pyramidal cells (**Figure 4.1**). Overall, the maturation of PV activity in the cortex appears to be tightly linked to the time window of the critical period, as studies have shown that the window for cortical plasticity does not open while PV cells are immature, but once PV cells have fully matured, the cortex is no longer plastic (van Versendaal and Levelt, 2016; Hooks and Chen, 2020). The reasons for this are unclear, but modeling studies suggest that PV-mediated inhibition serves to dampen noisy inputs and enhance important circuit-refining ones (Toyoizumi et al., 2013), which is somewhat reminiscent of the gain control function played by PV cells in adult V1.

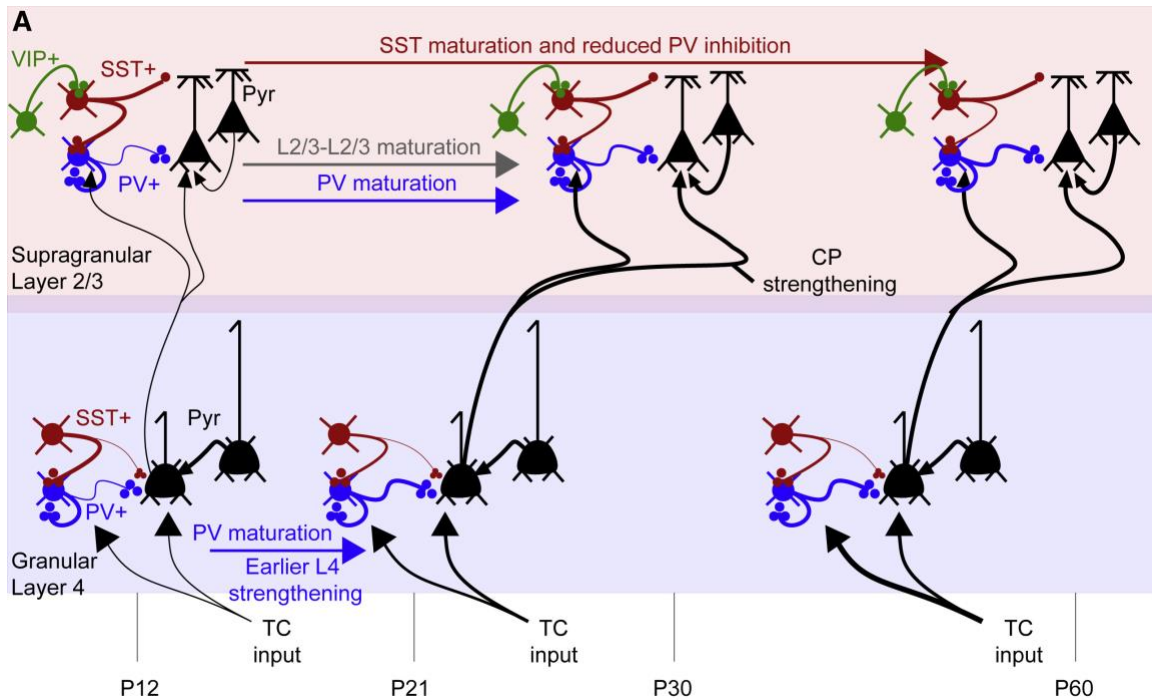


Figure 4.1. Changes in inhibitory innervation during the critical period. Adapted from (Hooks and Chen, 2020)

4.4 Disparity selectivity and stereovision

Throughout this dissertation, we have made references to the importance of disparity selectivity in V1 for stereovision. It should be noted that while V1 neurons are some of the earliest in the visual pathway to integrate binocular inputs, this does not equate to them being able to compute all the information needed for depth perception. Empirical evidence has shown that V1 neurons can be “fooled” into responding to stimuli that contain disparity that do not actually correlate to differences in real depth (Fleet et al., 1996).

In visual psychophysics and later computer vision, a perceptual system needs to be able to solve the correspondence problem in order to compute true depth (Read, 2005). This refers to the ability to determine which portions of one image correspond to the same points in a second image. In **Figure 4.2**, the top row displays two schematics, showing how 5 letters would project to locations on the retinae of two eyes. However, based on the way that the light rays cross over and given only the retinal images, the origins of the light rays could have two

different solutions – one with 5 letters at the same distance, and one with 6 total letters where 4 appear closer to the viewer. A cell that does not solve the correspondence problem would be unable to distinguish between the two solutions, and would fire in response to either correct or false matches, as depicted in the schematics on the bottom row.

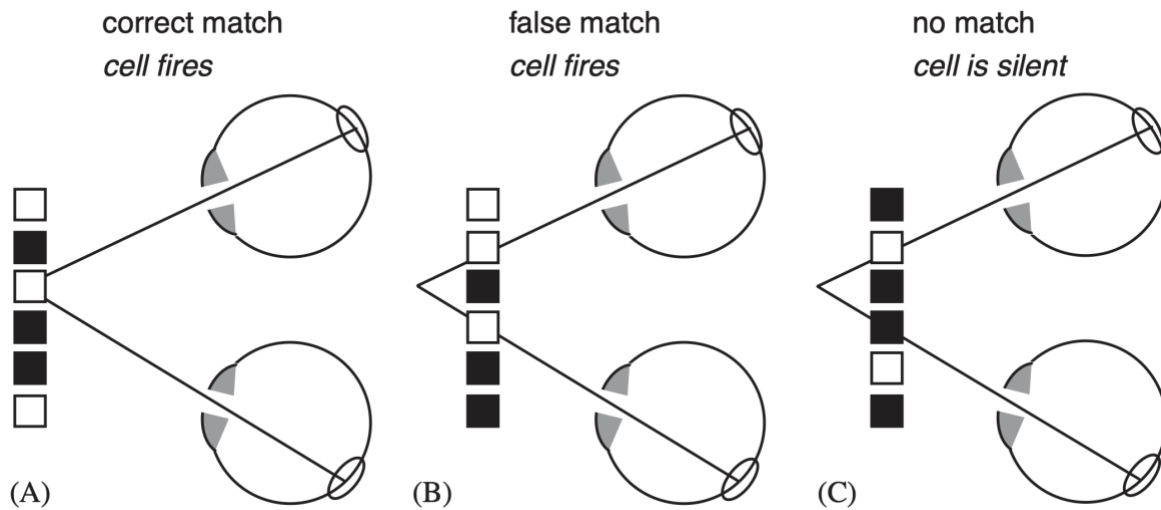
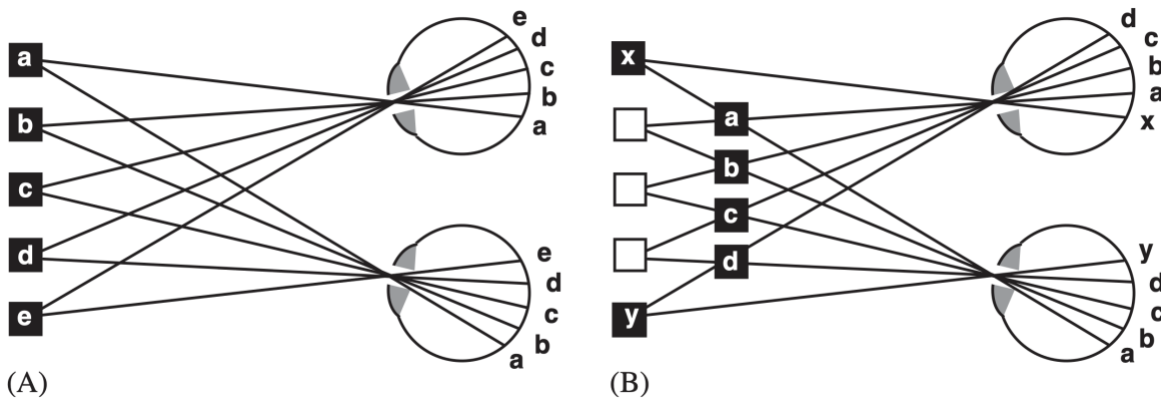


Figure 4.2. Stereoscopic correspondence problem. Schematics depicting two solutions to a correspondence problem (top). Stimuli that fulfill V1 neuron receptive field requirements, i.e. a particular disparity, will create a response regardless of whether they truly correspond to a real depth in space (bottom). Adapted from (Read, 2005).

A neuron or system able to solve the correspondence problem is therefore capable of global stereopsis, i.e. the ability to discern true depth given two disparate images, by processing the entirety of both views and finding their corresponding features. Binocular V1 neurons, due to the spatial limits and structures of their receptive fields, only perform local matches. However, the false match scenario shown in the schematic figure was found to be relatively rare when primate V1 was shown anticorrelated RDS images, which contain disparities but do not correspond to real depths (Cumming and Parker, 1997). This may indicate that V1 still plays a role in filtering out false matches before the information is passed to other areas for featural processing.

Although V1 itself does not generate the outputs needed for true global stereopsis, it plays a key role in preprocessing inputs and extracting the necessary information for depth perception. Future research in this direction is needed to determine whether V1 neurons in mice also filter out false correspondence matches, similar to V1 neurons in primates. It will be challenging that anticorrelated RDS-like stimuli would likely not be applicable to rodent studies, and so a computational approach where inputs are sent to synthetic mouse V1 neurons may be needed to address this question.

4.5 Concluding Remarks

Binocular integration by disparity selective cells provides a powerful framework for studying information processing in the visual system. In this dissertation, we highlight the prevalence of binocular neurons in adult and developing V1, by comprehensively characterizing visual response properties following dichoptic stimulation. Together, these results advance our understanding of how binocular processing emerges and can be measured, as well as how it matures over the course of the critical period.

References

- Ackman JB, Burbridge TJ, Crair MC (2012) Retinal waves coordinate patterned activity throughout the developing visual system. *Nature* 490:219–225.
- Adesnik H, Bruns W, Taniguchi H, Huang ZJ, Scanziani M (2012) A neural circuit for spatial summation in visual cortex. *Nature* 490:226–231.
- Anzai A, Ohzawa I, Freeman RD (1997) Neural mechanisms underlying binocular fusion and stereopsis: position vs. phase. *Proc Natl Acad Sci U S A* 94:5438–5443.
- Anzai A, Ohzawa I, Freeman RD (1999) Neural Mechanisms for Processing Binocular Information II. Complex Cells. *Journal of Neurophysiology* 82:909–924.
- Atencio CA, Schreiner CE (2008) Spectrotemporal Processing Differences between Auditory Cortical Fast-Spiking and Regular-Spiking Neurons. *J Neurosci* 28:3897–3910.
- Bae JA et al. (2025) Functional connectomics spanning multiple areas of mouse visual cortex. *Nature* 640:435–447.
- Banks MS, Hoffman DM, Kim J, Wetzstein G (2016) 3D Displays. *Annual Review of Vision Science* 2:397–435.
- Bansal A, Singer JH, Hwang BJ, Xu W, Beaudet A, Feller MB (2000) Mice Lacking Specific Nicotinic Acetylcholine Receptor Subunits Exhibit Dramatically Altered Spontaneous Activity Patterns and Reveal a Limited Role for Retinal Waves in Forming ON and OFF Circuits in the Inner Retina. *J Neurosci* 20:7672–7681.
- Barlow HB, Blakemore C, Pettigrew JD (1967) The neural mechanism of binocular depth discrimination. *The Journal of Physiology* 193:327–342.
- Boone HC, Samonds JM, Crouse EC, Barr C, Priebe NJ, McGee AW (2021) Natural binocular depth discrimination behavior In mice explained by visual cortical activity. *Current Biology* 0 Available at: [https://www.cell.com/current-biology/abstract/S0960-9822\(21\)00272-4](https://www.cell.com/current-biology/abstract/S0960-9822(21)00272-4) [Accessed March 24, 2021].
- Bruno RM, Simons DJ (2002) Feedforward Mechanisms of Excitatory and Inhibitory Cortical Receptive Fields. *J Neurosci* 22:10966–10975.
- Buccino AP, Garcia S, Yger P (2022) Spike sorting: new trends and challenges of the era of high-density probes. *Prog Biomed Eng* 4:022005.
- Butts DA (2002) Retinal Waves: Implications for Synaptic Learning Rules during Development. *Neuroscientist* 8:243–253.

- Callaway EM (2004) Feedforward, feedback and inhibitory connections in primate visual cortex. *Neural Networks* 17:625–632.
- Cang J, Fu J, Tanabe S (2023) Neural circuits for binocular vision: Ocular dominance, interocular matching, and disparity selectivity. *Frontiers in Neural Circuits* 17 Available at: <https://www.frontiersin.org/articles/10.3389/fncir.2023.1084027> [Accessed February 20, 2023].
- Cang J, Kaneko M, Yamada J, Woods G, Stryker MP, Feldheim DA (2005) Ephrin-as guide the formation of functional maps in the visual cortex. *Neuron* 48:577–589.
- Chang JT, Whitney D, Fitzpatrick D (2020) Experience-Dependent Reorganization Drives Development of a Binocularly Unified Cortical Representation of Orientation. *Neuron* 107:338-350.e5.
- Chen P-Y, Chen C-C, Tyler CW (2021) A gain-control disparity energy model for perceived depth from disparity. *Vision Research* 181:38–46.
- Chioma AL, Bonhoeffer T, Hübener M (2019) Area-Specific Mapping of Binocular Disparity across Mouse Visual Cortex. *Current Biology* 29:2954-2960.e5.
- Chioma AL, Bonhoeffer T, Hübener M (2020) Disparity Sensitivity and Binocular Integration in Mouse Visual Cortex Areas. *J Neurosci* 40:8883–8899.
- Chung JE, Magland JF, Barnett AH, Tolosa VM, Tooker AC, Lee KY, Shah KG, Felix SH, Frank LM, Greengard LF (2017) A Fully Automated Approach to Spike Sorting. *Neuron* 95:1381-1394.e6.
- Cumming BG, DeAngelis GC (2001) The physiology of stereopsis. *Annu Rev Neurosci* 24:203–238.
- Cumming BG, Parker AJ (1997) Responses of primary visual cortical neurons to binocular disparity without depth perception. *Nature* 389:280–283.
- DeAngelis GC, Ohzawa I, Freeman RD (1991) Depth is encoded in the visual cortex by a specialized receptive field structure. *Nature* 352:156–159.
- DeFelipe J et al. (2013) New insights into the classification and nomenclature of cortical GABAergic interneurons. *Nat Rev Neurosci* 14:202–216.
- Ding Z et al. (2025) Functional connectomics reveals general wiring rule in mouse visual cortex. *Nature* 640:459–469.
- Domínguez S, Ma L, Yu H, Pouchelon G, Mayer C, Spyropoulos GD, Cea C, Buzsáki G, Fishell G, Khodagholy D, Gelinás JN (2021) A transient postnatal quiescent period precedes emergence of mature cortical dynamics Nelson SB, Moore T, Nelson SB, Colonnese MT,

- eds. *eLife* 10:e69011.
- Espinosa JS, Stryker MP (2012) Development and Plasticity of the Primary Visual Cortex. *Neuron* 75:230–249.
- Feldheim DA, Kim YI, Bergemann AD, Frisén J, Barbacid M, Flanagan JG (2000) Genetic analysis of ephrin-A2 and ephrin-A5 shows their requirement in multiple aspects of retinocollicular mapping. *Neuron* 25:563–574.
- Feldheim DA, Nakamoto M, Osterfield M, Gale NW, DeChiara TM, Rohatgi R, Yancopoulos GD, Flanagan JG (2004) Loss-of-function analysis of EphA receptors in retinotectal mapping. *J Neurosci* 24:2542–2550.
- Finn IM, Priebe NJ, Ferster D (2007) The Emergence of Contrast-Invariant Orientation Tuning in Simple Cells of Cat Visual Cortex. *Neuron* 54:137–152.
- Fitzpatrick D (1996) The Functional Organization of Local Circuits in Visual Cortex: Insights from the Study of Tree Shrew Striate Cortex. *Cerebral Cortex* 6:329–341.
- Fleet DJ, Wagner H, Heeger DJ (1996) Neural encoding of binocular disparity: Energy models, position shifts and phase shifts. *Vision Research* 36:1839–1857.
- Fox MW (1965) The visual cliff test for the study of visual depth perception in the mouse. *Animal Behaviour* 13:232-IN3.
- Fu J, Tanabe S, Cang J (2023) Widespread and multifaceted binocular integration in the mouse primary visual cortex. *J Neurosci* Available at: <https://www.jneurosci.org/content/43/38/6495> [Accessed August 25, 2023].
- Glickfeld LL, Olsen SR (2017) Higher-Order Areas of the Mouse Visual Cortex. *Annu Rev Vis Sci* 3:251–273.
- Glickfeld LL, Reid RC, Andermann ML (2014) A mouse model of higher visual cortical function. *Current Opinion in Neurobiology* 24:28–33.
- Goltstein PM, Laubender D, Bonhoeffer T, Hübener M (2025) A column-like organization for ocular dominance in mouse visual cortex. *Nat Commun* 16:1926.
- Gordon JA, Stryker MP (1996) Experience-Dependent Plasticity of Binocular Responses in the Primary Visual Cortex of the Mouse. *J Neurosci* 16:3274–3286.
- Grubb MS, Rossi FM, Changeux JP, Thompson ID (2003) Abnormal functional organization in the dorsal lateral geniculate nucleus of mice lacking the beta 2 subunit of the nicotinic acetylcholine receptor. *Neuron* 40:1161–1172.
- Gu Y, Cang J (2016) Binocular matching of thalamocortical and intracortical circuits in the

- mouse visual cortex Nelson SB, ed. *eLife* 5:e22032.
- Guido W, Tuma N, Spear PD (1989) Binocular interactions in the cat's dorsal lateral geniculate nucleus. I. Spatial-frequency analysis of responses of X, Y, and W cells to nondominant-eye stimulation. *Journal of Neurophysiology* 62:526–543.
- Hagihara KM, Murakami T, Yoshida T, Tagawa Y, Ohki K (2015) Neuronal activity is not required for the initial formation and maturation of visual selectivity. *Nat Neurosci* 18:1780–1788.
- Haider B, Häusser M, Carandini M (2013) Inhibition dominates sensory responses in awake cortex. *Nature* 493:97–100.
- Hanganu IL, Ben-Ari Y, Khazipov R (2006) Retinal Waves Trigger Spindle Bursts in the Neonatal Rat Visual Cortex. *J Neurosci* 26:6728–6736.
- Hartigan JA, Hartigan PM (1985) The Dip Test of Unimodality. *The Annals of Statistics* 13:70–84.
- Hensch TK, Fagiolini M, Mataga N, Stryker MP, Baekkeskov S, Kash SF (1998) Local GABA Circuit Control of Experience-Dependent Plasticity in Developing Visual Cortex. *Science* 282:1504–1508.
- Hindges R, McLaughlin T, Genoud N, Henkemeyer M, O'Leary DDM (2002) EphB forward signaling controls directional branch extension and arborization required for dorsal-ventral retinotopic mapping. *Neuron* 35:475–487.
- Hofbauer A, Dräger UC (1985) Depth segregation of retinal ganglion cells projecting to mouse superior colliculus. *Journal of Comparative Neurology* 234:465–474.
- Hofer SB, Mrsic-Flogel TD, Bonhoeffer T, Hübener M (2006) Lifelong learning: ocular dominance plasticity in mouse visual cortex. *Current Opinion in Neurobiology* 16:451–459.
- Hoffmann K-P, Stone J (1971) Conduction velocity of afferents to cat visual cortex: a correlation with cortical receptive field properties. *Brain Research* 32:460–466.
- Honnuraiah S, Huang H, Ryan WJ, Broersen R, Connelly WM, Stuart GJ (2024) Cellular and circuit mechanisms underlying binocular vision. Available at: <http://biorxiv.org/lookup/doi/10.1101/2024.03.11.584536> [Accessed June 9, 2024].
- Hooks BM, Chen C (2020) Circuitry Underlying Experience-Dependent Plasticity in the Mouse Visual System. *Neuron* 106:21–36.
- Howarth M, Walmsley L, Brown TM (2014) Binocular Integration in the Mouse Lateral Geniculate Nuclei. *Current Biology* 24:1241–1247.
- Hoy JL, Niell CM (2015) Layer-Specific Refinement of Visual Cortex Function after Eye Opening

- in the Awake Mouse. *J Neurosci* 35:3370–3383.
- Hoy JL, Yavorska I, Wehr M, Niell CM (2016) Vision drives accurate approach behavior during prey capture in laboratory mice. *Current Biology* 26:3046–3052.
- Hubel DH, Wiesel TN (1962) Receptive fields, binocular interaction and functional architecture in the cat's visual cortex. *J Physiol* 160:106-154.2.
- Hubel DH, Wiesel TN (1963) Receptive fields of cells in striate cortex of very young, visually inexperienced kittens. *Journal of Neurophysiology* 26:994–1002.
- Hubel DH, Wiesel TN (1965) Binocular interaction in striate cortex of kittens reared with artificial squint. *Journal of Neurophysiology* 28:1041–1059.
- Huberman AD, Niell CM (2011) What can mice tell us about how vision works? *Trends in Neurosciences* 34:464–473.
- Huh CYL, Abdelaal K, Salinas KJ, Gu D, Zeitoun J, Velez DXF, Peach JP, Fowlkes CC, Gandhi SP (2019) Long-term monocular deprivation during juvenile critical period disrupts binocular integration in mouse visual thalamus. *J Neurosci* Available at: <https://www.jneurosci.org/content/early/2019/11/22/JNEUROSCI.1626-19.2019> [Accessed June 21, 2023].
- Jaepel J, Hübener M, Bonhoeffer T, Rose T (2017) Lateral geniculate neurons projecting to primary visual cortex show ocular dominance plasticity in adult mice. *Nat Neurosci* 20:1708–1714.
- Jang J, Song M, Paik S-B (2020) Retino-Cortical Mapping Ratio Predicts Columnar and Salt-and-Pepper Organization in Mammalian Visual Cortex. *Cell Reports* 30:3270-3279.e3.
- Jenks KR, Shepherd JD (2020) Experience-Dependent Development and Maintenance of Binocular Neurons in the Mouse Visual Cortex. *Cell Reports* 30:1982-1994.e4.
- Johnson KP, Fitzpatrick MJ, Zhao L, Wang B, McCracken S, Williams PR, Kerschensteiner D (2021) Cell-type-specific binocular vision guides predation in mice. *Neuron* Available at: <https://www.sciencedirect.com/science/article/pii/S0896627321001586> [Accessed April 20, 2021].
- Julesz B (1971) *Foundations of cyclopean perception*. Oxford, England: U. Chicago Press.
- Kameyama K, Sohya K, Ebina T, Fukuda A, Yanagawa Y, Tsumoto T (2010) Difference in Binocularity and Ocular Dominance Plasticity between GABAergic and Excitatory Cortical Neurons. *J Neurosci* 30:1551–1559.
- Kaneko M, Stryker MP (2017) Homeostatic plasticity mechanisms in mouse V1. *Philosophical Transactions of the Royal Society B: Biological Sciences* 372:20160504.

- Kara P, Boyd JD (2009) A micro-architecture for binocular disparity and ocular dominance in visual cortex. *Nature* 458:627–631.
- Kawaguchi Y, Kondo S (2002) Parvalbumin, somatostatin and cholecystokinin as chemical markers for specific GABAergic interneuron types in the rat frontal cortex. *J Neurocytol* 31:277–287.
- Kleiner M, Brainard D, Pelli D (2007) What's new in Psychtoolbox-3? *Perception* 36:14.
- Leinonen H, Tanila H (2018) Vision in laboratory rodents—Tools to measure it and implications for behavioral research. *Behavioural Brain Research* 352:172–182.
- LeVay S, Stryker MP, Shatz CJ (1978) Ocular dominance columns and their development in layer IV of the cat's visual cortex: A quantitative study. *Journal of Comparative Neurology* 179:223–244.
- LeVay S, Voigt T (1988) Ocular dominance and disparity coding in cat visual cortex. *Visual Neuroscience* 1:395–414.
- Levine JN, Chen H, Gu Y, Cang J (2017) Environmental Enrichment Rescues Binocular Matching of Orientation Preference in the Mouse Visual Cortex. *J Neurosci* 37:5822–5833.
- Li Y, Ma W, Pan C, Zhang LI, Tao HW (2012) Broadening of Cortical Inhibition Mediates Developmental Sharpening of Orientation Selectivity. *J Neurosci* 32:3981–3991.
- Liu B, Li P, Li Y, Sun YJ, Yanagawa Y, Obata K, Zhang LI, Tao HW (2009) Visual Receptive Field Structure of Cortical Inhibitory Neurons Revealed by Two-Photon Imaging Guided Recording. *J Neurosci* 29:10520–10532.
- Lohmann C, Kessels HW (2014) The developmental stages of synaptic plasticity. *The Journal of Physiology* 592:13–31.
- Martinez LM, Alonso J-M (2003) Complex Receptive Fields in Primary Visual Cortex. *Neuroscientist* 9:317–331.
- Martins JA, Lam RL, Rodrigues JMF, du Buf JMH (2018) Expression-invariant face recognition using a biological disparity energy model. *Neurocomputing* 297:82–93.
- Martins JA, Rodrigues JMF, du Buf JMH (2011) Disparity energy model using a trained neuronal population. In: 2011 IEEE International Symposium on Signal Processing and Information Technology (ISSPIT), pp 287–292 Available at: <https://ieeexplore.ieee.org/document/6151575> [Accessed March 16, 2025].
- Mazurek M, Kager M, Van Hooser SD (2014) Robust quantification of orientation selectivity and direction selectivity. *Front Neural Circuits* 8 Available at: <https://www.frontiersin.org/articles/10.3389/fncir.2014.00092/full> [Accessed April 6,

2021].

- McGee AW, Yang Y, Fischer QS, Daw NW, Strittmatter SM (2005) Experience-Driven Plasticity of Visual Cortex Limited by Myelin and Nogo Receptor. *Science* 309:2222–2226.
- McLaughlin T, Torborg CL, Feller MB, O’Leary DDM (2003) Retinotopic Map Refinement Requires Spontaneous Retinal Waves during a Brief Critical Period of Development. *Neuron* 40:1147–1160.
- Meyer AF, O’Keefe J, Poort J (2020) Two Distinct Types of Eye-Head Coupling in Freely Moving Mice. *Current Biology* 30:2116–2130.e6.
- Meyer HS, Schwarz D, Wimmer VC, Schmitt AC, Kerr JND, Sakmann B, Helmstaedter M (2011) Inhibitory interneurons in a cortical column form hot zones of inhibition in layers 2 and 5A. *Proceedings of the National Academy of Sciences* 108:16807–16812.
- Mitchell BA, Carlson BM, Westerberg JA, Cox MA, Maier A (2023) A role for ocular dominance in binocular integration. *Current Biology* 33:3884–3895.e5.
- Mitzdorf U (1985) Current source-density method and application in cat cerebral cortex: investigation of evoked potentials and EEG phenomena. *Physiological Reviews* 65:37–100.
- Mrsic-Flogel TD, Hofer SB, Ohki K, Reid RC, Bonhoeffer T, Hübener M (2007) Homeostatic Regulation of Eye-Specific Responses in Visual Cortex during Ocular Dominance Plasticity. *Neuron* 54:961–972.
- Niell CM, Scanziani M (2021) How Cortical Circuits Implement Cortical Computations: Mouse Visual Cortex as a Model. *Annu Rev Neurosci* 44:517–546.
- Niell CM, Stryker MP (2008) Highly selective receptive fields in mouse visual cortex. *J Neurosci* 28:7520–7536.
- Nishio N, Hayashi K, Ishikawa AW, Yoshimura Y (2021) The role of early visual experience in the development of spatial-frequency preference in the primary visual cortex. *The Journal of Physiology* 599:4131–4152.
- Ohzawa I, DeAngelis GC, Freeman RD (1990) Stereoscopic depth discrimination in the visual cortex: neurons ideally suited as disparity detectors. *Science* 249:1037–1041.
- Ohzawa I, DeAngelis GC, Freeman RD (1996) Encoding of binocular disparity by simple cells in the cat’s visual cortex. *J Neurophysiol* 75:1779–1805.
- Ohzawa I, DeAngelis GC, Freeman RD (1997) Encoding of binocular disparity by complex cells in the cat’s visual cortex. *J Neurophysiol* 77:2879–2909.

- Ohzawa I, Freeman RD (1986) The binocular organization of simple cells in the cat's visual cortex. *J Neurophysiol* 56:221–242.
- Osanai Y, Battulga B, Yamazaki R, Kouki T, Yatabe M, Mizukami H, Kobayashi K, Shinohara Y, Yoshimura Y, Ohno N (2022) Dark Rearing in the Visual Critical Period Causes Structural Changes in Myelinated Axons in the Adult Mouse Visual Pathway. *Neurochem Res* 47:2815–2825.
- Peysakhovich B, Zhu O, Tetrack SM, Shirhatti V, Silva AA, Li S, Ibos G, Rosen MC, Johnston WJ, Freedman DJ (2024) Primate superior colliculus is causally engaged in abstract higher-order cognition. *Nat Neurosci* 27:1999–2008.
- Poggio GF, Poggio T (1984) The Analysis of Stereopsis. *Annual Review of Neuroscience* 7:379–412.
- Policarpo F (2004) Chapter 41. Real-Time Stereograms. Available at: https://developer.nvidia.com/sites/all/modules/custom/gpugems/books/GPUGems/gpugems_ch41.html [Accessed April 19, 2021].
- Priebe NJ, Ferster D (2012) Mechanisms of neuronal computation in mammalian visual cortex. *Neuron* 75:194–208.
- Priebe NJ, McGee AW (2014) Mouse vision as a gateway for understanding how experience shapes neural circuits. *Front Neural Circuits* 8 Available at: <https://www.frontiersin.org/articles/10.3389/fncir.2014.00123/full> [Accessed April 14, 2021].
- Prince S j. d., Pointon AD, Cumming BG, Parker AJ (2002) Quantitative Analysis of the Responses of V1 Neurons to Horizontal Disparity in Dynamic Random-Dot Stereograms. *Journal of Neurophysiology* 87:191–208.
- Rao RPN (2002) Receptive Field. In: *Encyclopedia of the Human Brain* (Ramachandran VS, ed), pp 155–168. New York: Academic Press. Available at: <https://www.sciencedirect.com/science/article/pii/B0122272102002983> [Accessed April 30, 2025].
- Read J (2005) Early computational processing in binocular vision and depth perception. *Progress in Biophysics and Molecular Biology* 87:77–108.
- Read JCA, Cumming BG (2004) Ocular Dominance Predicts Neither Strength Nor Class of Disparity Selectivity With Random-Dot Stimuli in Primate V1. *Journal of Neurophysiology* 91:1271–1281.
- Ribic A (2020) Stability in the Face of Change: Lifelong Experience-Dependent Plasticity in the Sensory Cortex. *Frontiers in Cellular Neuroscience* 14 Available at: <https://www.frontiersin.org/articles/10.3389/fncel.2020.00076> [Accessed May 18,

2023].

- Ringach DL (2002) Spatial Structure and Symmetry of Simple-Cell Receptive Fields in Macaque Primary Visual Cortex. *Journal of Neurophysiology* 88:455–463.
- Ringach DL, Mineault PJ, Tring E, Olivas ND, Garcia-Junco-Clemente P, Trachtenberg JT (2016) Spatial clustering of tuning in mouse primary visual cortex. *Nat Commun* 7:12270.
- Russell AL, Dixon KG, Triplett JW (2022) Diverse modes of binocular interactions in the mouse superior colliculus. *Journal of Neurophysiology* 127:913–927.
- Russell JT (1932) Depth Discrimination in the Rat. *The Pedagogical Seminary and Journal of Genetic Psychology* 40:136–161.
- Sakai E, Bi H, Maruko I, Zhang B, Zheng J, Wensveen J, Harwerth RS, Smith EL, Chino YM (2006) Cortical effects of brief daily periods of unrestricted vision during early monocular form deprivation. *J Neurophysiol* 95:2856–2865.
- Salinas KJ, Velez DXF, Zeitoun JH, Kim H, Gandhi SP (2017) Contralateral Bias of High Spatial Frequency Tuning and Cardinal Direction Selectivity in Mouse Visual Cortex. *J Neurosci* 37:10125–10138.
- Samonds JM, Choi V, Priebe NJ (2019) Mice Discriminate Stereoscopic Surfaces Without Fixating in Depth. *J Neurosci* 39:8024–8037.
- Sanes JR, Masland RH (2015) The Types of Retinal Ganglion Cells: Current Status and Implications for Neuronal Classification. *Annual Review of Neuroscience* 38:221–246.
- Sarnaik R, Wang B-S, Cang J (2014) Experience-Dependent and Independent Binocular Correspondence of Receptive Field Subregions in Mouse Visual Cortex. *Cerebral Cortex* 24:1658–1670.
- Scholl B, Burge J, Priebe NJ (2013a) Binocular integration and disparity selectivity in mouse primary visual cortex. *J Neurophysiol* 109:3013–3024.
- Scholl B, Pattadkal JJ, Dilly GA, Priebe NJ, Zemelman BV (2015) Local integration accounts for weak selectivity of mouse neocortical parvalbumin interneurons. *Neuron* 87:424–436.
- Scholl B, Pattadkal JJ, Priebe NJ (2017) Binocular Disparity Selectivity Weakened after Monocular Deprivation in Mouse V1. *J Neurosci* 37:6517–6526.
- Scholl B, Tan AYY, Priebe NJ (2013b) Strabismus Disrupts Binocular Synaptic Integration in Primary Visual Cortex. *J Neurosci* 33:17108–17122.
- Seabrook TA, Burbridge TJ, Crair MC, Huberman AD (2017) Architecture, Function, and Assembly of the Mouse Visual System. *Annu Rev Neurosci* 40:499–538.

- Shen J, Colonnese MT (2016) Development of Activity in the Mouse Visual Cortex. *J Neurosci* 36:12259–12275.
- Siegle JH et al. (2021) Survey of spiking in the mouse visual system reveals functional hierarchy. *Nature* 592:86–92.
- Skottun BC, Bradley A, Sclar G, Ohzawa I, Freeman RD (1987) The effects of contrast on visual orientation and spatial frequency discrimination: a comparison of single cells and behavior. *Journal of Neurophysiology* 57:773–786.
- Skyberg R, Tanabe S, Chen H, Cang J (2022) Coarse-to-fine processing drives the efficient coding of natural scenes in mouse visual cortex. *Cell Reports* 38:110606.
- Soares CA, Mason CA (2015) Transient ipsilateral retinal ganglion cell projections to the brain: Extent, targeting, and disappearance. *Developmental Neurobiology* 75:1385–1401.
- Sommeijer J-P, Ahmadlou M, Saiepour MH, Seignette K, Min R, Heimel JA, Levelt CN (2017) Thalamic inhibition regulates critical-period plasticity in visual cortex and thalamus. *Nat Neurosci* 20:1715–1721.
- Stacy RC, Demas J, Burgess RW, Sanes JR, Wong ROL (2005) Disruption and Recovery of Patterned Retinal Activity in the Absence of Acetylcholine. *J Neurosci* 25:9347–9357.
- Stringer C, Pachitariu M (2024) Analysis methods for large-scale neuronal recordings. *Science* 386:eadp7429.
- Südhof TC (2018) Towards an Understanding of Synapse Formation. *Neuron* 100:276–293.
- Tan L, Ringach DL, Zipursky SL, Trachtenberg JT (2021) Vision is required for the formation of binocular neurons prior to the classical critical period. *Current Biology* 31:4305–4313.e5.
- Tan L, Tring E, Ringach DL, Zipursky SL, Trachtenberg JT (2020) Vision Changes the Cellular Composition of Binocular Circuitry during the Critical Period. *Neuron* 108:735–747.e6.
- Tanabe S, Fu J, Cang J (2022) Strong tuning for stereoscopic depth indicates orientation-specific recurrent circuitry in tree shrew V1. *Current Biology* Available at: <https://www.sciencedirect.com/science/article/pii/S0960982222017110> [Accessed November 22, 2022].
- Tanaka S (1997) Topological analysis of point singularities in stimulus preference maps of the primary visual cortex. *Proceedings of the Royal Society of London Series B: Biological Sciences* 261:81–88.
- Thompson A, Gribizis A, Chen C, Crair MC (2017) Activity-dependent development of visual receptive fields. *Curr Opin Neurobiol* 42:136–143.

- Tian N, Copenhagen DR (2001) Visual Deprivation Alters Development of Synaptic Function in Inner Retina after Eye Opening. *Neuron* 32:439–449.
- Toyoizumi T, Miyamoto H, Yazaki-Sugiyama Y, Atapour N, Hensch TK, Miller KD (2013) A Theory of the Transition to Critical Period Plasticity: Inhibition Selectively Suppresses Spontaneous Activity. *Neuron* 80:51–63.
- Troyer TW, Krukowski AE, Priebe NJ, Miller KD (1998) Contrast-Invariant Orientation Tuning in Cat Visual Cortex: Thalamocortical Input Tuning and Correlation-Based Intracortical Connectivity. *J Neurosci* 18:5908–5927.
- Tsao DY, Conway BR, Livingstone MS (2003) Receptive Fields of Disparity-Tuned Simple Cells in Macaque V1. *Neuron* 38:103–114.
- Valverde F (1971) Rate and extent of recovery from dark rearing in the visual cortex of the mouse. *Brain Research* 33:1–11.
- van Versendaal D, Levelt CN (2016) Inhibitory interneurons in visual cortical plasticity. *Cell Mol Life Sci* 73:3677–3691.
- Vorobyov V, Schwarzkopf DS, Mitchell DE, Sengpiel F (2007) Monocular deprivation reduces reliability of visual cortical responses to binocular disparity stimuli. *Eur J Neurosci* 26:3553–3563.
- Wade NJ (2002) Charles Wheatstone (1802 – 1875). *Perception* 31:265–272.
- Walters S (2020) *Psychology - 1st Canadian Edition*. Available at: <https://pressbooks.bccampus.ca/psychcapilano/> [Accessed April 30, 2025].
- Wang B-S, Feng L, Liu M, Liu X, Cang J (2013) Environmental enrichment rescues binocular matching of orientation preference in mice that have a precocious critical period. *Neuron* 80:198–209.
- Wang B-S, Sarnaik R, Cang J (2010a) Critical period plasticity matches binocular orientation preference in the visual cortex. *Neuron* 65:246–256.
- Wang L, Sarnaik R, Rangarajan K, Liu X, Cang J (2010b) Visual Receptive Field Properties of Neurons in the Superficial Superior Colliculus of the Mouse. *Journal of Neuroscience* 30:16573–16584.
- Wiesel TN, Hubel DH (1963a) Effects of visual deprivation on morphology and physiology of cells in the cat's lateral geniculate body. *Journal of Neurophysiology* 26:978–993.
- Wiesel TN, Hubel DH (1963b) Single-cell responses in striate cortex of kittens deprived of vision in one eye. *Journal of Neurophysiology* 26:1003–1017.

- Wiesel TN, Hubel DH (1965a) Comparison of the effects of unilateral and bilateral eye closure on cortical unit responses in kittens. *Journal of Neurophysiology* 28:1029–1040.
- Wiesel TN, Hubel DH (1965b) Extent of recovery from the effects of visual deprivation in kittens. *Journal of Neurophysiology* 28:1060–1072.
- Yang L, Lee K, Villagrancia J, Masmanidis SC (2020) Open source silicon microprobes for high throughput neural recording. *J Neural Eng* 17:016036.
- Young BK, Brennan JN, Wang P, Tian N (2018) Virtual reality method to analyze visual recognition in mice. *PLOS ONE* 13:e0196563.
- Zhou Q, Li H, Yao S, Takahata T (2023) Visual experience-dependent development of ocular dominance columns in pigmented rats. *Cerebral Cortex* 33:9450–9464.
- Zhuang J, Ng L, Williams D, Valley M, Li Y, Garrett M, Waters J (2017) An extended retinotopic map of mouse cortex Kleinfeld D, ed. *eLife* 6:e18372.
- Znamenskiy P, Kim M-H, Muir DR, Iacaruso MF, Hofer SB, Mrsic-Flogel TD (2024) Functional specificity of recurrent inhibition in visual cortex. *Neuron* 112:991-1000.e8.